

**Pore water expulsion at submarine cold seeps:
geochemical evidence for short-cuts between
crust, sediments and ocean**

DISSERTATION

zur Erlangung des Doktorgrades

an der Mathematisch-Naturwissenschaftlichen Fakultät

der Christian-Albrechts-Universität zu Kiel

vorgelegt von

Florian Scholz

Kiel, 2009

Referent: Prof. Dr. Klaus Wallmann

Koreferent: Prof. Dr. Martin Frank

Tag der mündlichen Prüfung: 29.01.2010

Zum Druck genehmigt: Kiel, 29.01.2010

Der Dekan

Hiermit erkläre ich, dass ich die vorliegende Doktorarbeit selbständig und ohne Zuhilfenahme unerlaubter Hilfsmittel erstellt habe. Weder diese noch eine ähnliche Arbeit wurde an einer anderen Abteilung oder Hochschule im Rahmen eines Prüfungsverfahrens vorgelegt, veröffentlicht oder zur Veröffentlichung vorgelegt. Ferner versichere ich, dass die Arbeit unter Einhaltung der Regeln guter wissenschaftlicher Praxis der Deutschen Forschungsgemeinschaft entstanden ist.

Florian Scholz

*„... Ach, rief Humboldt, was sei Wissenschaft denn dann?
Gauß sog an der Pfeife. Ein Mann allein am Schreibtisch.
Ein Blatt Papier vor sich, allenfalls noch ein Fernrohr,
vor dem Fenster der klare Himmel. Wenn dieser Mann nicht
aufgebe, bevor er verstehe. Das sei vielleicht Wissenschaft. ...“*

Daniel Kehlmann

Die Vermessung der Welt, 2005

Acknowledgements

This study was realized under supervision of Dr. Christian Hensen. I am grateful for his support, his readiness for discussion and for the pleasant and amicable working atmosphere throughout the period of my PhD.

I sincerely thank Prof. Dr. Klaus Wallmann for accepting me as a PhD student within the Research Unit Marine Geosystems and for acting as a referee for this dissertation. Furthermore, I would like to give sincere thanks to Prof. Dr. Martin Frank for acting as a co-referee.

The present work significantly benefited from collaboration and discussion with Dr. Anja Reitz, Dr. Matthias Haeckel, Dr. Marianne Nuzzo and Dr. Volker Liebetrau. I want to thank them for their support and for granting me insights into various aspects of scientific work.

During my PhD, I took part in four seagoing expeditions. Much of the work at sea would not have been possible without the outstanding expertise and the endeavor of the IFM-GEOMAR laboratory technicians. In particular, I want to thank Anke Bleyer, Bettina Domeyer and Regina Surberg for excellent collaboration; even under sometimes adverse conditions. Moreover, I owe thanks to Ana Kolevica, Anette Meixner and Cathrin Schulz for supporting me in the isotope labs of IFM-GEOMAR and GFZ.

I am grateful to Prof. Dr. Gert J. De Lange, Prof. Dr. Rolf L. Romer and Prof. Dr. Udo Fehn for the fruitful cooperation and for hosting me in their labs at Utrecht, Potsdam and Rochester.

I also want to thank all my colleagues and friends at IFM-GEOMAR for the friendly atmosphere.

Finally, I want to express my gratitude to Anna Dammshäuser for her encouragement and the affectionate companionship during the past years.

Abstract

Active pore water expulsion from marine sediments has been observed on continental margins worldwide and is therefore considered a potentially important link in global geochemical cycles. Understanding element recycling through submarine fluid discharge on a global scale requires a profound knowledge of the fluids' origin and the geochemical processes affecting their composition. Consequently, the present thesis investigates the chemical and isotopic composition of cold seep fluids as a function of the tectonic context, the lithology and thickness of ambient sediments and other relevant geological factors.

Chapter II deals with pore water data of five mud volcanoes that are aligned on an E-W transect across the Gulf of Cadiz in the NE Atlantic Ocean. In this area, mud volcanism and other phenomena of fluid flow are closely tied to thrust and strike-slip motion along the African-Eurasian plate boundary. Stable lithium and radiogenic strontium isotope data reveal a systematic pattern of deep fluid sources and diagenetic processes across the continental margin. High lithium concentrations and light $\delta^7\text{Li}$ values, both similar to those observed at hydrothermal vents, indicate a high-temperature fluid origin in the deep subsurface. Decreasing $^{87}\text{Sr}/^{86}\text{Sr}$ ratios reflect the seaward thinning of terrigenous sediments and the increasing importance of a non-radiogenic fluid component originating in the underlying oceanic basement. The collected data represent new geochemical evidence for a hydrological connection between buried oceanic crust and the water column at this crustal age (>140 Ma) and distance from the spreading axis.

The well-defined continent-ocean transition in the Gulf of Cadiz is revisited in Chapter III to investigate how iodine and its radioisotope, ^{129}I , respond to lateral changes in sediment thickness and fluid origin. Iodine is a biophilic element and the cosmogenic ^{129}I system therefore has been used to date organic sources of marine pore waters. In the Gulf of Cadiz, however, pore fluids receive additional ^{129}I produced through spontaneous fission of ^{238}U in uranium-rich, terrigenous sediments. Seaward decreasing $^{129}\text{I}/\text{I}$ ratios and a pronounced correlation with $^{87}\text{Sr}/^{86}\text{Sr}$ ratios are in line with the progressive change from continental to oceanic fluid sources. Comparison of the new data with literature data from sediment cores of

the Ocean Drilling Program (ODP) and terrestrial groundwater aquifers reveals a systematic relationship between fissiogenic ^{129}I , radiogenic ^{87}Sr and the lithology or provenance of rocks and sediments, respectively. This relationship places valuable constraints on the applicability of ^{129}I dating in different geological settings.

Chapter IV provides a comprehensive analysis of lithium isotope fractionation during diagenetic or hydrothermal fluid/mineral exchange in marine systems. New pore water data for cold seeps in different ocean basins and geological settings are compared with new and literature data for shallow marine sediments, ODP cores, hydrothermal fluids and marine brines. Most of the fluid data follow a general relationship between lithium concentration and isotopic composition reflecting lithium release from sediment and fractionation during uptake into authigenic minerals. Deviations from this trend are related to the varying lithology of sediments and rocks or to transport-related fractionation mechanisms. Application of a numerical transport-reaction model demonstrates that little pore water advection suffices to transfer deep-seated lithium isotope signals into shallow sediments. It is shown that lithium isotopes may provide a valuable record of fluid/mineral interaction that has been inherited hundreds or thousands of meters below the seafloor

Comparison of seep fluids in different geological settings reveals that deep-sourced fluid flow may occur in much more diverse manifestation than previously thought. Some cold seep fluids bear witness of exchange with minerals at temperatures beyond the typical diagenetic range ($>150\text{ }^{\circ}\text{C}$) or share other geochemical characteristics with fluids from sediment-covered ridge crest or ridge flank hydrothermal systems. This applies in particular to the abyssal seep locations in the Gulf of Cadiz where fluids carry a signature from interaction with the oceanic basement. Further manifestations of such fluid pathways intermediate between mid-ocean ridge hydrothermal vent and shallow marginal cold seep most likely exist on sediment-covered seamounts and fracture zones in the deep-sea. Exploration of these largely disregarded structures is essential for a sound understanding of material exchange between the oceanic lithosphere and the ocean.

Kurzfassung

Die Freisetzung von Porenwässern am Meeresboden durch kalte Quellen ist ein weltweit an Kontinentalrändern beobachtetes Phänomen und muss folglich als potentiell wichtiges Bindeglied in globalen geochemischen Stoffkreisläufen betrachtet werden. Ein globales Verständnis der Rückführung von Elementen durch submarine Fluidfreisetzung erfordert detaillierte Kenntnisse über die Herkunft der Fluide und die ihre Zusammensetzung bestimmenden Prozesse. Die vorliegende Arbeit beschäftigt sich mit der chemischen und isotopischen Zusammensetzung von Fluiden an submarinen, kalten Quellen, in Abhängigkeit des tektonischen Kontexts, der Sedimentmächtigkeit und anderer relevanter geologischer Faktoren.

Kapitel II behandelt Porenwasserdaten von fünf Schlammvulkanen, die entlang eines von Ost nach West verlaufenden Transekts durch den Golf von Cadiz im Nordost-Atlantik angeordnet sind. In diesem Gebiet sind Schlammvulkanismus und andere mit Fluidaustritten zusammenhängende Phänomene eng mit lateralen, tektonischen Bewegungen entlang der afrikanisch-eurasischen Plattengrenze verknüpft. Stabile Lithium und radiogene Strontium Isotopendaten belegen, wie sich tiefe Fluidquellen und diagenetische Prozesse in einer systematischen Abfolge über den Kontinentalrand hin ändern. Hohe Lithium-Konzentrationen und leichte $\delta^7\text{Li}$ -Werte, beide ähnlich derer von hydrothermalen Fluiden, weisen auf eine Fluidentstehung im tiefen Untergrund bei hohen Temperaturen hin. Zudem zeigen über den Kontinentalrand abnehmende $^{87}\text{Sr}/^{86}\text{Sr}$ -Verhältnisse die Ausdünnung terrigener Sedimente, die mit dem zunehmenden Einfluss einer unradiogenen Fluidkomponente aus der ozeanischen Kruste einhergeht. Die erhobenen Daten liefern neue Hinweise für eine hydrologische Verbindung zwischen einem von mächtigen Sedimenten bedeckten, alten (>140 Ma) ozeanischen Krustensegment und der Wassersäule.

Der in Kapitel II untersuchte Übergang zwischen Kontinent und Ozean im Golf von Cadiz wird in Kapitel III neu aufgegriffen, um zu untersuchen, wie die sich ändernden Sedimentmächtigkeiten und Fluidquellen auf die Iod-Konzentrationen und Iodisotopenverhältnisse im Porenwasser auswirken. Im Allgemeinen entstammt der

Hauptteil des im Porenwasser gelösten Iods der im Untergrund abgebauten organischen Substanz. Aus diesem Grunde wurde das kosmogene ^{129}I -System vorwiegend zur Datierung organischer Komponenten im Porenwasser genutzt. Im Gegensatz zu diesem generellen Trend enthalten tiefe Porenwässer im Golf von Cadiz zusätzliches Iod aus dem spontanen Zerfall von ^{238}U in uranreichen, terrigenen Sedimenten. Abnehmende $^{129}\text{I}/\text{I}$ -Verhältnisse über den Kontinentalrand und eine ausgeprägte Korrelation mit $^{87}\text{Sr}/^{86}\text{Sr}$ -Verhältnissen stehen im Einklang mit den sich seewärts ändernden Fluidquellen. Eine vergleichende Betrachtung neuer Daten und Literaturdaten aus Sedimentkernen des Ocean Drilling Program (ODP) und terrestrischer Grundwasseraquifere belegen einen systematischen Zusammenhang zwischen ^{129}I aus dem Zerfall von ^{238}U , radiogenem ^{87}Sr und der Lithologie oder Herkunft der umgebenden Sedimente und Gesteine. Diese generelle Systematik bietet wertvolle Hinweise für die Anwendbarkeit der Iodisotopdatierung in verschiedenen geologischen Systemen.

Kapitel IV beschäftigt sich mit einer umfassenden Analyse der Prozesse, die bei diagenetischen oder hydrothermalen Austauschreaktionen in marinen Systemen, zur Lithiumisotopenfraktionierung führen. Porenwasserdaten von submarinen kalten Quellen in unterschiedlichen Gebieten werden mit neu erhobenen und aus der Literatur bezogenen Daten mariner Sedimentporenwässer, hydrothermalen Fluide und mariner Solen verglichen. Größtenteils zeigen die Fluiddaten eine systematische Beziehung zwischen Lithiumkonzentration und $\delta^7\text{Li}$ -Isotopenzusammensetzung, die die Freisetzung von Lithium aus Tonmineralen und die Isotopenfraktionierung beim Einbau in authigene Minerale widerspiegelt. Abweichungen von diesem generellen Trend sind auf Unterschiede in der Herkunft der Sedimente oder deren Zusammensetzung sowie auf transportbedingte Fraktionierungsmechanismen zurückzuführen. Die Anwendung eines numerischen Transport-Reaktions-Modells beweist, dass bereits geringe Fluidaufstiegsgeschwindigkeiten ausreichen, um die in großer Tiefe generierten Lithiumisotopensignale in Oberflächensedimente zu transferieren. Lithiumisotope können daher als ein wertvoller Anzeiger für Interaktionen zwischen Fluiden und Mineralen in tiefen Sedimenten genutzt werden.

Die vergleichende Untersuchung von Fluiden aus submarinen, kalten Quellen in unterschiedlichen geologischen Situationen macht deutlich, dass Fluidtransport in deutlich vielgestaltigerer Form auftritt, als dies bisher angenommen wurde. Viele Fluide zeugen von Austauschprozessen mit Mineralen bei Temperaturen jenseits des typischen diagenetischen Bereichs ($>150\text{ °C}$) oder teilen andere geochemische Eigenschaften mit Fluiden aus sedimentbedeckten Hydrothermalsystemen an Spreizungsachsen oder deren Flanken. Dies

gilt insbesondere für die abyssalen Porenwasseraustritte im Golf von Cadiz, wo die geförderten Fluide Spuren von Interaktionen mit der ozeanischen Kruste tragen. Damit können sie als intermediäre Fluidtransportsysteme zwischen den hydrothermalen Fluidaustritten an mittelozeanischen Rücken und den flachwurzelnden, kalten Quellen an Kontinentalrändern angesehen werden. Weitere solche intermediären Fluidaustritte existieren höchst wahrscheinlich an sedimentbedeckten Seamounts und Bruchzonen in der Tiefsee. Eine Untersuchung dieser bisher weitgehend unbeachteten Strukturen ist unerlässlich für ein vollständiges Verständnis des stofflichen Austauschs zwischen der ozeanischen Lithosphäre und dem Ozean.

Table of contents

ABSTRACT.....	I
KURZFASSUNG.....	III
TABLE OF CONTENTS.....	VI

I. GENERAL INTRODUCTION

I.1. Geochemical budget of the global ocean	1
I.2. Significance of fluid expulsion on continental margins	3
I.3. Diagenetic processes in marine sediments.....	5
<i>I.3.1. Early diagenesis of organic matter.....</i>	6
<i>I.3.2. Diagenetic alteration of silicate minerals.....</i>	8
<i>I.3.3. Water/rock interaction within buried basement rocks.....</i>	9
I.4. The oceanic lithium cycle	10
I.5. Thesis outline	12
References.....	13

II. ISOTOPIC EVIDENCE ($^{87}\text{Sr}/^{86}\text{Sr}$, $\delta^7\text{Li}$) FOR ALTERATION OF THE OCEANIC CRUST AT DEEP-ROOTED MUD VOLCANOES IN THE GULF OF CADIZ, NE ATLANTIC OCEAN

Abstract.....	17
II.1. Introduction	18
II.2. Material and methods.....	20
<i>II.2.1. Geological setting</i>	20
<i>II.2.2. Sediment sampling and pore water recovery.....</i>	22
<i>II.2.3. Chemical analyses.....</i>	22
<i>II.2.4. Isotope analyses</i>	23
II.3. Results.....	24
<i>II.3.1. Pore water chemistry</i>	24
<i>II.3.2. Isotope data</i>	24
II.4. Discussion	27
<i>II.4.1. Diagenetic characterization of pore fluids.....</i>	27

<i>II.4.2. Evolution of saline fluids at the proximal mud volcanoes</i>	29
<i>II.4.3. Strontium isotope geochemistry of pore fluids</i>	31
<i>II.4.4. Lithium isotope geochemistry of pore fluids</i>	34
<i>II.4.4.1. Lithium in pore fluids: source or temperature controlled?</i>	34
<i>II.4.4.2. Lithium isotope constraints on fluid formation temperatures</i>	36
II.5. Summary and conclusions	39
Acknowledgements.....	41
References.....	42

III. TRACING ORGANIC AND INORGANIC SOURCES TO DEEP-SEATED MARINE INTERSTITIAL FLUIDS: IODINE AND ¹²⁹I SYSTEMATICS IN THE GULF OF CADIZ

Abstract.....	49
III.1. Introduction.....	50
<i>III.1.1. Scientific objective</i>	50
<i>III.1.2. Geochemistry of iodine in marine sediments</i>	51
<i>III.1.3. Geological setting</i>	52
III.2. Sampling and analytical methods.....	54
III.3. Results.....	57
III.4. Discussion.....	58
<i>III.4.1. Diagenetic controls on iodide in pore waters</i>	58
<i>III.4.2. Iodine isotope systematics</i>	60
<i>III.4.2.1. Sources of old iodine</i>	60
<i>III.4.2.2. Sources of excess ¹²⁹I</i>	62
<i>III.4.2.3. Controls on fissiogenic ¹²⁹I in deep-seated marine interstitial fluids</i>	65
III.5. Summary and conclusions.....	67
Acknowledgments	68
References.....	69

IV. LITHIUM ISOTOPE GEOCHEMISTRY OF MARINE PORE WATERS – INSIGHTS FROM COLD SEEP FLUIDS

Abstract.....	73
IV.1. Introduction.....	74
IV.2. Samples.....	75
<i>IV.2.1. Regional settings</i>	76

<i>IV.2.2. Diagenetic characterization of pore fluids</i>	77
IV.3. Methods	80
<i>IV.3.1. Sediment sampling and pore water recovery</i>	80
<i>IV.3.2. Laboratory analyses</i>	81
<i>IV.3.3. Transport-reaction modeling</i>	82
IV.4. Results	83
IV.5. Discussion	87
<i>IV.5.1. Controls on the lithium isotope composition of marine pore fluids</i>	87
<i>IV.5.1.1. Hydrothermal fluids</i>	89
<i>IV.5.1.2. Sediment interstitial fluids</i>	90
<i>IV.5.1.3. Cold seep fluids</i>	91
<i>IV.5.1.4. Marine brines</i>	94
<i>IV.5.2. Lithium isotope fractionation during fluid advection</i>	96
IV.6. Summary and conclusions	101
Acknowledgements	102
References.....	102
V. SYNTHESIS	109
References.....	110
APPENDIX A. SUPPORTING MATERIAL TO CHAPTER IV	111

General Introduction

I.1. Geochemical budget of the global ocean

The world ocean directly interacts with most other geochemical reservoirs on earth and, therefore, plays a key role in global geochemical cycles. In order to understand its geochemical budget it is necessary to evaluate the composition, magnitude and temporal variability of element fluxes into and out of the oceanic reservoir. This global framework of input and output fluxes is illustrated as a conceptual box model in Figure I.1.

Major natural sources or sinks of material to the ocean are the continental crust, the oceanic crust and the atmosphere. Material that has been mobilized from the continental crust by subaerial weathering and erosion reaches the ocean mostly via fluvial or aeolian transport. River inputs to the ocean are well constrained from studies on the runoff and chemical composition of the dissolved and particulate load of the world's major rivers and streams (Martin and Maybeck, 1979; Martin and Whitfield, 1983). In principle, the chemical composition of river water and particulate matter chiefly depends on the geology and climatic regime of the catchment area. However, chemical and biological reactions in the river itself and, especially, in the estuarine mixing zone have to be considered for the evaluation of the river flux into the ocean (Boyle et al., 1974). The atmospheric flux has attracted considerable attention in recent years because of its important role in controlling primary productivity in nutrient-limited ocean regions (Jickells et al., 2005). Estimates of the continental input flux via the atmospheric pathway have been obtained by combining the quantity and chemical composition of locally collected dry and wet deposition with global wind and precipitation data (Duce et al., 1991). Other approaches concentrate on diagnostic elements in surface waters (e.g. aluminum; Measures and Vink, 2000) or involve remote sensing data on the global aerosol distribution (Kaufman et al., 2005). The chemical composition of the airborne input to the ocean depends, similar to that of the fluvial input, on the geology of the source region but also on the extent of chemical alteration during transport in the atmosphere.

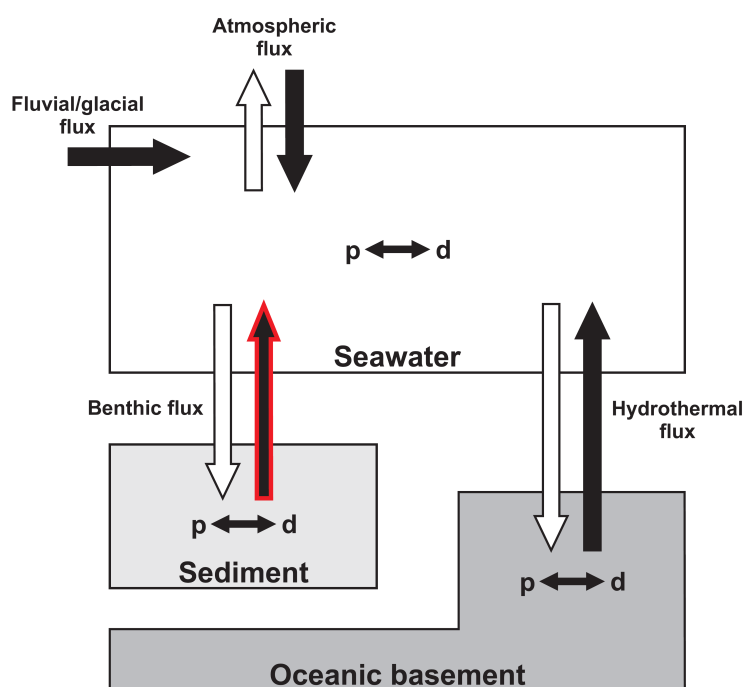


Figure I.1. Schematic representation of the global ocean geochemical reservoir. The large black arrows indicate transport from material sources and the large white arrows indicate transport into material sinks. Small arrows denote transitions between particulate/solid (p) and dissolved (d) phase. The main subject of the present thesis, i.e. pore water expulsion from sediments, is highlighted by the red arrow.

The most prominent manifestation of chemical exchange between the ocean and the oceanic crust is hydrothermal venting at the crests of mid-ocean ridges. It is a result of the emplacement of hot rock at divergent plate boundaries and the accompanying circulation of seawater through the oceanic basement. Depending on the reaction temperature, hydrothermal fluids are strongly depleted in magnesium and sulfate and enriched in hydrogen sulfide, alkali elements and certain trace metals (Edmond et al., 1979; Von Damm, 1990). Global estimates suggest that the entire ocean interacts every 8 – 10 Ma with fresh basalt at the high-temperature ridge axial zone. The importance of hydrothermal activity for ocean chemistry has been further underscored by studies on hydrothermal circulation at low to intermediate temperatures at the ridge flanks. For instance, it has been suggested that most of the riverine input of magnesium to the ocean is balanced by removal during off-axis hydrothermal circulation (Wheat and Mottl, 2000). Furthermore, the heat transferred through the seafloor at ridge flanks exceeds that of the ridge axis by a factor of 2 - 4 (Elderfield and Schulz, 1996). Low-temperature weathering of basalt that is exposed on the seafloor or interaction with hot lava that is extruded onto the sea bed at submarine volcanoes are further examples for exchange between seawater and the oceanic crust.

Marine sediments represent the ultimate sink for all particulate components that survive destruction in the oceanic reservoir. The sediments are also the major sink for dissolved elements which become scavenged by particles or incorporated in organic tissues or biogenous precipitates. Tectonic uplift above sea level and subduction at convergent ocean margins are the major mechanisms by which sediments may be transferred into adjacent geochemical reservoirs. Prior to uplift or recycling to the earth mantle, however, sediments undergo multiple physical and chemical alterations leading to a significant modification of the primary sediment-forming signal. Many elements or components contained in the sediments at the time of deposition are dissolved and recycled during these processes. This back-flux of dissolved elements from marine sediments is one of the least-constrained input pathways to the ocean. Especially the expulsion of deep-sourced pore fluids from thick sediment accumulations on continental margins is likely to be an important source of volatile elements to the global oceanic reservoir.

I.2. Significance of fluid expulsion on continental margins

The most common transport mechanism by which solute elements are transported across the sediment/bottom water boundary is molecular diffusion. It is driven by concentration gradients which result from chemical or biological processes within the sediments. However, on continental margins with high sedimentation rates, this process does only affect the uppermost meters of the sediment column. In contrast to molecular diffusion, active fluid advection is a more efficient transport mechanism by which pore fluids from sediment depths of several kilometers below seafloor may be transferred to the sediment surface.

The actual reasons for upward directed, advective transport of fluids in sedimentary environments may be comprehended by examining Figure I.2 showing a compilation of worldwide locations where either hydrothermal venting or sediment fluid expulsion occurs. Submarine hydrothermalism is closely tied to magmatic activity at mid-ocean ridges, back-arc spreading centers or intra-plate hot spots. In a hydrothermal convection cell, seawater that has penetrated the oceanic crust along fractures or fissures is heated to temperatures of 350 - 400 °C close to the top of the magma chamber and then driven upwards towards the seafloor (Lowell et al., 1995). In contrast to hydrothermal venting, phenomena related to active sediment dewatering and degassing are concentrated on thickly sedimented continental margins and at convergent plate boundaries (Figure I.2). During deposition of

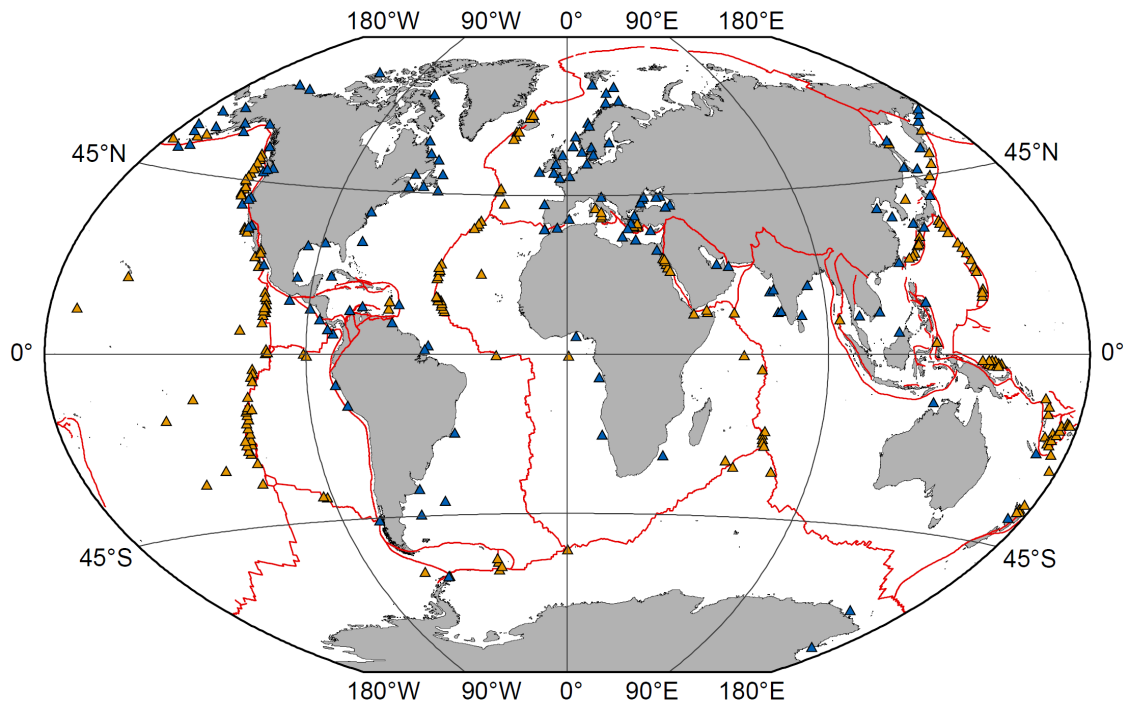


Figure I.2. Global distribution of phenomena related to seafloor hydrothermal activity (yellow triangles) and active fluid expulsion from sediments (blue triangles). Tectonic plate boundaries are depicted by red lines (data from Herzig and Hannington, 2005; Judd, 2003).

sediments with normal consolidation, pore fluids move upward with respect to the solid grains and relative to the underlying crust. However, provided that the porosity at the bottom does not become zero, both solid grains and fluids are continually added to the sediment section at the top. In other words, as long as such a situation of equilibrium consolidation is maintained, there is no pore fluid expulsion from the seafloor (Hyndman and Davis, 1995). Active upward migration of fluids with respect to the seafloor requires one of the following particular geological conditions: Sediment sections must be (i) subjected to compressional forces and undergo tectonic thickening, e.g. in accretionary wedges in subduction zones, (ii) loaded and compressed when underthrust and subducted at non-accretionary margins or (iii) so rapidly deposited that equilibrium consolidation is no longer maintained and fluid expulsion has to occur in order to redress the balance (Hyndman and Davis, 1995). Examples for the first two cases are the Mediterranean Ridge accretionary complex and the non-accretionary Central American margin, respectively. The Nile deep-sea fan in the eastern Mediterranean Sea may be an example for the third case. Pore water geochemical data for all of these examples will be treated in Chapter IV of this thesis.

In addition to the above-listed mechanisms, geochemical processes within the sediments, such as generation of hydrocarbon gases, dehydration of clay minerals or dissolution of gas

hydrates, may further amplify pore pressure and thus upward movement of interstitial fluids. In continental margin settings with huge accumulation rates of terrigenous, fine-grained sediments, clay mineral dehydration and tectonic compression may cause liquefaction and vertical emplacement of sediments themselves. The combined process of pore fluid, gas and mud (i.e. liquefied sediment) extrusion is referred to as ‘mud volcanism’. It has to be stressed, however, that at most mud volcanoes, fluids and mud are unlikely to be derived from the same depth within the sedimentary complex (Dimitrov, 2002; Kopf, 2002).

One major problem in quantifying the contribution of pore fluid expulsion on continental margins to the geochemical budget of the world ocean is the poorly constrained number of seep locations, as well as their size and activity. A global map of regions where fluid seepage has been documented is given in Figure I.2. However, analogical to the occurrence of hydrothermal vents, the actual number of fluid expulsion sites is likely to be considerably higher. Another limitation for a quantitative evaluation of fluid seepage is the lack of a general systematic on how geological conditions such as the tectonic setting or the thickness, provenance and/or lithology of sediments influence the chemical and isotopic composition of pore fluids. A brief overview about (bio)geochemical processes that may be encountered in shallow and deeply buried sediments on continental margins is given in the following section. This general overview will prepare the ground for a detailed treatise of the behavior of specific elemental and isotopic proxies under varying environmental conditions in Chapter II to IV.

I.3. Diagenetic processes in marine sediments

Interstitial waters are aqueous solutions that occupy the pore space between particles in sediments or rocks. For most marine sediments, the pore water originated as seawater trapped from the overlying water column. Exceptions to this rule are coastal or estuarine sediments where groundwater seepage can occur and sediments at mid-ocean ridge flanks where circulating basement fluids may enter the sediment column. The sediment-pore water continuum is a site of intense physical, chemical and biological reaction leading to compaction, dissolution of detrital minerals or precipitation of new, so-called authigenic minerals and, consequently, to changes in the composition of pore waters themselves (Chester, 2003). These processes are grouped together under the term ‘diagenesis’ which has been defined by Berner (1980) as “the sum total of processes that bring about changes in a

sediment or sedimentary rock subsequent to deposition in water”. This section focuses on diagenetic processes and concepts that are relevant to the following chapters. Therefore, special attention is given to the inorganic geochemical aspects of diagenesis.

I.3.1. Early diagenesis of organic matter

Diagenetic processes occurring up to a burial depth of a few hundred meters and at temperatures close to that prevailing at the seafloor are referred to as ‘early diagenesis’ (Berner, 1980). Most early diagenetic processes are related to the microbial degradation of organic matter. Organic substance is produced by photosynthetic algae in the water column, transported through the food chain and repeatedly recycled until sedimentation and burial in the sediments. Chemoheterotrophic microorganisms oxidize sedimented organic matter by transferring electrons from organic carbon to an electron acceptor. The major electron acceptors are dissolved oxygen, nitrate (NO_3^-), sulfate (SO_4^{2-}) and carbon dioxide (CO_2) as well as solid manganese (Mn(IV)) and iron (Fe(III)) in the form of oxyhydroxides. Since bacteria aim to optimize their metabolic energy yield, different microbial communities exist which are specialized for specific oxidizing agents. Oxidants are consumed successively according to the decreasing Gibbs free energy yield (ΔG^0) of the corresponding metabolic pathway. This results in a vertical sequence of predominantly occurring redox-reactions: the so-called ‘early diagenetic sequence’ (Figure I.3; Froelich et al., 1979). The early diagenetic sequence is reflected by the pore water profiles of the involved redox species. With increasing sediment depth, concentrations of reduced species (e.g. HS^-) increase at the expense of the corresponding oxidized species (e.g. SO_4^{2-}). Such concentration-depth gradients promote vertical, diffusive transport of pore water constituents. Upward-diffusing reduced species may reach the interface at which they are not stable anymore. Microorganisms occupy such transition zones and gain energy through re-oxidation. A prominent example for such an interfacial redox process is sulfate reduction coupled to the anaerobic oxidation of methane which results from a syntrophic relationship between sulfate reducing bacteria and methanotrophic archaeans (Boetius et al., 2000). This process plays an outstanding role in oxidizing deep-sourced methane in surficial sediments of submarine fluid escape structures (Wallmann et al., 2006).

According to the predominantly occurring metabolic pathway or the presence of specific authigenic minerals, sediments have been classified into oxic, sub- or post-oxic, anoxic-sulfidic and methanic (Figure I.3; Berner, 1981). Especially the ambiguous definition of

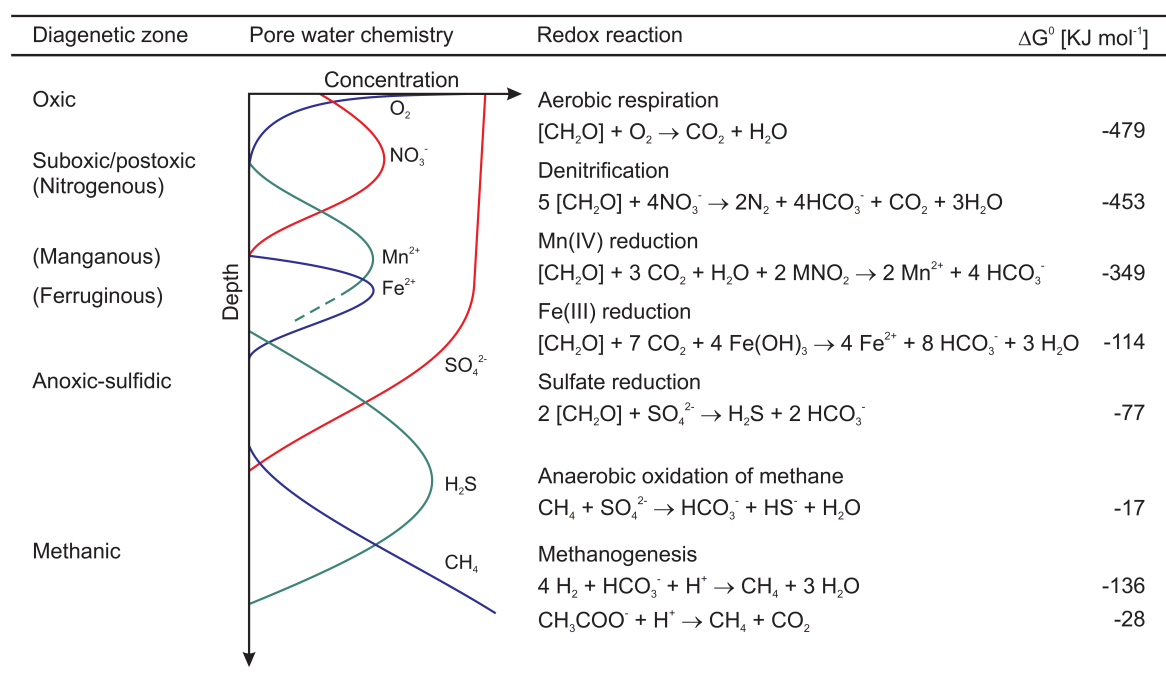


Figure I.3. Schematic representation of the early diagenetic sequence in marine sediments (after Froelich et al., 1979). The names of the major redox zones are taken from Froelich et al. (1979), Berner (1981) and Canfield and Thamdrup (2009). The reaction equations for organic matter oxidation, methanogenesis as well as anaerobic methane oxidation and their corresponding Gibbs free energy yield (ΔG^0 at pH = 7) are given according to Jørgensen (2006).

‘suboxic’ conditions, however, has led to considerable confusion in literature. In a recent article, Canfield and Thamdrup (2009) proposed a more precise terminology for conditions, where neither dissolved oxygen nor sulfide is present. According to these authors, geochemical environments should be denominated ‘nitrogenous’, ‘manganous’ and ‘ferruginous’, depending on the predominant redox species in pore water. Although not yet accepted by the scientific community, this classification is shown in parentheses in Figure I.3.

The vertical extent of redox zones varies from a few centimeters to several meters, depending on the availability of organic matter and electron acceptors. In pelagic deep-sea sediments, where the organic matter flux and, as a result, microbial respiration is low, oxic or suboxic diagenesis may prevail up to a depth of several meters (Froelich et al., 1979). By contrast, in near-shore environments with high biological productivity or in semi-enclosed basins, most electron acceptors are rapidly depleted and sulfate reduction or even methanogenesis becomes the dominant organic matter degradation pathway at or shortly below the sediment/bottom water interface (Jørgensen, 1982; Claypool and Kvenholden, 1983).

In ocean regions with high primary productivity, considerable amounts of organic matter may survive early diagenesis and become buried to greater sediment depth (Pedersen and

Calvert, 1990). Hegdes and Keil (1995) demonstrated that organic matter preservation in such environments largely depends on its residence time in the oxic diagenetic zone. Furthermore, these authors pointed out that formation of protective clay-organic aggregates leads to an enhanced burial of organic matter to the anoxic zone. Once buried and subjected to temperatures and pressures beyond the early diagenetic range, organic matter is slowly transformed into non-hydrolysable degradation products referred to as kerogen. Depending on temperature, pressure and its composition, kerogen may later transform into light (i.e. gas) or heavy hydrocarbons (i.e. oil). Such deeply buried organic matter in continental margin sediments represents an important reservoir in the long-term carbon cycle (Berner, 2003).

I.3.2. Diagenetic alteration of silicate minerals

The pore water chemistry of many major and minor seawater constituents is determined by interactions with detrital or authigenic silicate minerals. Those interactions occur over a broad depth and temperature range and can lead to significant changes in the bulk geochemistry of the solid phase. The most readily altered siliciclastic components of marine sediments are ash particles and other fresh volcanogenic material. This has important implications for the composition of pore waters in convergent margin settings where huge amounts of volcanogenic matter are delivered from the volcanic arc (Kastner et al., 1991). During low-temperature diagenesis, ash particles are transformed into authigenic minerals such as smectite or zeolites. Authigenic smectite formation decreases pore water magnesium and lithium, increases calcium and strontium and consumes water. Since most volcanic matter in subduction zones has an intermediate, i.e. andesitic, composition, interstitial $^{87}\text{Sr}/^{86}\text{Sr}$ ratios become generally less radiogenic during this process (Lawrence et al., 1979). Depending on the respective zeolite mineral formed, pore fluids become depleted in e.g. potassium, sodium or calcium (Kastner and Rudnicki, 2004).

At temperatures above 60 °C, authigenic or detrital smectite is progressively transformed into illite or smectite/illite mixed layer minerals. In a generalized manner, this process may be expressed as a reaction of smectite and potassium to illite, magnesium, sodium, some minor elements (e.g. strontium and lithium) and water. Depending on the provenance of the precursor smectite (oceanic/volcanic versus terrigenous), pore water $^{87}\text{Sr}/^{86}\text{Sr}$ ratios can become less radiogenic or more radiogenic during this process (Środoń, 1999; Kastner and Rudnicki, 2004). Pore fluids that are influenced by clay mineral transformation in adjacent sediments commonly display reduced salinities due to dilution with interlayer water.

Furthermore, dehydration of clay minerals may increase pore pressure which enhances negative buoyancy of already overpressured pore fluids in compressional sedimentary settings. The interlayer water released during smectite/illite transformation has a characteristic oxygen and hydrogen isotopic composition ($\delta^{18}\text{O} > \text{SMOW}$ and $\delta\text{D} < \text{SMOW}$) (Sheppard and Gilg, 1996). Oxygen and hydrogen isotope systematics may therefore be used to distinguish between clay mineral dehydration and other reasons for pore fluid freshening, such as gas hydrate dissolution ($\delta^{18}\text{O}, \delta\text{D} > \text{SMOW}$) or seepage of meteoric groundwater ($\delta^{18}\text{O}, \delta\text{D} < \text{SMOW}$) (Dählmann and De Lange, 2003). At temperatures ≤ 160 °C smectite/illite conversion is mostly completed, which is also indicated by near-complete potassium depletion in pore water.

At temperatures between 160 °C and 250 °C, geochemical exchange processes between fluids and sediments become similar to those typically observed in ridge crest hydrothermal systems. For instance, plagioclase is replaced by albite, smectite or illite are transformed into chlorite/smectite mixed layer minerals or pure chlorite and fluids leach mobile elements such as potassium, rubidium, lithium and boron from the solid phase (Alt et al., 1986; Alt, 1995; You et al., 1996; Kastner and Rudnicki, 2004). Further interaction between pore fluids and silicate minerals at higher temperatures and pressures occurs during ongoing subduction of sediments at convergent plate boundaries.

1.3.3. Water/rock interaction within buried basement rocks

Strictly speaking, water/solid interactions within basement rocks should not be dealt with in a section on sediment-diagenetic processes. However, in particular geological settings, such as sedimented ridge flank hydrothermal systems (e.g. eastern flank of the Juan de Fuca Ridge), basement fluids may enter the sediment column. In these cases, a detailed understanding of seawater/basalt interaction at low to intermediate temperatures is a basic requirement to distinguish sediment- and basement-derived geochemical signals in pore water.

Critical factors for fluid flow within buried basement rocks on sedimented ridge flanks are the location and abundance of basement outcrops that provide sites for fluid recharge (Fisher et al., 2003). In general, basement fluids become more geochemically evolved with increasing basement temperature which, in turn, is determined by the thickness of the overlying sediments. For instance, fluids sampled on a W-E transect across the eastern flank of the Juan

de Fuca Ridge showed increasing concentrations of calcium and decreasing concentrations of magnesium, sodium, potassium and lithium with increasing distance from the recharge zone and with temperature increasing from ~ 16 °C to 63 °C. Interstitial $^{87}\text{Sr}/^{86}\text{Sr}$ ratios decreased towards an end member value intermediate between those of fresh basalt and modern seawater (Wheat and Mottl, 1994; Elderfield et al., 1999). Most of these geochemical signals have been explained with transformation of plagioclase and volcanic glass to smectite and related mineral phases (see above) (Wheat and Mottl, 2000).

The factors controlling reaction of basement fluids with overlying sediments or mixing with pore waters are less well constrained. James et al. (2003) suggested that reaction with sediments becomes dominant at slow upwelling rates (e.g. <0.1 cm a^{-1}). This has important implications for the pore water geochemistry of sediments that are in hydraulic contact with the underlying oceanic basement. For instance, lithium is taken up by basalt at temperatures up to 250 °C but released from terrigenous sediments at temperatures as low as 50 °C (James et al., 2003). Considering intense reaction of a slowly upwelling basement fluid with sediments, the original basement-derived lithium signal would be entirely overprinted after passage through the sediment column.

Once the sediment cover has reached a thickness of a few hundred meters, pore fluid advection largely ceases confining flow to the basement aquifer (McDuff, 1981; Rudnicki et al., 2001). In certain ocean areas, there is geophysical evidence for continued hydrothermal circulation within the upper oceanic basement at crustal ages of ~ 60 – 175 Ma. Because of the thick sediment cover, however, such basement aquifers are unlikely to possess a hydrological connection to the ocean (Von Herzen, 2004).

I.4. The oceanic lithium cycle

Investigating the geochemical processes described above on a global scale yields a more quantitative picture of the input and output fluxes to the world ocean than depicted in Figure I.1. Two of the following chapters deal with lithium and its isotopes as tracers for mineral/water interactions in the marine subsurface. Therefore, this element will be used here to illustrate how an oceanic mass balance may be obtained.

The magnitude of the fluvial lithium input has been evaluated by measuring concentrations in the world's major rivers and multiplying the resulting average concentration with the global

fluvial discharge into the ocean (Huh et al., 1998). Estimates of the hydrothermal lithium flux to the ocean were obtained from the lithium to mantle-derived ^3He ratio in vent fluids extrapolated to the total ^3He inventory of the ocean. The validity of this calculation is based on the fact that extrapolation of the heat to ^3He ratio measured in hydrothermal fluids results in a global heat flux which is similar to that estimated based on the heat flow anomaly near to active ridges (Edmond et al., 1979). Later studies refined the hydrothermal lithium flux by correcting for off-axis heat flow and by comparing the fluxes to the amount of oceanic crust formed per year at mid-ocean ridges (Stoffyn-Egli and Mackenzie, 1984; Chan et al., 2002). Lithium inputs through fluid expulsion at convergent plate boundaries have been estimated by multiplying averaged concentrations in décollement fluids with the associated global dewatering flux (You et al., 1995).

The rate of lithium removal by uptake onto basalt at low to moderate temperatures has been determined by measuring the authigenic lithium enrichment in weathered basalt with respect to freshly formed basalt and, again, by extrapolating this concentration difference to the global volume of new oceanic crust formed per year (Stoffyn-Egli and Mackenzie, 1984; Chan et al., 2002). The diffusive benthic flux of lithium into marine sediments has been calculated based on concentration-depth profiles in sediment pore waters. Multiplying the average diffusive lithium flux with the total sediment-covered seafloor area where authigenic clay mineral formation takes place yields an estimate of the global lithium uptake by sediments (Stoffyn-Egli and Mackenzie, 1984; Zhang et al., 1998).

The resulting oceanic lithium budget is largely balanced which is illustrated in a modified version of Figure I.1 in Figure I.4. Most of the flux estimates, however, vary over broad ranges demonstrating that parts of the oceanic lithium cycle are still poorly constrained. Input fluxes to the ocean, that are less well studied so far, could be missed in that manner. For instance, the back-flux of lithium from sediments into the water column in Figure I.4 does not account for fluid flow at cold seeps on passive continental margins. Such missing sinks or sources are unlikely to be important for the element budget itself, but could exert a certain influence on the lithium isotope budget of the ocean. A recent lithium mass balance, published in a paper on lithium and its isotopes as tracers for global silicate weathering (Hathorne and James, 2006), is based on average values for the most important lithium input and output fluxes (bold values in Figure I.4). Because of the broad range of the actual flux estimates, however, their calibration for the modern ocean underlies large uncertainties. Ongoing refinement of element fluxes is therefore an important requirement for the development of new environmental tracers and paleo-proxies.

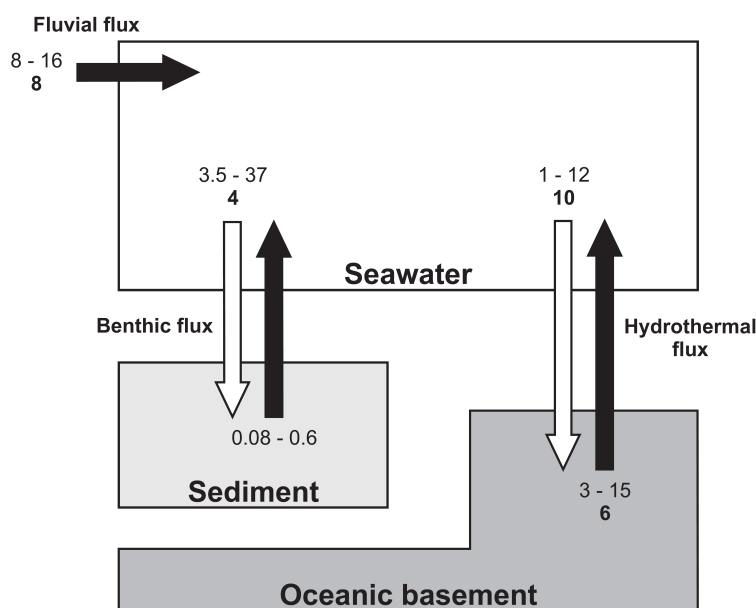


Figure I.4. Schematic representation of the global oceanic lithium budget. The flux values (in 10^9 mol a^{-1}) are taken from Chan et al. (2002), Huh et al. (1998), Stoffyn-Egli and Mackenzie (1984), You et al. (1995) and Zhang et al. (1998). Values in bold are average fluxes which were applied for mass balance calculations by Hathorne and James (2006).

1.5. Thesis outline

The following three chapters represent stand-alone articles which have been published or submitted for publication in scientific journals. They revisit different aspects which have been raised in the general introduction given above.

Chapter II deals with the inorganic geochemistry of deep-sourced pore fluids from five mud volcanoes that were sampled on a transect across the Gulf of Cadiz in the NE Atlantic Ocean. For the first time, lithium isotopes are applied as a tracer for fluid/mineral interactions in the context of mud volcanism and fluid seepage on continental margins. A combination of lithium and radiogenic strontium isotope data reveals a consistent transition of diagenetic processes and fluid sources from the near-shore to the deep-sea locations. Findings from Chapter II are revisited in Chapter III to assess how iodine and the $^{129}\text{I}/^{127}\text{I}$ system respond to lateral changes in tectonic setting and sediment thickness. Comparison of the presented results with pore water data from the Ocean Drilling Program (ODP) yields new insights into the cycling of iodine and its radioisotope, ^{129}I , in marine sediments. Chapter IV provides a comprehensive analysis of lithium isotope systematics in the context of diagenesis and fluid seepage. Data for

deep-sourced pore fluids from cold seep sites in differing geological settings are compared with literature data from pore waters of ODP cores and hydrothermal fluids from bare ridge-crest and sediment-hosted hydrothermal systems. A numerical transport-reaction model is applied to simulate the fractionation of lithium isotopes during fluid advection through sediments. This study aims at establishing a general reference frame for Li isotope exchange between fluids and silicate minerals in marine systems.

A general summary and an evaluation of the presented conclusions in the context of the current state of research will be given in Chapter V.

In addition to the work presented here, I contributed to the following, complementary articles:

Origin of light volatile hydrocarbon gases in mud volcano fluids, Gulf of Cadiz - evidence for multiple sources and transport mechanisms in active sedimentary wedges

Authors: Nuzzo M., Hornibrook E.R.C., Gill F., Hensen C., Pancost R.D., Haeckel M., Reitz A., Scholz F., Magalhães V.H., Brückmann W. and Pinheiro L.M.

Status: published in *Chemical Geology* (2009) **266**, 359-372.

Active mud volcanoes on the upper slope of the western Nile deep-sea fan - first results from the P362/2 cruise of R/V Poseidon

Authors: Feseker T., Brown K., Blanchet C., Scholz F., Nuzzo M., Reitz A., Schmidt M. and Hensen C.

Status: submitted to *GeoMarine Letters*.

Sources of fluids and gases expelled at cold seeps offshore Georgia, eastern Black Sea

Authors: Reitz A., Pape T., Schmidt M., Haeckel M., Scholz F., Aloisi G., Liebetrau V., Wallmann K., Berner U. and Weise S.M.

Status: in preparation.

References

- Alt J.C., Honnorez J., Laverne C. and Emmermann R. (1986). Hydrothermal alteration of a 1 km section through the upper oceanic crust, Deep-Sea Drilling Project Hole 504b: mineralogy, chemistry, and evolution of seawater-basalt interactions. *Journal of Geophysical Research* **91**, 309-335.
- Alt J.C. (1995). Subseafloor processes in mid-ocean ridge hydrothermal systems. *American Geophysical Union, Geophysical Monograph* **91**, 85-114.

- Berner R.A. (1980). *Early diagenesis, a theoretical approach*. Princeton University Press, Princeton, NJ.
- Berner R.A. (1981). A new geochemical classification of sedimentary environments. *Journal of Sedimentary Petrology* **51**, 359-365.
- Berner R.A. (2003). The long-term carbon cycle, fossil fuels and atmospheric composition. *Nature* **426**, 323-326.
- Boetius A., Ravensschlag K., Schubert C.J., Rickert D., Widdel F., Gieseke A., Amann R., Jørgensen B.B., Witte U. and Pfannkuche O. (2000). A marine microbial consortium apparently mediating anaerobic oxidation of methane. *Nature* **407**, 623-626.
- Boyle E., Collier R., Dengler A.T., Edmond J.M., Ng A.C. and Stallard R.F. (1974). On the chemical mass-balance in estuaries. *Geochimica et Cosmochimica Acta* **38**, 1719-1728.
- Canfield D. E. and Thamdrup (2009). Towards a consistent classification scheme for geochemical environments, or, why we wish the term 'suboxic' would go away. *Geobiology* **7**, 385-392.
- Chan L.H., Alt J.C. and Teagle D.A.H. (2002). Lithium and lithium isotope profiles through the upper oceanic crust: a study of seawater-basalt exchange at ODP Sites 504B and 896A. *Earth and Planetary Science Letters* **201**, 187-201.
- Chester R. (2003). *Marine Geochemistry*. Blackwell Publishing, Malden, MA.
- Claypool G.E. and Kvenvolden K.A. (1983). Methane and other hydrocarbon gases in marine sediment. *Annual Review of Earth and Planetary Sciences* **11**, 299-327.
- Dählmann A. and De Lange G.J. (2003). Fluid-sediment interactions at Eastern Mediterranean mud volcanoes: a stable isotope study from ODP Leg 160. *Earth and Planetary Science Letters* **212**, 377-391.
- Dimitrov L.I. (2002). Mud volcanoes - the most important pathway for degassing deeply buried sediments. *Earth Science Reviews* **59**, 49-76.
- Duce R.A., Liss P.S., Merrill J.T., Atlas E.L., Buat-Menard P., Hicks B.B., Miller J.M., Prospero J.M., Arimoto R., Church T.M., Ellis W., Galloway J.N., Hansen L., Jickells T.D., Knap A.H., Reinhardt K.H., Schneider B., Soudine A., Tokos J.J., Tsunogai S., Wollast R. and Zhou M. (1991). The atmospheric input of trace species to the world ocean. *Global Biogeochemical Cycles* **5**, 193-259.
- Edmond J.M., Measures C., McDuff R.E., Chan L.H., Collier R., Grant B., Gordon L.I. and Corliss J.B. (1979). Ridge crest hydrothermal activity and the balances of the major and minor elements in the ocean – the Galapagos data. *Earth and Planetary Science Letters* **46**, 1-18.
- Elderfield H. and Schultz A. (1996). Mid-ocean ridge hydrothermal fluxes and the chemical composition of the ocean. *Annual Review of Earth and Planetary Sciences* **24**, 191-224.
- Elderfield H., Wheat C.G., Mottl M.J., Monnin C. and Spiro B. (1999). Fluid and geochemical transport through oceanic crust: a transect across the eastern flank of the Juan de Fuca Ridge. *Earth and Planetary Science Letters* **172**, 151-165.
- Fisher A.T., Davis E.E., Hutnak M., Spiess V., Zuhlsdorff L., Cherkaoui A., Christiansen L., Edwards K., Macdonald R., Villinger H., Mottl M.J., Wheat C.G. and Becker K. (2003). Hydrothermal recharge and discharge across 50 km guided by seamounts on a young ridge flank. *Nature* **421**, 618-621.
- Froelich P.N., Klinkhammer G.P., Bender M.L., Luedtke N.A., Heath G.R., Cullen D., Dauphin P., Hammond D., Hartman B. and Maynard V. (1979). Early oxidation of organic matter in pelagic sediments of the eastern equatorial Atlantic: suboxic diagenesis. *Geochimica et Cosmochimica Acta* **43**, 1075-1090.
- Hathorne E.C. and James R.H. (2006). Temporal record of lithium in seawater: a tracer for silicate weathering? *Earth and Planetary Science Letters* **246**, 393-406.
- Hedges J.I. and Keil R.G. (1995). Sedimentary organic matter preservation: an assessment and speculative synthesis. *Marine Chemistry* **49**, 81-115.

- Herzig P.M. and Hannington M.D. (2006). Input from the deep: hot vents and cold seeps. In: *Marine Geochemistry* (eds. Schulz H.D. and Zabel M.), 457-480. Springer Verlag, Berlin.
- Hyndman R.D. and Davis E.E. (1992). A mechanism for the formation of methane hydrate and seafloor bottom-simulating reflectors by vertical fluid expulsion. *Journal of Geophysical Research* **97**, 7025-7041.
- Huh Y., Chan L.H., Zhang L. and Edmond J.M. (1998). Lithium and its isotopes in major world rivers: implications for weathering and the oceanic budget. *Geochimica et Cosmochimica Acta* **62**, 2039-2051.
- James R.H., Allen D.E. and Seyfried W.E. (2003). An experimental study of alteration of oceanic crust and terrigenous sediments at moderate temperatures (51 to 350 °C): insights as to chemical processes in near-shore ridge-flank hydrothermal systems. *Geochimica et Cosmochimica Acta* **67**, 681-691.
- Jickells T.D., An Z.S., Andersen K.K., Baker A.R., Bergametti G., Brooks N., Cao J.J., Boyd P.W., Duce R.A., Hunter K.A., Kawahata H., Kubilay N., La Roche J., Liss P.S., Mahowald N., Prospero J.M., Ridgwell A.J., Tegen I. and Torres R. (2005). Global iron connections between desert dust, ocean biogeochemistry, and climate. *Science* **308**, 67-71.
- Jørgensen B.B. (1982). Mineralization of organic matter in the sea bed - the role of sulphate reduction. *Nature* **296**, 643-645.
- Jørgensen B.B. (2006). Bacteria and marine biogeochemistry. In: *Marine Geochemistry* (eds. Schulz H.D. and Zabel M.), 169-206. Springer Verlag, Berlin.
- Judd A.G. (2003). The global importance and context of methane escape from the seabed. *Geo-Marine Letters* **23**, 147-154.
- Kastner M. and Rudnicki M.D. (2004). Ridge flank sediment-fluid interactions. In: *Hydrogeology of the oceanic lithosphere* (eds. Davis E.E. and Elderfield H.), 534-571. Cambridge University Press, Cambridge, NJ.
- Kastner M., Elderfield H. and Martin J.B. (1991). Fluids in convergent margins: what do we know about their composition, origin, role in diagenesis and importance for oceanic chemical fluxes. *Philosophical Transactions of the Royal Society of London: Physical Sciences and Engineering* **335**, 243-259.
- Kaufman Y.J., Koren I., Remer L.A., Tanre D., Ginoux P. and Fan S. (2005). Dust transport and deposition observed from the Terra-Moderate Resolution Imaging Spectroradiometer (MODIS) spacecraft over the Atlantic Ocean. *Journal of Geophysical Research* **110**, D10S12, doi:10.1029/2003JD004436.
- Kopf A.J. (2002). Significance of mud volcanism. *Reviews of Geophysics* **40**, doi:10.1029/2000RG000093.
- Lowell R.P., Rona P.A. and Von Herzen R.P. (1995). Seafloor hydrothermal systems. *Journal of Geophysical Research* **100**, 327-352.
- Martin J.M. and Meybeck M. (1979). Elemental mass-balance of material carried by major world rivers. *Marine Chemistry* **7**, 173-206.
- Martin J.M. and Whitfield M. (1983). The significance of the river input of chemical elements to the ocean. In: *Trace metals in sea water* (eds. Wong C.S., Boyle E., Bruland K.W., Burton J.D. and Goldberg E.D.), 265-296. Plenum Press, New York, NY.
- McDuff R.E. (1981). Major cation gradients in DSDP interstitial waters: the role of diffusive exchange between seawater and upper oceanic crust. *Geochimica et Cosmochimica Acta* **45**, 1705-1713.
- Measures C.I. and Vink S. (2000). On the use of dissolved aluminum in surface waters to estimate dust deposition to the ocean. *Global Biogeochemical Cycles* **14**, 317-327.
- Pedersen T.F. and Calvert S.E. (1990). Anoxia vs. productivity: what controls the formation of organic-carbon-rich sediments and sedimentary rocks? *AAPG Bulletin* **74**, 454-466.
- Rudnicki M.D., Elderfield H. and Mottl M.J. (2001). Pore fluid advection and reaction in sediments of the eastern flank, Juan de Fuca Ridge, 48 °N. *Earth and Planetary Science Letters* **187**, 173-189.
- Sheppard S.M.F. and Gilg H.A. (1996). Stable isotope geochemistry of clay minerals. *Clay Minerals* **31**, 1-24.

- Środoń J. (1999). Nature of mixed-layer clays and mechanism of their formation and alteration. *Annual Review of Earth and Planetary Sciences* **27**, 19-53.
- Stoffyn-Egli P. and Mackenzie F.T. (1984). Mass balance of dissolved lithium in the oceans. *Geochimica et Cosmochimica Acta* **48**, 859-872.
- Von Damm K.L. (1990). Seafloor hydrothermal activity: black smoker chemistry and chimneys. *Annual Review of Earth and Planetary Sciences* **18**, 173.
- Von Herzen R.P. (2004). Geothermal evidence for continuing hydrothermal circulation in older (>60 M.y.) ocean crust. In: *Hydrogeology of the oceanic lithosphere* (eds. Davis E.E. and Elderfield H.), 534-571. Cambridge University Press, Cambridge, NJ.
- Wallmann K, Drews M, Aloisi G. and Bohrmann G. (2006). Methane discharge into the Black Sea and the global ocean via fluid flow through submarine mud volcanoes. *Earth and Planetary Science Letters* **248**, 545-560.
- Wheat C.G. and Mottl M.J. (1994). Hydrothermal circulation, Juan de Fuca Ridge eastern flank: factors controlling basement water composition. *Journal of Geophysical Research* **99**, 3067-3080.
- Wheat C.G. and Mottl M.J. (2000). Composition of pore and spring waters from Baby Bare: global implications of geochemical fluxes from a ridge flank hydrothermal system. *Geochimica et Cosmochimica Acta* **64**, 629-642.
- You C.F., Chan L.H., Spivack A.J. and Gieskes J.M. (1995). Lithium, boron, and their isotopes in sediments and pore waters of Ocean Drilling Program Site 808, Nankai Trough: implications for fluid expulsion in accretionary prisms. *Geology* **23**, 37-40.
- You C.F., Castillo P.R., Gieskes J.M., Chan L.H. and Spivack A.J. (1996). Trace element behavior in hydrothermal experiments: implications for fluid processes at shallow depths in subduction zones. *Earth and Planetary Science Letters* **140**, 41-52.
- Zhang L., Chan L.H. and Gieskes J.M. (1998). Lithium isotope geochemistry of pore waters from ocean drilling program Sites 918 and 919, Irminger Basin. *Geochimica et Cosmochimica Acta* **62**, 2437-2450.

Isotopic evidence ($^{87}\text{Sr}/^{86}\text{Sr}$, $\delta^7\text{Li}$) for alteration of the oceanic crust at deep-rooted mud volcanoes in the Gulf of Cadiz, NE Atlantic Ocean

Florian Scholz^{a,*}, Christian Hensen^a, Anja Reitz^a, Rolf L. Romer^b, Volker Liebetrau^a, Anette Meixner^b, Stephan M. Weise^c and Matthias Haeckel^a

^a*Leibniz Institute of Marine Sciences, IFM-GEOMAR, Wischhofstraße 1-3, D-24148 Kiel, Germany*

^b*Deutsches GeoForschungsZentrum, GFZ, Telegrafenberg, D-14473 Potsdam, Germany*

^c*Helmholtz Centre for Environmental Research, UFZ, Theodor-Lieser-Straße 4, D-06120 Halle, Germany*

Published in 2009 in *Geochimica et Cosmochimica Acta* 73, 5444-5459

Abstract

The chemical and isotopic composition of pore fluids is presented for five deep-rooted mud volcanoes aligned on a transect across the Gulf of Cadiz continental margin at water depths between 350 m and 3860 m. Generally decreasing interstitial Li concentrations and $^{87}\text{Sr}/^{86}\text{Sr}$ ratios with increasing distance from shore are attributed to systematically changing fluid sources across the continental margin. Although highest Li concentrations at the near-shore mud volcanoes coincide with high salinities derived from dissolution of halite and late stage evaporites, clayey, terrigenous sediments are identified as the ultimate Li source to all pore fluids investigated. Light $\delta^7\text{Li}$ values, partly close to those of hydrothermal vent fluids ($\delta^7\text{Li}$: +11.9 ‰), indicate that Li has been mobilized during high-temperature fluid/sediment

* Corresponding author: Florian Scholz; e-mail address: fscholz@ifm-geomar.de.

or fluid/rock interactions in the deep subsurface. Intense leaching of terrigenous clay has led to radiogenic $^{87}\text{Sr}/^{86}\text{Sr}$ ratios (~ 0.7106) in pore fluids of the near-shore mud volcanos. In contrast, non-radiogenic $^{87}\text{Sr}/^{86}\text{Sr}$ ratios (~ 0.7075) at the distal locations are attributed to admixing of a basement-derived fluid component, carrying an isotopic signature from interaction with the basaltic crust. This inference is substantiated by temperature constraints from Li isotope equilibrium calculations suggesting exchange processes at particularly high temperatures (>200 °C) for the least radiogenic pore fluids of the most distal location.

Advective pore fluids in the off-shore reaches of the Gulf of Cadiz are influenced by successive exchange processes with both oceanic crust and terrigenous, fine-grained sediments, resulting in a chemical and isotopic signature similar to that of fluids in near-shore ridge flank hydrothermal systems. This suggests that deep-rooted mud volcanoes in the Gulf of Cadiz represent a fluid pathway intermediate between mid-ocean ridge hydrothermal vent and shallow, marginal cold seep. Due to the thicker sediment coverage and slower fluid advection rates, the overall geochemical signature is shifted towards the sediment-diagenetic signal compared to ridge flank hydrothermal environments.

II.1. Introduction

Mud volcanoes (MVs) and cold seeps are ubiquitous manifestations of sediment dewatering and degassing on continental margins (Milkov, 2000; Kopf, 2002). In most cases, the chemical and isotopic composition of the emitted fluids differs significantly from seawater. Therefore, fluid expulsion at MVs and cold seeps has been considered a potentially important recycling process in global biogeochemical cycles (e.g. Milkov et al., 2003; Aloisi et al., 2004a,b). The composition of a given pore fluid results from various diagenetic reactions occurring at any depth of the sedimentary complex beneath the MV. Such processes involve e.g. high-temperature interactions with sediments and rocks (Martin et al., 1991; Chan and Kastner, 2000), clay mineral transformation reactions (Kastner et al., 1991; Dählmann and De Lange, 2003; Saffer and Scretton, 2003; Hensen et al., 2004), the microbial or thermal mineralization of organic matter (Martin et al., 1993; Fehn et al., 2007; Tomaru et al., 2007), the admixing of evaporated seawater or the dissolution of evaporites (Charlou et al., 2003; Reitz et al., 2007) and the dissolution or precipitation of authigenic minerals such as carbonates, barite and sulfides (Luff and Wallmann, 2003; Gieskes et al., 2005; Castellini et al., 2006). Some of these processes can have opposing effects on the fluid chemistry. Thus, attempts to decipher their

respective influence can lead to ambiguous results, and the most promising approach to understand the often complex diagenetic evolution of a pore fluid is to combine complementary geochemical tracers (Martin et al., 1996; You et al., 2004; Hensen et al., 2007).

In a recent article, Hensen et al. (2007) presented geochemical evidence that fluids emanating at MVs in the Gulf of Cadiz are dominantly formed by clay mineral dehydration processes at a sediment depth of up to 5 km below seafloor. In addition, high concentrations of dissolved Li were attributed to interactions with sediments or basement rocks at temperatures beyond the range typical for clay mineral diagenetic processes (>150 °C). In consideration of apparently hydrothermal signals preserved in shallow MV fluids, the authors suggested a close coupling of high- and low-temperature processes in deep-rooted cold seep environments.

In order to further elucidate structural controls on mud volcanism and regional variability across the margin, another sampling campaign was carried out in 2006. The sampled MVs are aligned on a transect across the entire Gulf of Cadiz from E to W at water depths between 350 m and 3860 m. During this second campaign, exceptionally high Li concentrations were detected in saline fluids at Mercator MV on the Moroccan shelf. Although the admixing of brines has been identified before (Hensen et al., 2007), these findings shed new light on fluid formation processes in the Gulf of Cadiz and demand a more systematic examination of crucial elements such as Li and Sr. Consequently, the present study aims to: (i) identify the processes responsible for Li enrichments in pore fluids throughout the study area; (ii) find out if $^{87}\text{Sr}/^{86}\text{Sr}$ ratios reflect interactions with different types of basement rocks (i.e. locate the transition between oceanic and continental crust), and (iii) further constrain the fluid origin by involving Li isotope systematics. Lithium isotopes are a promising tracer in that context since they have been successfully applied to trace fluid/sediment and fluid/rock interactions at different temperatures and to characterize the diagenetic evolution of pore fluids in general (e.g. You et al., 1995; Chan and Kastner, 2000; Chan et al., 2002). Overall, the multi-elemental and multi-isotopic approach adopted in this study, reveals a systematic pattern of diagenetic processes and fluid sources across the Gulf of Cadiz continental margin.

II.2. Material and methods

II.2.1. Geological setting

The Gulf of Cadiz is located west of the strait of Gibraltar (Figure II.1) at the boundary between the African and Eurasian plates. The area has a complex geological history comprising several phases of rifting, convergence and strike-slip motion since the Triassic (Maldonado et al., 1999). At present, comparably slow plate convergence (4 mm a^{-1} ; Argus et al., 1989) is accommodated over a wide and diffuse deformation zone with maximum compressional stress in WNW-ESE direction (Sartori et al., 1994). The poorly defined transition from continental to oceanic crust (Contrucci et al., 2004; Rovere et al., 2004) is concealed beneath up to 13 km thick sedimentary deposits (Thiebot and Gutscher, 2006) whose emplacement was linked to the build-up of the Arc of Gibraltar in Mid- to Upper Miocene (Maldonado et al., 1999). The sedimentary cover consists of Mesozoic and Cenozoic limestones, marls and shales which are overlain by up to 1 km thick Plio-Quaternary

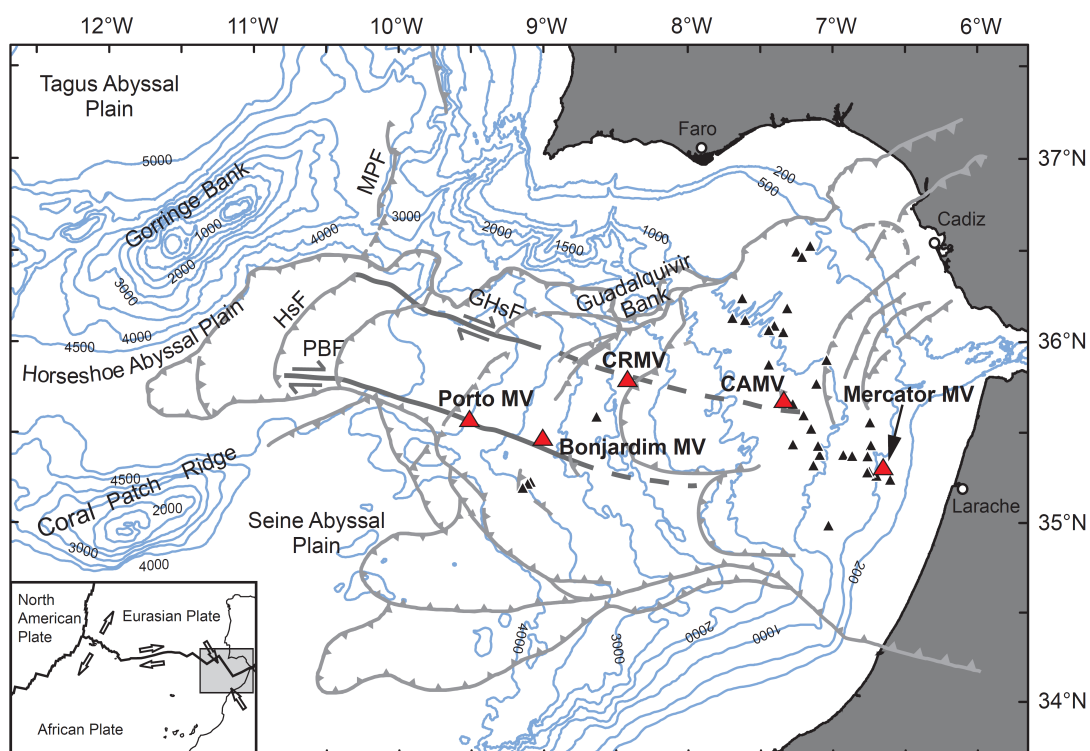


Figure II.1. Structural and bathymetrical map of the Gulf of Cadiz within the NE Atlantic Ocean. The major tectonic features (after Medialdea et al., 2004; bathymetry from Diez et al., 2005) are the Marques de Pombal (MPF) and Horseshoe (HsF) thrust faults, the Porto-Bonjardim (PBF) and Gorringe-Horseshoe (GHsF) strike-slip faults as well as the basement highs Gorringe Bank, Guadalquivir Bank and Coral Patch Ridge. The five MVs investigated within this study (Table II.1) are represented by large triangles; smaller triangles represent other MVs discovered to date.

Table II.1. Geographical position of MVs sampled in the framework of this study. The MVs are ordered from E to W according to increasing water depth.

Sampling location	Gravity core	Latitude N	Longitude W	Water depth [m]
Mercator MV	239 GC20	35°17.917'	6°38.700'	353
	263 GC28	35°17.866'	6°38.797'	351
Captain Arutyunov MV (CAMV)	174 GC9	35°39.736'	7°19.959'	1322
	205 GC13	35°39.697'	7°20.082'	1326
Carlos Ribeiro MV (CRMV)	154 GC5	35°47.257'	8°25.357'	2198
Bonjardim MV	130 GC1	35°27.817'	9°00.136'	3049
Porto MV	143 GC3	35°33.703'	9°30.439'	3860
	163 GC8	35°33.734'	9°30.438'	3861

hemipelagic sediments and locally penetrated by rising salt diapirs (Hayes et al., 1972; Medialdea et al., 2004; Pinheiro et al., 2005). These evaporites were originally deposited during the early rifting phase of the N Atlantic Ocean in Triassic to Jurassic time (Evans, 1978; Holser et al., 1983).

Mud volcanism and other phenomena related to seepage of fluids and hydrocarbon gases are widespread in the Gulf of Cadiz. The MVs are mainly located along major E-W trending strike-slip faults delineating the diffuse plate boundary or at intersections of these faults with arcuate thrusts associated with the formation of the Gibraltar Arc (Pinheiro et al., 2003; Pinheiro et al., 2005; Figure II.1). In comparison with other continental margin settings, the intensity of fluid flow has been characterized as moderate in the Gulf of Cadiz (<0.05 – 15 cm a⁻¹; Niemann et al., 2006; Hensen et al., 2007).

This study is based on samples which were obtained during the MSM1-3 cruise of *RV Maria S. Merian* in April and May 2006. The geographical positions of the sampling locations are summarized in Table II.1. The recovered sediment cores are composed of greenish to dark gray mud, mostly overlain by a thin layer of brownish hemipelagic sediments. Some of the cores contain mm- to cm-sized rock clasts, mainly composed of clayey material. Finely dispersed gas hydrates were discovered at all MVs with the exception of Mercator MV. Due to geographical and geochemical conformities the study sites will be sub-grouped in proximal MVs (Mercator MV and Captain Arutyunov MV (CAMV)) and distal MVs (Carlos Ribeiro MV (CRMV), Bonjardim MV and Porto MV) in the following sections.

II.2.2. Sediment sampling and pore water recovery

Sediment samples were obtained using a 6 m long gravity corer equipped with plastic liners. Companion multiple cores (MUCs) were taken at most of the stations in order to obtain bottom water samples and accurate pore water profiles of the sediment/water boundary. Upon recovery, the gravity cores (GCs) were sectioned into 1 m segments and then cut lengthwise into a work and an archive half. All further sample processing was carried out in a cooled laboratory close to in-situ (i.e. seafloor) temperature. Sediment samples were taken from the work half at 20 – 40 cm intervals. Multiple cores were stepwise extruded from the liner and cut into 1 – 3 cm thick discs. A sediment squeezer operated with argon gas at a pressure of 1 – 5 bar was used for pore water recovery. The extruded pore water was filtered through 0.2 μm cellulose acetate membrane filters and sub-sampled for on-board and shore-based analyses. Samples for cation analyses were acidified with HCl (30 %, suprapur) to prevent any mineral precipitation or adsorption. The archive core halves, sediment squeeze cakes and pore water samples were stored refrigerated or frozen until further processing after the cruise.

II.2.3. Chemical analyses

Pore water chlorinity and SO_4^{2-} concentrations were analyzed on-board by Ion Exchange Chromatography (761 IC-Compact, Metrohm) within few hours after sampling. The Cl concentrations of brine samples were additionally checked by titration with 0.01 N AgNO_3 (Grasshoff et al., 2002). Cation concentrations (Li^+ , Na^+ , Mg^{2+} , K^+ , Ca^{2+} and Sr^{2+}) were determined by Inductively Coupled Plasma Optical Emission Spectrometry (ICP-OES, JY 170 Ultrace, Jobin Yvon). Analytical precision based on repeated analysis of IAPSO seawater standard was found to be <1 % for Cl and SO_4^{2-} , <2 % for Na^+ , Mg^{2+} , K^+ , Ca^{2+} and Sr^{2+} and <5 % for Li^+ .

For solid phase analyses, rock clasts were collected from the archive core halves at the IFM-GEOMAR core repository. The total carbon (TC) and total organic carbon (TOC) content of freeze-dried and ground sediment samples and air-dried and ground rock clasts was determined by flash combustion in a Carlo Erba Element Analyzer (NA1500) with an analytical precision of about 1 % for replicate analyses. Carbonate carbon was driven out with HCl prior to TOC analysis and total inorganic carbon (TIC) was obtained by subtracting

TOC from TC. Further information about the above described analytical techniques is given on the IFM-GEOMAR web site.

II.2.4. Isotope analyses

Analyses of hydrogen and oxygen isotopes were carried out at UFZ using a High-Temperature Pyrolysis (HTP) system coupled with an Isotope Ratio Mass Spectrometer (IRMS, Delta S, Finnigan MAT) (Gehre and Strauch, 2003). The results are reported relative to V-SMOW with a precision (2σ) of ± 1.5 ‰ for δD and ± 0.4 ‰ for $\delta^{18}O$.

Lithium isotope analyses were carried out at GFZ by Multi Collector Inductively Coupled Plasma Mass Spectrometry (MC ICP-MS, NEPTUNE ThermoFisher Scientific) after chromatographical Li separation following a modified procedure after Tomascak et al. (1999). A detailed description of the ion chromatographic and mass spectrometric procedures is given in Wunder et al. (2006, 2007). The Li standard NIST SRM 8545 (L-SVEC) and seawater were repeatedly included in the chromatographic separation to check the accuracy of the procedure. The resulting Li isotope values are given relative to the standard NIST SRM 8545 according to $\delta^7Li = ((^7Li/^6Li)_{sample}/(^7Li/^6Li)_{standard} - 1) \times 1000$. Repeated analysis of seawater yielded a δ^7Li of $+30.8 \pm 0.2$ ‰ (2σ , $n = 9$).

For the calculation of isotope fractionation factors it is necessary to define the isotopic composition of the solid phase which has interacted with the fluids at depth. The sediment matrix is not an appropriate representation of deeply buried sediments since it is composed of both deep and shallow material (Stadnitskaia et al., 2008). As a consequence, solid phase analyses were carried out on rock clasts which, given their consolidated state, are necessarily derived from great depth. In order to separate loosely bound Li from silicate Li, 200 mg of air-dried and ground sample were treated at 80 °C with 5 ml of 4 N acetic acid (sub-boiled distilled) for 24 h. This fraction consists of exchangeable Li from the interlayer positions of clay minerals, carbonate- and other loosely bound Li. The remainder was then treated at 120 °C with 3 ml concentrated HF (sub-boiled distilled) for 48 h, evaporated and subsequently treated with 4 N HNO₃ (sub-boiled distilled) for further 24 h to dissolve precipitated fluorides. Finally, the supernatant was filtered through black ribbon cellulose filters to separate the liquid from the remaining solid phase (organic matter, heavy minerals). This step aims to extract structural Li from clay minerals. Each leaching step was followed by one washing step with bi-distilled water. The leaching and washing solutions were combined, evaporated and re-dissolved for ion exchange chromatography.

Strontium isotope ratios were determined at IFM-GEOMAR by Thermal Ionization Mass Spectrometry (TIMS, TRITON, ThermoFisher Scientific) after chemical separation via cation exchange chromatography using SrSpec resin (Eichrom). All isotope ratios were internally normalized to an $^{86}\text{Sr}/^{88}\text{Sr}$ ratio of 0.1194. Repeated analysis of the standard NIST SRM 987 during this study yielded an average value of 0.710232 ± 11 (2σ , $n = 30$). For comparison with literature values all $^{87}\text{Sr}/^{86}\text{Sr}$ were normalized to a value of 0.710248 for the NIST SRM 987.

II.3. Results

II.3.1. Pore water chemistry

Pore water depth profiles of Cl, SO_4^{2-} , Na, Mg, K, Ca, Li and Sr are shown in Figure II.2. Most of the parameters show an almost uniform downward decrease or increase from normal seawater concentration towards a near-constant value in the lower core section. The only core where the concentrations at the top are considerably below or above the normal value of seawater is 154-GC5 from CRMV (Figure II.2). Close-by retrieved MUCs do not show such cut off profiles suggesting that approximately 50 cm of surface sediment were lost during recovery of this core.

II.3.2. Isotope data

Results of the hydrogen and oxygen isotope analyses are plotted in Figure II.3 together with previously published data (Hensen et al., 2007) for CAMV, Bonjardim MV and four other MVs in the Gulf of Cadiz. The data show a pronounced negative correlation, i.e. decreasing δD and increasing $\delta^{18}\text{O}$ with increasing sediment depth.

The Li and Sr concentration and isotopic composition of pore waters are summarized in Table II.2. Similar to the concentration depth profiles for Li and Sr (Figure II.2g and h), down core isotope trends obtained for 143-GC3 and 239-GC20 show a progressive convergence from the isotope value of modern seawater towards a near-constant isotopic composition in the lower core section. Such rising deep fluids with almost uniform elemental and isotopic composition are assumed to be essentially unaltered by mixing with seawater.

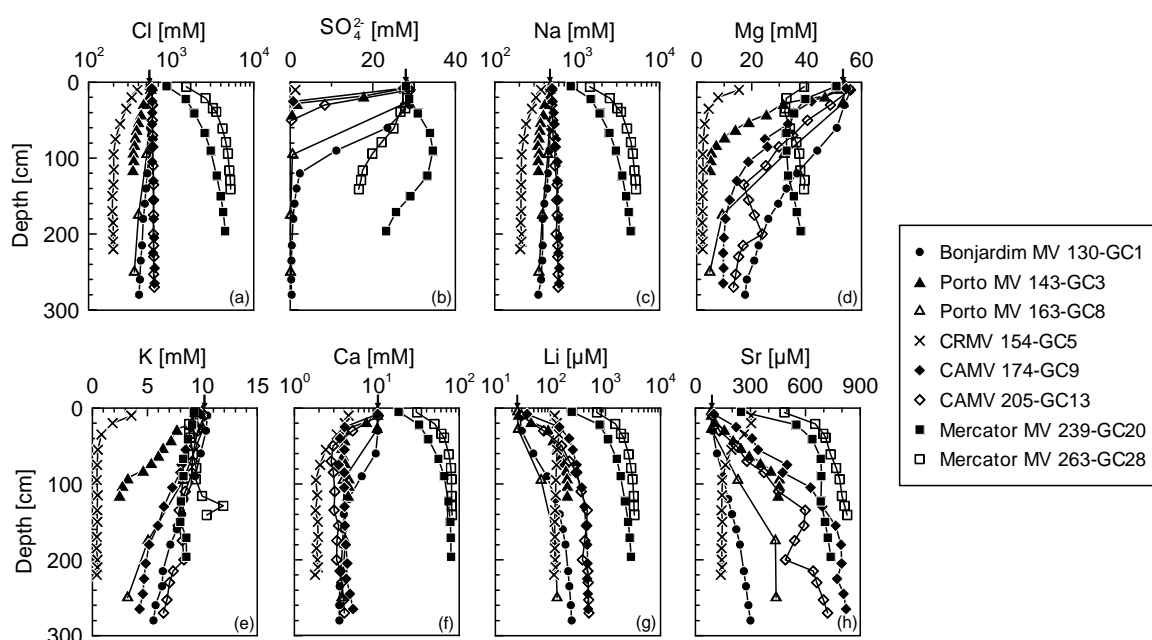


Figure II.2. Pore water profiles of (a) Cl, (b) SO_4^{2-} , (c) Na, (d) Mg, (e) K, (f) Ca, (g) Li and (h) Sr in sediment cores from all study sites. Vertical arrows (on x axis) indicate seawater values. Note logarithmic scale of x-axis in (a), (c), (f) and (g).

All investigated pore fluids show higher Li concentrations and lighter $\delta^7\text{Li}$ values than seawater (Li: 26 μM , $\delta^7\text{Li}$: +31.0 ‰; Millot et al., 2004) and local bottom water, respectively. Exceptionally high Li concentrations were encountered at CAMV and especially Mercator MV (up to 3360 μM) where Li concentrations are among the highest reported so far in similar environments (Dia et al., 1995; De Lange and Brumsack, 1998; Aloisi et al., 2004a; Hensen et al., 2007; Reitz et al., 2007). The largest offset from seawater in $\delta^7\text{Li}$ is observed in deep fluids of Mercator MV and Porto MV ($\delta^7\text{Li}$ as low as +11.9 ‰).

Pore fluids of CAMV and Mercator MV display more radiogenic $^{87}\text{Sr}/^{86}\text{Sr}$ ratios ($^{87}\text{Sr}/^{86}\text{Sr}$ up to 0.710626) than modern seawater ($^{87}\text{Sr}/^{86}\text{Sr}$: 0.70916; Banner, 2004) whereas the $^{87}\text{Sr}/^{86}\text{Sr}$ ratios of pore fluids of Bonjardim MV, CRMV and especially Porto MV ($^{87}\text{Sr}/^{86}\text{Sr}$ as low as 0.707526) lie below that of modern seawater. The single value obtained for Bonjardim MV is in excellent agreement with previously published data for this MV (Hensen et al., 2007).

The carbon and Li content and Li and Sr isotopic composition of the leached MV clasts is summarized in Table II.3. Lithium in the loosely bound fraction of rock clasts is on average lighter than Li in the silicate fraction which has a $\delta^7\text{Li}$ around 0 ‰. The $^{87}\text{Sr}/^{86}\text{Sr}$ of the silicate fraction is always more radiogenic than modern seawater.

Table II.2. Concentration and isotopic composition of Sr and Li in deep fluids. The $^{87}\text{Sr}/^{86}\text{Sr}$ ratios were normalized to a value of 0.710248 for the NIST SRM 987.

Sampling location	Gravity core	Sediment depth [cm]	Sr [μM]	$^{87}\text{Sr}/^{86}\text{Sr}$	Li [μM]	$\delta^7\text{Li}$ [‰]
Reference station		Bottom water	89.6	0.709179	24.0	+30.9
Bonjardim MV	130-GC1	160	223	0.708694	167	+19.6
		180	243		187	+19.6
Porto MV	143-GC3	18	107	0.708676	44.5	+24.2
		62	294	0.707668	160	+15.3
		92	411	0.707534	202	+12.1
		102	459	0.707536	192	+12.1
		115	451	0.707526	202	
	163-GC8	175	436	0.707569	222	
		175-r		0.707568		
CRMV	154-GC5	170	145	0.708327	121	
		200	144	0.708208	122	+19.7
		220	138	0.708208	116	+20.0
CAMV	174-GC9	155	794	0.709931	445	
		180	773	0.709921	465	
		205	808	0.709922	479	+16.3
	205-GC13	215	642	0.709896	477	
		253	699	0.709910	497	
		270	721		503	+17.2
Mercator MV	239-GC20	5	249	0.710151	244	+15.5
		90	688	0.710630	1890	+14.1
		171	723	0.710626	2770	+12.5
		196	739	0.710613	2910	+12.5
	263-GC28	116	800	0.710628	3270	+11.9
Seawater				0.709178		+30.8

Table II.3. Carbon and Li content and Li and Sr isotopic composition of rock clasts. The Li concentrations were determined by MC ICP-MS.

Sampling location	Bonjardim MV	CAMV	Mercator MV
Gravity core	130-GC1	174-GC9	239-GC20
Sediment depth [cm]	283	249	125
TIC [wt.%]	0.09	3.2	1.60
TOC [wt.%]	0.39	0.46	0.36
<i>Loosely bound fraction</i>			
Li [mg kg^{-1}]	7.8	8.8	12.7
$\delta^7\text{Li}$ [‰]	-4.9	-1.4	-8.4
<i>Silicate fraction</i>			
Li [mg kg^{-1}]	40	26.9	43.7
$\delta^7\text{Li}$ [‰]	+1.3	+0.4	-1.7
$^{87}\text{Sr}/^{86}\text{Sr}$	0.714959	0.709355	0.714173

II.4. Discussion

II.4.1. Diagenetic characterization of pore fluids

In advective systems such as cold seeps or MVs, two different types of diagenetic signals can be distinguished by examining the pore water profiles of surficial sediments. Shallow, i.e. early diagenetic processes are demonstrated by the deviation of an element or isotope profile from a simple mixing relationship between bottom water and deep fluid. By contrast, the depth integrated effect of diagenetic processes beneath the sampled sediment interval is represented by the overall difference in chemical or isotopic composition between the deep fluid and seawater (e.g. Aloisi et al., 2004a; Haese et al., 2006; Hensen et al., 2007). At most of the study sites, pore water SO_4^{2-} is completely consumed within the topmost 50 – 150 cm (Figure II.2b). Sulfate reduction coupled to decomposition of organic matter cannot explain this since the TOC content of surface sediments is generally below 0.5 wt%. Instead, shallow SO_4^{2-} depletion in surficial MV deposits in the Gulf of Cadiz is caused by sulfate reduction coupled to the anaerobic oxidation of, chiefly thermogenic, methane (AOM) and higher hydrocarbons (Niemann et al., 2006; Stadnitskaia et al., 2006; Hensen et al., 2007; Nuzzo et al., 2008). Below the AOM zone the downward mixing of bottom water due to pore water irrigation and diffusion becomes negligible (Luff and Wallmann, 2003; Hensen et al., 2007), enabling the investigation of essentially unaltered deep fluids.

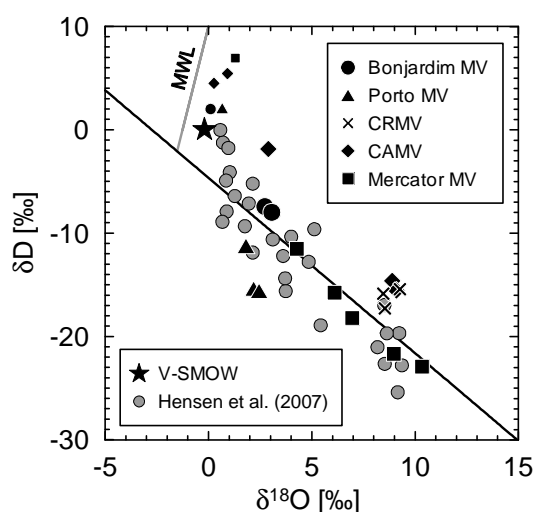


Figure II.3. Plot of δD versus $\delta^{18}\text{O}$ for bottom water samples (small symbols) and pore water samples (large symbols) from various sediment depths at all study sites. Data from Hensen et al. (2007) for CAMV, Bonjardim MV and four other Gulf of Cadiz MVs are shown for comparison. The black line represents a linear regression through all pore water data. The gray line represents the global meteoric water line (MWL) (Craig, 1961).

Deep fluids of the various sampled MVs are, on average, depleted in Cl, Na, Mg, K and Ca and enriched in Li and Sr (Figure II.2). Exceptions are CAMV and Mercator MV where salty brines enriched in e.g. Cl and Na are encountered (Figure II.2a and c). In a previous study, clay mineral transformation and dehydration processes such as the conversion of smectite to illite have been identified as a major mechanism of fluid formation within deeply buried sediments of the Gulf of Cadiz (Hensen et al., 2007). During this transformation interlayer water of smectite is released into the pore space producing an interstitial fluid with a distinct δD and $\delta^{18}O$ signature (Kastner et al., 1991; Sheppard and Gilg, 1996; Dählmann and De Lange, 2003). The hydrogen and oxygen isotope data of pore water samples from various core depths of all MVs investigated, including CAMV and Mercator MV, are in line with the typical downcore trend of decreasing δD and increasing $\delta^{18}O$ (Figure II.3). Additional evidence for clay mineral diagenesis is provided in Figure II.4 where element/Cl ratios in the lowermost sample of each core are plotted with respect to the dilution and evaporation pathway of seawater. Enrichment of Na and depletion of K with respect to diluted seawater (Figure II.4a and b) is a direct consequence of Na release and K consumption during the reaction of smectite to illite (Środoń, 1999). The major temperature field for the smectite to illite conversion ranges between ~ 60 °C and 150 °C (Środoń, 1999). Grevenmeyer et al. (2009) reported a geothermal gradient increasing seaward from 30 °C km⁻¹ to 38 °C km⁻¹ across the continental margin. It is thus inferred that fluids are formed at an approximate depth of ~ 1.5 - 5 km below seafloor.

Depletion of Mg and Ca (Figure II.4d and e) has been attributed to carbonate precipitation and/or dolomitization (Hensen et al., 2007) of Cenozoic and Mesozoic carbonates (Maldonado et al., 1999; Medialdea et al., 2004). Coinciding enrichment of Li and Sr (Figure II.2g and h; Figure II.4g-i) was interpreted as indication for long-term leaching of deeply buried sediments and crustal rocks at temperatures above 150 °C (Hensen et al., 2007). In this study, however, the highest Sr and Li concentrations were detected in pore fluids of CAMV and especially Mercator MV where the diagenetic signal of clay dehydration is overprinted by admixing of brines. Such salty solutions are known to accumulate Sr and Li depending on their respective evolution and origin (Fontes and Matray, 1993; Bottomley et al., 1999). A detailed examination of the minerals and mechanism involved in the generation of saline pore fluids at CAMV and Mercator MV is therefore an important prerequisite for the understanding of Li and Sr systematics in all pore fluids discussed here.

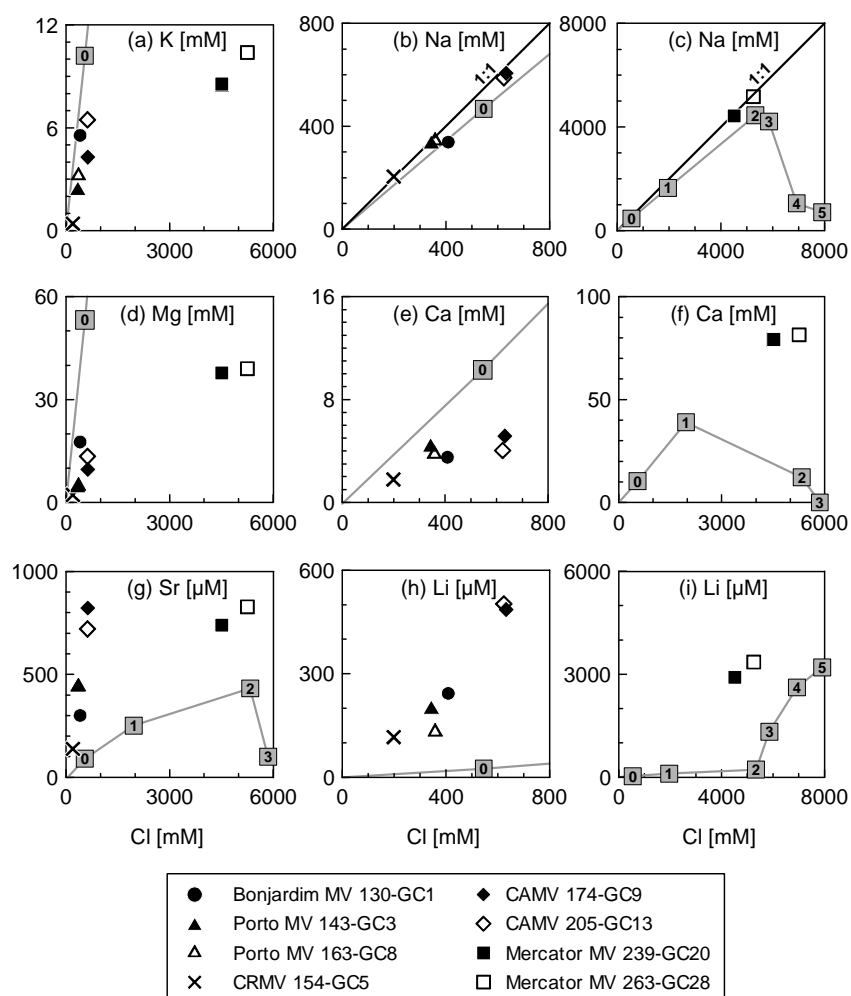


Figure II.4. Plots of (a) K, (b), (c) Na, (d) Mg, (e), (f) Ca, (g) Sr and (f), (i) Li versus Cl in deep fluids. See Figure II.2 for symbols. Gray lines and gray squares represent the dilution and evaporation pathway of seawater (0 = seawater, 1 = gypsum, 2 = halite, 3 = epsomite, 4 = sylvite, 5 = carnallite; from Fontes and Matray, 1993). Solid black lines in (b) and (c) indicate Na/Cl ratios of unity. Strongly deviating values of Mercator MV are shown in separate plots of (c) Na, (f) Ca and (i) Li versus Cl with extended scale in the right column.

II.4.2. Evolution of saline fluids at the proximal mud volcanoes

The generation of saline pore fluids in sedimentary environments is usually attributed to either admixing of evaporated and subsequently infiltrated seawater (primary brine) or to partial dissolution of interbedded evaporite minerals (secondary brine) (Hanor, 1994). Deep fluids of CAMV and Mercator MV reveal Na/Cl ratios close to unity (Figure II.4b and c) which is a clear indication for dissolution of halite (e.g. De Lange et al., 1990; Reitz et al., 2007). A mild leaching of NaCl at CAMV has previously been recognized by Hensen et al. (2007). In the case of Mercator MV, however, fluids are saturated with respect to halite (Na and Cl:

Table II.4. Excess Mg, K (relative to Bonjardim MV and CRMV) and Cl (calculated and measured) in pore fluid end members of Mercator MV. See text for further explanation.

Pore fluid end members	Excess Mg [mM]	Excess K [mM]	Excess Cl (2 x Mg + 1 x K) [mM]	Excess Cl (Cl-Na) [mM]
239-GC20 (-130-GC1)	20.2	2.99	43.3	79.1
263-GC28 (-130-GC1)	21.4	4.83	47.6	82.4
239-GC20 (-154-GC5)	35.6	8.14	79.3	79.1
263-GC28 (-154-GC5)	36.8	9.98	83.6	82.4

~5000 mM; Fontes and Matray, 1993) suggesting intense leaching of evaporites in the subsurface. During DSDP Leg 79, Holser et al. (1983) sampled a salt diapir SW of Mercator MV (Site 546) and identified halite, anhydrite and minor amounts of potash minerals (mainly carnallite) within this evaporite deposit. Dissolution of sulfate minerals at Mercator MV is indicated by Ca concentrations beyond gypsum equilibrium (Ca: ~40 mM; Fontes and Matray, 1993) in cores 239-GC20 and 263-GC28 (Figure II.2f, Figure II.4f). Most of the hereby liberated SO_4^{2-} is likely to have been lost due to sulfate reduction. Leaching of potash minerals is more difficult to detect since bulk concentrations of K and Mg are governed by different processes (see Section II.4.1). The amount of K and Mg potentially derived from such late-stage evaporite minerals may be estimated by comparison with diluted deep fluids of another MV where no interactions with evaporites take place. Accordingly, excess Mg and K in deep fluids of Mercator MV (Table II.4) have been calculated by subtracting the concentrations in deep fluids of Bonjardim MV (130-GC1) and CRMV (154-GC5) which are the most and least depleted in Mg and K (Figure II.2d and e), respectively. The Cl potentially derived from potash minerals has been estimated on two different ways: (i) based on excess K and Mg (Mg: 2 Cl, K: 1 Cl) and (ii) by subtracting the measured Cl from measured Na. An almost perfect fit between calculated and measured excess Cl (both ~80 mM) is achieved using 154-GC5 as a reference (Table II.4), or in other words, assuming that pore fluids of Mercator MV had been similarly depleted in Mg and K as fluids of CRMV prior to interaction with the evaporites. This assumption is reasonable considering that similar deviations in δD and $\delta^{18}\text{O}$ from SMOW (Figure II.3) denote comparably intense clay mineral dewatering, and thus dilution, at the two sites. The above calculations show that fluids of Mercator MV have indeed interacted with late stage evaporite minerals (e.g. sylvite, carnallite), which places the salt deposit, similar to that encountered near-by during ODP Leg 79 (Holser et al., 1983), into the potash evaporite facies.

The amount of Sr and Li derived from evaporite dissolution may be estimated by comparing the major element to Sr or Li proportion in the fluids with the average Sr and Li content in the

respective evaporite minerals. Gypsum and anhydrite minerals are often enriched in Sr (up to 5900 mg kg⁻¹ Sr; Usdowski, 1973) and Ca concentrations in fluids of Mercator MV are more than one order of magnitude higher than at the other MVs. The Sr concentrations, however, range in the same order of magnitude suggesting that Sr derived from dissolving sulfate minerals is negligible. Lithium has a preference for anions with high charge/radius ratio and thus little affinity to form Cl complexes or minerals (Olsher, 1991). As a consequence, Li behaves conservatively in the estuarine mixing zone (Stoffyn-Egli, 1982; Brunskill et al., 2003) and is not incorporated in evaporite minerals, except at extreme concentrations in the parent solution (Sonnenfeld, 1984). Theoretical Li concentrations in potash minerals at Mercator MV, calculated based on the relative proportions of excess Mg, K, Li and Cl in the lowermost samples of 239-GC20 and 263-GC28, lie in the order of 1600 mg kg⁻¹ for sylvite and 8000 mg kg⁻¹ for carnallite. These values are two to three orders of magnitude higher than average Li contents of these minerals (sylvite: 16 mg kg⁻¹, carnallite: 9 mg kg⁻¹; Sonnenfeld, 1984). Another explanation for coinciding enrichments in Li and Cl could be admixing of the primary brine from which the potash minerals had precipitated. Lithium concentrations in deep fluids of Mercator MV lie between those of evaporated seawater in the stages of sylvite (~2400 µM) and carnallite (~3100 µM) precipitation (Fontes and Matray, 1993; Figure II.4i). However, admixing of this brine would produce a Na/Cl ratio of 0.16 which is far lower than the measured ratio of 0.98. It is therefore concluded that neither the above demonstrated interactions with late stage evaporites nor admixing of the corresponding primary brine can explain the extreme Li enrichments in fluids of Mercator MV. Instead, interactions with underlying sediments or basement rocks must be responsible for variable but significant Li and Sr enrichments at all MVs investigated.

II.4.3. Strontium isotope geochemistry of pore fluids

Deep interstitial fluids acquire distinct ⁸⁷Sr/⁸⁶Sr ratios during diagenetic or hydrothermal interactions with underlying sediments or rocks. Strontium isotope ratios well above seawater in fluids of the proximal sites Mercator MV and CAMV (Table II.2, Figure II.5) indicate interactions with continental crust and terrigenous material, respectively (Elderfield and Gieskes, 1982). Large parts of the sedimentary cover in the Gulf of Cadiz consist of compacted clays and shale which have their continental origin in the Arc of Gibraltar (Maldonado et al., 1999). Furthermore, highly radiogenic ⁸⁷Sr/⁸⁶Sr ratios in rock clasts from Mercator MV and Bonjardim MV (Table II.3) confirm the terrigenous character of deeply

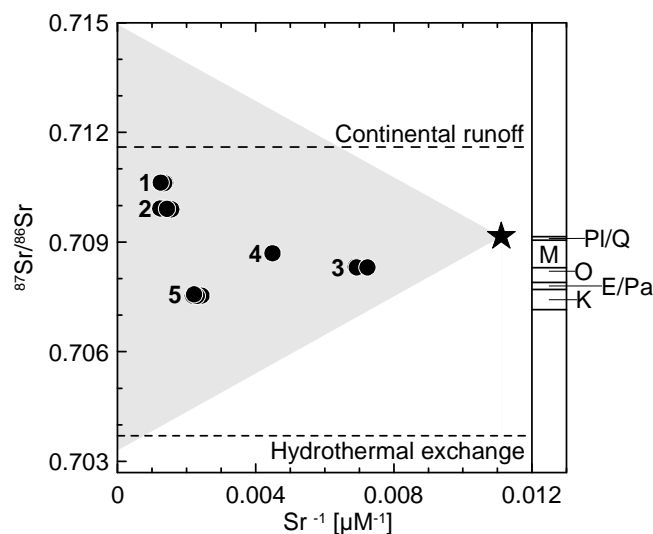


Figure II.5. Plot of $^{87}Sr/^{86}Sr$ versus Sr^{-1} for deep fluids of (1) Mercator MV, (2) CAMV, (3) CRMV, (4) Bonjardim MV and (5) Porto MV. Seawater is represented by the black star. Dashed lines indicate the average isotopic composition of major Sr inputs to the ocean (i.e. continental runoff and hydrothermal exchange; after Palmer and Edmond, 1989; Banner, 2004). The $^{87}Sr/^{86}Sr$ evolution of the ocean from Cretaceous to present is indicated by the vertical bar on the right side (Burke et al., 1982; McArthur and Howarth, 2004). The corners of the shaded triangle represent assumed Sr sources to the investigated fluids, i.e. seawater as well as interaction with terrigenous sediments (upper left corner, represented by the isotopic composition of the most radiogenic clast, Table II.3) and oceanic crust (lower left corner).

buried sediments and rocks in large parts of the study area. The radiogenic Sr has likely been mobilized, upon burial and at increasing temperatures, during clay mineral alteration processes and other fluid/sediment and fluid/rock interactions (e.g. Chaudhuri and Clauer, 1993; Ohnuki et al., 1994).

Pore fluids of the distal sites Bonjardim MV, CRMV and Porto MV display $^{87}Sr/^{86}Sr$ ratios below that of modern seawater (Table II.2, Figure II.5); although these MVs are also underlain by terrigenous sediments (Maldonado et al., 1999) (Table II.3) and even though fluids carry a strong signature from clay mineral diagenesis as is indicated by pore water freshening, K depletion and characteristic deviations in δD and $\delta^{18}O$ from SMOW (Figure II.2a and e, Figure II.3, Figure II.4a). Thus, admixing of non-radiogenic Sr from an additional source must have led to lower $^{87}Sr/^{86}Sr$ ratios at these sites. In general, pore water $^{87}Sr/^{86}Sr$ ratios below that of modern seawater may be generated through diagenetic re-crystallization of carbonates or by alteration of mafic material such as volcanogenic sediments or oceanic crust (Elderfield and Gieskes, 1982). Interactions with volcanic matter can be excluded since no widespread occurrence of such material has been reported in the Gulf of Cadiz. In the case of carbonate re-crystallization the interstitial $^{87}Sr/^{86}Sr$ ratios would be close to contemporaneous

seawater. Comparison with the Phanerozoic seawater evolution curve (stratigraphic bar in Figure II.5; Burke et al., 1982; McArthur and Howarth, 2004) yields carbonate ages between upper Cretaceous and Miocene at the distal MVs. Thus, diagenetic reactions within the widespread Cenozoic and Mesozoic limestones (Maldonado et al., 1999; Medialdea et al., 2004) could explain decreasing $^{87}\text{Sr}/^{86}\text{Sr}$ ratios across the margin. However, interpreting $^{87}\text{Sr}/^{86}\text{Sr}$ ratios in terms of a pure carbonate signal is not appropriate, since admixing of radiogenic Sr from the above described interactions with terrigenous sediments must have shifted the ratios to higher values. Consequently, the pure, non-radiogenic source at the distal MVs has most likely an $^{87}\text{Sr}/^{86}\text{Sr}$ ratio below that of Cretaceous seawater or even below seawater of any point of time in the Phanerozoic.

Another process that produces non-radiogenic $^{87}\text{Sr}/^{86}\text{Sr}$ ratios in marine pore fluids is leaching of oceanic basement rocks (Palmer and Edmond, 1989). Laboratory experiments and field studies in ridge flank hydrothermal systems have shown that seawater/basalt interactions at low to moderate temperatures produce pore water isotope ratios close to those found at the distal MVs in the Gulf of Cadiz (Elderfield et al., 1999; Butterfield et al., 2001; James et al., 2003). Similarly, Sr isotope ratios intermediate between seawater and basalt in advective interstitial fluids from ODP Site 1251 on Hydrate Ridge (Leg 204) have been interpreted as a clear indication for interactions with the oceanic basement deep within the Cascadia subduction zone (Teichert et al., 2005). Specifically, these fluids represent a meaningful analog to those studied here, since they are also influenced by clay mineral dehydration processes within terrigenous sediments (Torres et al., 2004). Furthermore, fluid/basalt interactions are in line with near-complete Mg depletion at CRMV and Porto MV (Figure II.2d, Figure II.4d) (Elderfield and Schulz, 1996). The distal MVs in the Gulf of Cadiz are located on E-W trending strike-slip faults (Figure II.1) cutting deep into the underlying sedimentary complex and the basement (Maldonado et al., 2004). The upward transport of fluids, carrying a strong signal of interactions with basalt, is likely favored by concurrent strike slip motion and thrusting along these faults. Subsequent mixing with interstitial water from the overlying sediments finally yields a fluid showing both the basement and sediment-diagenetic signature.

According to the above discussion, the Sr isotope variability across the margin is best explained by three component mixing between seawater and at least two other Sr sources (see shaded triangle in Figure II.5). At the proximal MVs, fluids are primarily influenced by interactions with terrigenous sediments leading to highly radiogenic interstitial $^{87}\text{Sr}/^{86}\text{Sr}$ ratios. In contrast, $^{87}\text{Sr}/^{86}\text{Sr}$ ratios below that of modern seawater at the distal MVs most

likely result from admixing of a basement derived fluid component. Strontium from diagenetic alteration of Cenozoic and Mesozoic limestones could have further influenced the fluid composition but is unlikely to represent the pure non-radiogenic end member.

II.4.4. Lithium isotope geochemistry of pore fluids

II.4.4.1. Lithium in pore fluids: source or temperature controlled?

Considering the thick sedimentary cover overlying the basement in the Gulf of Cadiz (5 – 13 km; Thiebot and Gutscher, 2006), any interactions between deep fluids and the oceanic crust likely occur at temperatures beyond the range typical for diagenetic processes (i.e. >150 °C). Hensen et al. (2007) interpreted strong Li enrichments in MV fluids in the Gulf of Cadiz as an indication for hydrothermal exchange processes at the sediment/basement interface. A more comprehensive understanding of Li enrichments in deep interstitial fluids and possible implications for their origin may be obtained by applying the temperature-sensitive Li isotope system. Low-temperature alteration of sediments or rocks is accompanied by Li uptake from ambient pore waters. As the light isotope is preferentially incorporated in secondary minerals, fluids become increasingly heavy during this process. By contrast, during exchange reactions at high temperatures Li is leached from the solid phase,

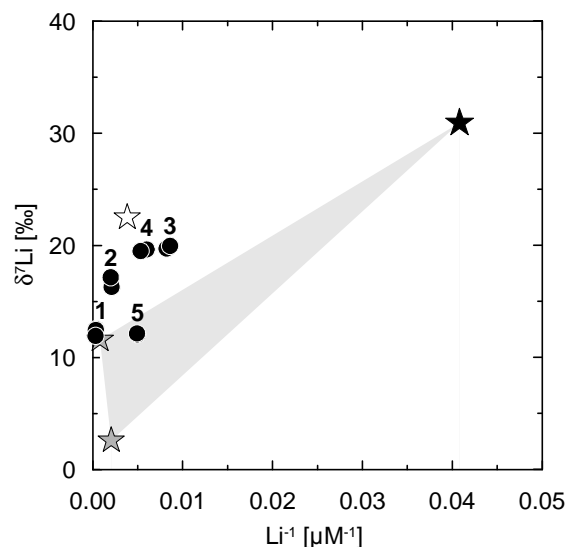


Figure II.6. Plot of $\delta^7\text{Li}$ versus Li^{-1} for deep fluids of (1) Mercator MV, (2) CAMV, (3) CRMV, (4) Bonjardim MV and (5) Porto MV. The white star represents the average Li concentration and isotopic composition of deep-sourced décollement fluids in the Costa Rica subduction zone (Chan and Kastner, 2000). The shaded array represents mixing between seawater (black star) and end members for hydrothermal solutions (gray stars) (after Tomascak, 2004 and references therein).

resulting in Li enrichments and lighter isotopic compositions in the fluid (e.g. Chan et al., 1994; You et al., 1995; Chan and Kastner, 2000; Chan et al., 2002). Finally, at very high temperatures the $\delta^7\text{Li}$ of the fluid approaches the isotopic composition of the ambient solid phase (James et al., 2003). As a result, highest Li concentrations and lowest $\delta^7\text{Li}$ values have been observed in fluids of mid-ocean ridge hydrothermal vents and sediment covered hydrothermal systems (20- to 50-fold seawater concentration, $\delta^7\text{Li}$: +2.6 to +11.6 ‰; Tomascak, 2004 and references therein) where Li is intensely leached from underlying basalt and sediments (Butterfield et al., 1994; Elderfield and Schulz, 1996), respectively.

All pore fluids investigated within this study display lighter isotopic compositions than seawater (Table II.2). For comparison, deep-sourced décollement fluids in the Costa Rica subduction zone (Chan and Kastner, 2000) have a slightly heavier Li isotopic composition than MV fluids in the Gulf of Cadiz and the lowest $\delta^7\text{Li}$ values, measured in deep fluids of Mercator MV and Porto MV, plot close to or along mixing lines between seawater and hydrothermal end members (shaded array in Figure II.6). The isotopic similarity between the fluids investigated here and those from décollement zone and hydrothermal vent settings clearly indicates a high-temperature origin within the deep sub-surface. However, Li concentrations and $\delta^7\text{Li}$ values are not correlated at the various locations suggesting that they are not controlled by the same source or process. This is particularly evident when comparing fluids from Mercator MV and Porto MV showing an almost identical $\delta^7\text{Li}$ but strongly diverging Li concentrations (Table II.2, Figure II.6).

Terrigenous clay and silt are the primary Li source to sediment interstitial fluids (up to 70 mg kg⁻¹; Chan et al., 2006). Substitution of Li for Mg or Mg for Al in the structural, octahedral sites of clay minerals produces a negative layer charge which is compensated by uptake of Li into the interlayers (Huh et al., 1998; Williams and Hervig, 2005). High amounts of total leachable Li (up to 56 mg kg⁻¹) in rock clasts (Table II.3) are in line with radiogenic ⁸⁷Sr/⁸⁶Sr ratios and a terrigenous provenance of deeply buried sediment beneath the MVs. Strontium isotope ratios below seawater at the distal MVs were attributed to an additional input of non-radiogenic Sr from basalt and, possibly, from Mesozoic and Cenozoic carbonates (see Section II.4.3).

Lithium concentrations in carbonates (Li: 0.5 – 2.6 mg kg⁻¹; Delaney et al., 1985; Hoefs and Sywall, 1997; Huh et al., 1998) are much lower than in terrigenous sediments. Moreover, laboratory experiments conducted by James et al. (2003) showed that there is no net release of Li from basalt at temperatures between 50 °C and 250 °C. By contrast, Li was leached from

terrigenous sediments at temperatures as low as 50 °C (James et al., 2003). Consequently, irrespective if derived from carbonate diagenesis or interactions with the oceanic crust at intermediate temperatures (~150 – 250 °C), non-radiogenic $^{87}\text{Sr}/^{86}\text{Sr}$ ratios at the distal locations are accompanied by lower Li concentrations.

During high-temperature fluid/sediment interactions ^6Li is preferably retained in the re-crystallized phase. Referring to hydrothermally altered sediments, Li isotope values below 0 ‰ in the loosely bound fraction of rock clasts (Table II.3.) are therefore interpreted as the immediate result of such high-temperature alterations (Chan et al., 1994; You et al., 1995; James et al., 1999). The structural or silicate Li has an average $\delta^7\text{Li}$ of 0 ‰ (Table II.3) which is within the range typical for detrital marine sediments (-1.5 to 5 ‰; Chan et al., 2006) or shales ($\delta^7\text{Li}$: -3.2 to +3.9 ‰; Teng et al., 2004) and, furthermore, in perfect agreement with the average value for upper continental crust ($\delta^7\text{Li}$: 0.0 ± 2.0 ‰; Teng et al., 2004). Most of the Li in excess over seawater is likely derived from such fine-grained terrigenous sediments with a relatively narrow range of $\delta^7\text{Li}$ values around 0 ‰. However, $\delta^7\text{Li}$ values differ significantly from each other at the various locations (Table II.3, Figure II.6) suggesting that temperature is an additional factor influencing the final $\delta^7\text{Li}$ of the pore fluids.

II.4.4.2. Lithium isotope constraints on fluid formation temperatures

The transport of fluids and solid matter in a mud volcano is mediated through interaction of multiple processes (e.g. Kopf, 2002; Haese et al., 2006). During periods where the transport of fluids and liquefied sediments is coupled and during stagnant periods where no upward transport takes place, Li isotopes in pore water may come to equilibrium with the ambient solid phase. By contrast, during prolonged periods of fluid flow, without transport of liquefied sediments, the Li isotope geochemistry of the fluids may switch to an open system. Because of the large number of unknowns regarding the temporal and spatial variability of transport processes and mineral-water interactions, a simplified model is applied here to test the probability of certain fluid sources and ranges of reaction temperature.

Assuming that pore water Li in excess of seawater concentration is derived from interactions with sediments or rocks the total amount of Li in the pore fluids (PF) can be expressed with a mass balance equation:

$$[\text{Li}]_{PF} = f_{SW} \cdot [\text{Li}]_{SW} + f_{INT} \cdot [\text{Li}]_{INT} \quad (\text{II.1})$$

where the indices SW and INT refer to seawater and water/solid (sediment and rock) interactions, respectively. Note that $f_{SW} + f_{INT} = 1$. Lithium isotope values intermediate between seawater and the solid phase result from simultaneous release of Li from sediments or rocks and uptake into secondary minerals. Both the distribution coefficient between fluid and solid and the extent of isotope fractionation during formation of authigenic minerals are temperature dependent (Berger et al., 1988; Chan et al., 1994). Assuming that $[Li]_{INT}$ is in isotopic equilibrium with deeply buried sediments or rocks, the δ^7Li of the pore fluid is given by:

$$\delta^7 Li_{PF} = f_{SW} \cdot \delta^7 Li_{SW} + f_{INT} \cdot \delta^7 Li_{INT} \quad (II.2)$$

The Li isotopic composition of the dissolved Li derived from interaction with sediments or rocks may then be obtained by rearranging Equation II.2:

$$\delta^7 Li_{INT} = \frac{\delta^7 Li_{PF} - f_{SW} \cdot \delta^7 Li_{SW}}{f_{INT}} \quad (II.3)$$

Table II.5 shows δ^7Li_{INT} values calculated for all MVs based on average values in deep fluids and an average δ^7Li_{SW} of +31 ‰ (Millot et al., 2004). The solid phase-fluid fractionation factors (α_{SP-INT}) given in Table II.5 were calculated according to:

$$\alpha_{SP-INT} = \frac{1000 + \delta^7 Li_{SP}}{1000 + \delta^7 Li_{INT}} \quad (II.4)$$

assuming that the solid phase in equilibrium with the fluids has a δ^7Li equal to the structural Li of rock clasts and upper continental crust (i.e. δ^7Li_{SP} : 0 ‰; Teng et al., 2004), respectively. By applying the fractionation factors to the empirical relationship between Li isotope fractionation and temperature (Figure II.7a; Chan et al. 1994) it is possible to estimate temperature values for fluid/sediment or fluid/rock interaction at the various locations (Table II.5). The relationship between the isotopic composition of dissolved Li derived from interaction with sediments or rocks ($[Li]_{INT}$) and temperature is highlighted by the dashed lines in Figure II.7b. The temperatures compiled in Table II.5 are regarded as minimum estimates since continuous alteration of the Li isotope composition during upward transport of fluids cannot be excluded. For instance, admixing of pristine pore water and uptake of isotopically light Li by sediments at lower temperatures could have increased the δ^7Li of fluids (Zhang et al., 1998; James and Palmer, 2000). Another limitation is that clay-rich sediments and rocks could represent a finite reservoir for Li which becomes increasingly lighter with increasing reaction progress. In a flow through system fluids would also become

Table II.5. Calculated Li isotope fractionation factors for fluid/sediment or fluid/rock interactions at the various locations. See text for further explanation.

Sampling location	Li _{PF} [μM]	δ ⁷ Li _{PF} [‰]	f _{SW}	f _{INT}	δ ⁷ Li _{INT} ^a [‰]	α _{SP-INT} ^b	T [°C]
Mercator MV	2980	+12.3	0.01	0.99	+12.0	0.988	100
CAMV	463	+16.8	0.06	0.94	+14.9	0.985	55
CRMV	120	+19.9	0.22	0.78	+11.2	0.989	115
Bonjardim MV	177	+19.6	0.15	0.85	+14.2	0.986	64
Porto MV	199	+12.1	0.13	0.87	+7.4	0.993	208

^a Calculated assuming δ⁷Li_{SW} = 31 ‰.

^b Calculated assuming δ⁷Li_{SP} = 0 ‰.

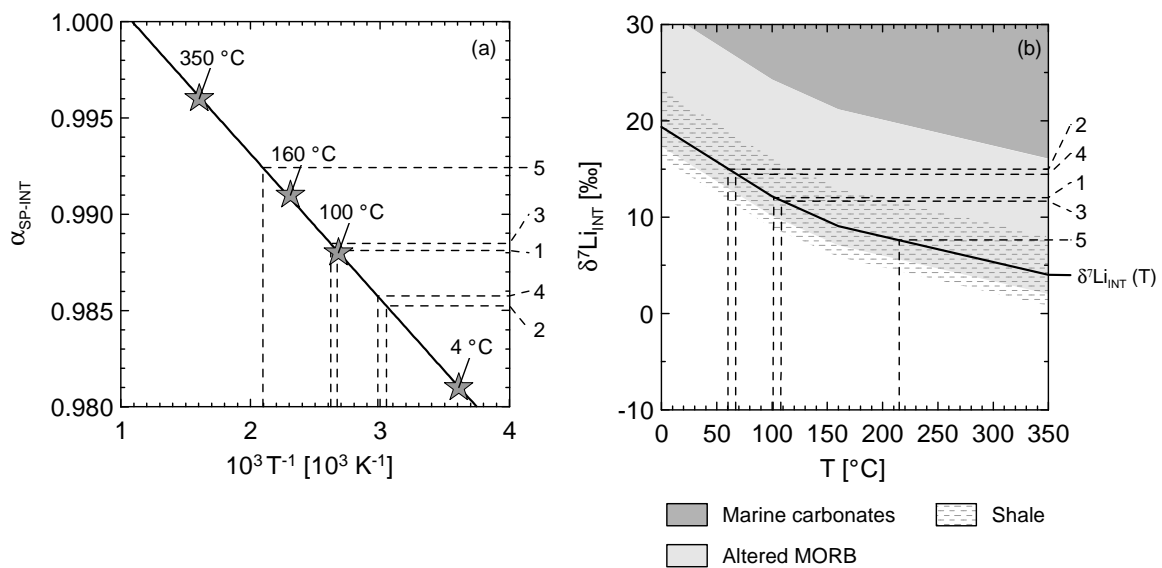


Figure II.7. (a) Empirical relationship between Li isotope fractionation factor (α) and temperature (gray stars, black regression line) (from Chan et al., 1994). (b) Plot showing the isotopic composition of dissolved Li in equilibrium with the silicate fraction of rock clasts ($\delta^7\text{Li}_{\text{SP}}$: 0 ‰) (Table II.3) as a function of temperature ($\delta^7\text{Li}_{\text{INT}}(T)$, solid line). The temperature-dependent isotopic composition of Li in equilibrium with other sediment and rock types may be obtained by shifting $\delta^7\text{Li}_{\text{INT}}(T)$ into the corresponding shaded area (calculated based on: $\delta^7\text{Li}$ of biogenic carbonates: $>+12$ ‰; altered mid-ocean ridge basalt (MORB): -2 to $+12$ ‰; shale: -3.2 to $+3.9$ ‰; from Teng et al., 2004, Tomascak, 2004). The dashed lines in both (a) and (b) depict the relationship between the calculated isotopic composition of dissolved Li derived from interactions with sediments or rocks ($\delta^7\text{Li}_{\text{INT}}$) (Table II.5) and temperature at (1) Mercator MV, (2) CAMV, (3) CRMV, (4) Bonjardim MV and (5) Porto MV.

lighter with time. In this respect, low $\delta^7\text{Li}$ values could also reflect more persistent fluid pathways or higher fluid advection rates. Nonetheless, the temperature estimates are in line with previous interpretations which are based on findings from other, independent tracers. Considering a small off-set due to secondary alteration processes, the temperatures in Table II.5 fall mostly in the range of smectite to illite conversion ($\sim 60 - 150$ °C; Środoń, 1999). Similar observations have been made by Chan and Kastner (2000) who proposed clay

mineral transformation as the major process contributing light Li to décollement fluids in the Costa Rica subduction zone (Figure II.6). Liberation of Li during the conversion of smectite to illite might be due to the strongly reduced exchange capacity (2 – 6 times lower; Appelo and Postma, 2005) of the reaction product. High temperatures corresponding to deep-reaching fluid mobilization and thus more advanced transformation of smectite to illite at CRMV is in agreement with intense pore water freshening and K depletion (Figure II.2a and e, Figure II.4a). A similar temperature calculated for Mercator MV reinforces the assumption that fluids were similarly depleted in Cl, K and Mg as those of CRMV prior to dissolution of evaporite minerals (see Section II.4.2). The lower temperatures at CAMV and Bonjardim MV correspond to the onset of smectite to illite conversion which is corroborated by less intense K depletion compared to CRMV (Figure II.2e, Figure II.4a).

Porto MV is the only site where the calculated temperature is clearly beyond the range typical for diagenetic processes (Table II.5). Non-radiogenic $^{87}\text{Sr}/^{86}\text{Sr}$ ratios at the distal MVs are attributed to a fluid component derived from interaction with basalt and possibly influenced by overlying carbonates. The dashed line corresponding to the $\delta^{7}\text{Li}_{\text{INT}}$ of Porto MV in Figure II.7b does not enter the shaded area representing fluids in equilibrium with carbonates at any reasonable temperature. Moreover, pore waters corresponding to strongly re-crystallized carbonates in the E equatorial Pacific display the heaviest $\delta^{7}\text{Li}$ values ever reported for marine pore fluids ($\delta^{7}\text{Li}$ up to +55 ‰; You et al., 2003). Consequently, only interaction with basalt is compatible with both the light $\delta^{7}\text{Li}$ and non-radiogenic $^{87}\text{Sr}/^{86}\text{Sr}$ of the pore fluids. An approximate depth of fluid formation may be estimated by dividing the temperature values in Table II.5 by the local background geothermal gradient of 38 °C per km (Grevemeyer et al., 2009). The resulting depth of 5.5 km at Porto MV is close the anticipated sediment/basement interface in this area (Thiebot and Gutscher, 2006). Thus, Li isotope systematics do also reveal a deep-sourced fluid component being generated within the upper oceanic crust at a depth of several km below seafloor.

II.5. Summary and conclusions

Recently collected data for five MVs, aligned on an E-W transect across the Gulf of Cadiz continental margin, reveal generally decreasing $^{87}\text{Sr}/^{86}\text{Sr}$ ratios and Li concentrations with increasing distance from shore. Exceptionally high Li concentrations are observed in saline pore fluids of the proximal MVs which have been formed through interactions with an

evaporite deposit composed of halite, gypsum and potash minerals. Mass balance calculations reveal that extreme Li concentrations cannot be ascribed to evaporite dissolution. Instead, fine-grained, terrigenous sediments are identified as the ultimate Li source to pore fluids throughout the study area. Hence, frequently reported correlations between Li and Cl in marine pore fluids (e.g. Bernasconi, 1999; Aloisi et al., 2004a; Reitz et al., 2008) are attributed to the common coincidence of evaporite deposits and Li-rich, terrigenous sediments in continental margin environments.

Intense diagenetic alteration of terrigenous sediments has led to highly radiogenic $^{87}\text{Sr}/^{86}\text{Sr}$ ratios in pore fluids of the proximal MVs. At the distal sites, admixing of non-radiogenic Sr from an additional source has overprinted the terrigenous isotopic signature. Lithium isotope systematics reveal that re-crystallization of carbonates cannot explain the observed Sr isotope trend. Instead, $^{87}\text{Sr}/^{86}\text{Sr}$ ratios below modern seawater at the distal sites are attributed to a basement-derived fluid component, carrying an isotopic signature from interactions with the basaltic crust. This inference is substantiated by temperature constraints from Li isotope equilibrium calculations suggesting exchange processes at temperatures above 200 °C for the least radiogenic pore fluids of the most distal site. The injection of basement fluid is likely driven by strike-slip motion and simultaneous thrusting along deep-rooted faults belonging to the African-Eurasian plate boundary. Collectively, Sr and Li isotope systematics of advective pore fluids sampled close to the sediment/water interface reveal a systematic pattern of diagenetic processes and deep fluid sources across the Gulf of Cadiz continental margin. The spatial relationship of tectonics, crustal transition, sediment input and fluid formation is highlighted in a conceptual box model in Figure II.8.

With respect to their chemical and isotopic composition, advective interstitial fluids at Gulf of Cadiz MVs are remarkably similar to pore and basement fluids in near-shore ridge flank hydrothermal systems (e.g. Juan de Fuca Ridge; Elderfield et al., 1999). This analogy arises from successive exchange processes with both oceanic crust and terrigenous, fine-grained sediments (Elderfield et al., 1999; Wheat et al., 2000; James et al., 2003). James et al. (2003) suggested that the geochemical signal from reaction with sediments becomes dominant at slow upwelling rates. Following their conclusion, we suggest that deep-rooted MVs in the Gulf of Cadiz represent a fluid pathway intermediate between mid-ocean ridge hydrothermal vent and shallow, marginal cold seep. In such intermediate systems, reduced heat flow, a thicker sediment coverage and slower fluid advection rates lead to a more pronounced sediment-diagenetic signal compared to ridge flank hydrothermal environments. Although the particular geological setting of the Gulf of Cadiz complicates broad extrapolations, our

findings shed new light on the functioning of deep-rooted cold seeps and their role in global element recycling processes.

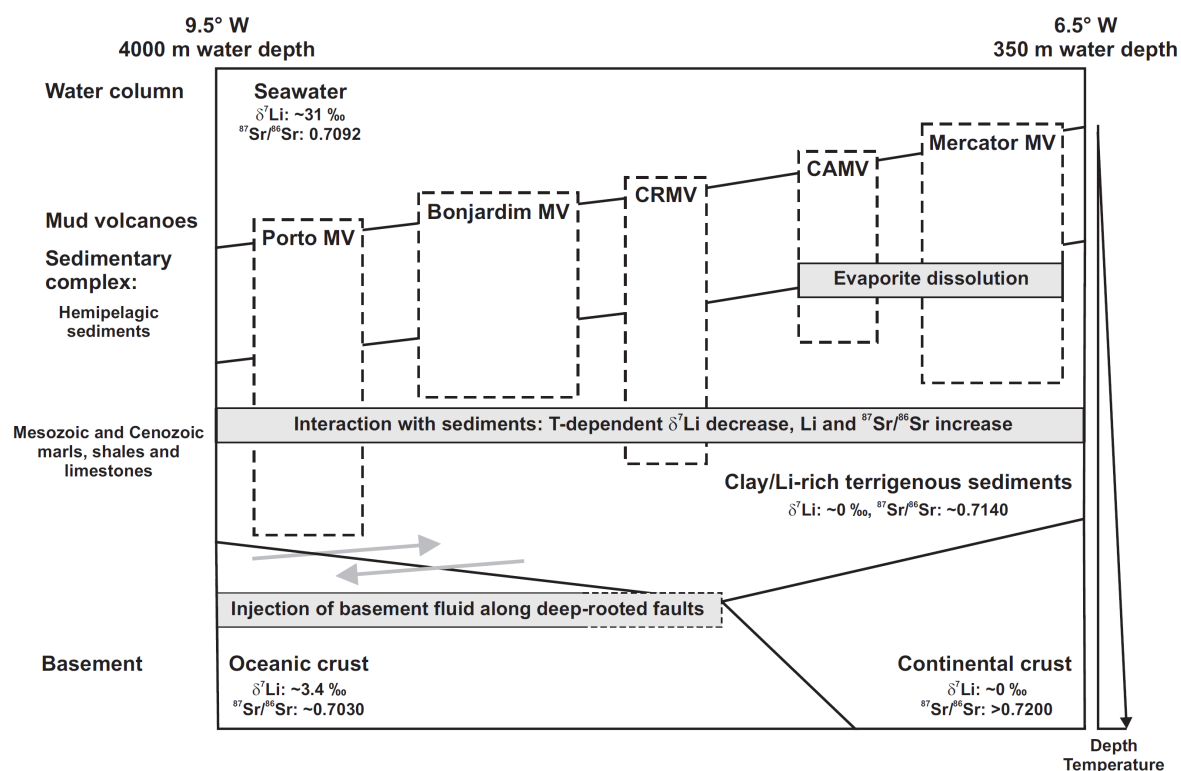


Figure II.8. Conceptual box model illustrating the systematic pattern of diagenetic processes and deep fluid sources across the Gulf of Cadiz continental margin. The variable vertical extent of the dashed boxes denotes different fluid source depths at the various locations. High Li concentrations and radiogenic $^{87}\text{Sr}/^{86}\text{Sr}$ ratios in fluids of the proximal mud volcanoes are caused by clay mineral dehydration processes and other diagenetic reactions within fine-grained terrigenous sediments. At the distal sites, this terrigenous, diagenetic signal is overprinted by admixing of a basement-derived fluid component carrying an isotopic signature from interactions with basalt. Injection of this basement fluid is favoured by thrusting and strike-slip motion along deep-rooted faults belonging to the African-Eurasian plate boundary. Geological framework after Medialdea et al. (2004) and Thiebot and Gutscher (2006). Isotope values for seawater, oceanic and continental crust are from Banner (2004), Millot et al. (2004), Teng et al. (2004) and Tomascak et al. (2008).

Acknowledgements

The authors thank the officers and crew of *RV Maria S. Merian* for their excellent support at sea. Thanks are due to our colleagues A. Bleyer, B. Domeyer, A. Kolevica, C. Schulz and R. Surberg for manifold help in shipboard and shore-based laboratories. The manuscript benefited from fruitful discussions with G. Aloisi, B. Kısakürek, M. Nuzzo and K. Wallmann. Thoughtful comments by P. B. Tomascak, two anonymous reviewers and the associate editor

J. C. Alt are gratefully acknowledged. This is publication no. 173 of the Sonderforschungsbereich 574 “Volatiles and Fluids in Subduction Zones” at Kiel University and publication no. GEOTECH-329 of the R&D program GEOTECHNOLOGIEN. Financial support was obtained by RWE-Dea through R&D project West Nile Delta (WND) and by the Federal Ministry of Education and Research (BMBF) (COMET, grant no. 03G0600D).

References

- Aloisi G., Drews M., Wallmann K. and Bohrmann G. (2004a). Fluid expulsion from the Dvurechenskii mud volcano (Black Sea) Part I. Fluid sources and relevance to Li, B, Sr, I and dissolved inorganic nitrogen cycles. *Earth and Planetary Science Letters* **225**, 347-363.
- Aloisi G., Wallmann K., Drews M. and Bohrmann G. (2004b). Evidence for the submarine weathering of silicate minerals in Black Sea sediments: possible implications for the marine Li and B cycles. *Geochemistry, Geophysics, Geosystems* **5**, Q04007. doi:10.1029/2003GC000639.
- Appelo C. A. J. and Postma D. (2005). *Geochemistry, Groundwater and Pollution*. Taylor & Francis, London.
- Argus D.F., Gordon R.G., Demets C. and Stein S. (1989). Closure of the Africa Eurasia North America Plate Motion Circuit and Tectonics of the Gloria Fault. *Journal of Geophysical Research* **94**, 5585-5602.
- Banner J.L. (2004). Radiogenic isotopes: systematics and applications to earth surface processes and chemical stratigraphy. *Earth-Science Reviews* **65**, 141-194.
- Berger G., Schott J. and Guy C. (1988). Behavior of Li, Rb and Cs during basalt glass and olivine dissolution and chlorite, smectite and zeolite precipitation from seawater: experimental investigations and modelization between 50 °C and 300 °C. *Chemical Geology* **71**, 297-312.
- Bernasconi S.M. (1999). Interstitial water chemistry in the Western Mediterranean: results from leg 161. *Proceedings of the Ocean Drilling Program Scientific Results* **161** (eds. Zahn R., Comas K.C. and Klaus A.), 423-432.
- Bottomley D.J., Katz A., Chan L.H., Starinsky A., Douglas M., Clark I.D. and Raven K.G. (1999). The origin and evolution of Canadian Shield brines: evaporation or freezing of seawater? New lithium isotope and geochemical evidence from the Slave craton. *Chemical Geology* **155**, 295-320.
- Brunskill G.J., Zagorskis I. and Pfitzner J. (2003). Geochemical mass balance for lithium, boron, and strontium in the Gulf of Papua, Papua New Guinea (project TROPICS). *Geochimica et Cosmochimica Acta* **67**, 3365-3383.
- Burke W.H., Denison R.E., Hetherington E.A., Koepnick R.B., Nelson H.F. and Otto J.B. (1982). Variation of seawater $^{87}\text{Sr}/^{86}\text{Sr}$ throughout Phanerozoic time. *Geology* **10**, 516-519.
- Butterfield D.A., McDuff R.E., Franklin J. and Wheat C.G. (1994). Geochemistry of hydrothermal vent fluids from middle valley, Juan de Fuca Ridge. *Proceedings of the Ocean Drilling Program Scientific Results* **139** (eds. Mottl M.J., Davis E.E., Fisher A.T. and Slack A.F.), 395-410.
- Butterfield D.A., Nelson B.K., Wheat C.G., Mottl M.J. and Roe K.K. (2001). Evidence for basaltic Sr in mid-ocean ridge-flank hydrothermal systems and implications for the global oceanic Sr isotope balance. *Geochimica et Cosmochimica Acta* **65**, 4141-4153.
- Castellini D.G., Dickens G.R., Snyder G.T. and Ruppel C.D. (2006). Barium cycling in shallow sediment above active mud volcanoes in the Gulf of Mexico. *Chemical Geology* **226**, 1-30.

- Chan L.H. and Kastner M. (2000). Lithium isotopic compositions of pore fluids and sediments in the Costa Rica subduction zone: implications for fluid processes and sediment contribution to the arc volcanoes. *Earth and Planetary Science Letters* **183**, 275-290.
- Chan L.H., Gieskes J.M., You C.F. and Edmond J.M. (1994). Lithium isotope geochemistry of sediments and hydrothermal fluids of the Guaymas Basin, Gulf of California. *Geochimica et Cosmochimica Acta* **58**, 4443-4454.
- Chan L.H., Starinsky A. and Katz A. (2002). The behavior of lithium and its isotopes in oilfield brines: evidence from the Heletz-Kokhav field, Israel. *Geochimica et Cosmochimica Acta* **66**, 615-623.
- Chan L.H., Leeman W.P. and Plank T. (2006). Lithium isotopic composition of marine sediments. *Geochemistry Geophysics Geosystems* **7**, Q06005. doi:10.1029/2005GC001202.
- Charlou J.L., Donval J.P., Zitter T., Roy N., Baptiste P.J., Foucher J.P. and Woodside J. (2003). Evidence of methane venting and the geochemistry of brines on mud volcanoes of the eastern Mediterranean Sea. *Deep-Sea Research* **50**, 941-958.
- Chaudhuri S. and Clauer N. (1993). Strontium isotopic compositions and potassium and rubidium contents of formation waters in sedimentary basins: clues to the origin of the solutes. *Geochimica et Cosmochimica Acta* **57**, 429-437.
- Contrucci I., Klingelhöfer F., Perrot J., Bartolome R., Gutscher M.A., Sahabi M., Malod J. and Rehault J.P. (2004). The crustal structure of the NW Moroccan continental margin from wide-angle and reflection seismic data. *Geophysical Journal International* **159**, 117-128.
- Craig H. (1961). Isotopic Variations in Meteoric Waters. *Science* **133**, 1702-1703.
- Dählmann A. and De Lange G.J. (2003). Fluid-sediment interactions at Eastern Mediterranean mud volcanoes: a stable isotope study from ODP Leg 160. *Earth and Planetary Science Letters* **212**, 377-391.
- Delaney M.L., Bé A.W.H. and Boyle E.A. (1985). Li, Sr, Mg, and Na in foraminiferal calcite shells from laboratory culture, sediment traps, and sediment cores. *Geochimica et Cosmochimica Acta* **49**, 1327-1341.
- De Lange G.J. and Brumsack H.J. (1998). Pore-water indications for the occurrence of gas hydrates in Eastern Mediterranean Mud Dome Structures. *Proceedings of the Ocean Drilling Program Scientific Results* **160** (eds. Robertson A.H.F., Emeis K.C., Richter C. and Camerlenghi A.), 569-574.
- De Lange G.J., Middelburg J.J., Van der Weijden C.H., Catalano G., Luther III G.W., Hydes D.J., Woititez J.R.W. and Klinkhammer G.P. (1990). Composition of anoxic hypersaline brines in the Tyro and Bannock Basins, eastern Mediterranean. *Marine Chemistry* **31**, 63-88.
- Dia A.N., Castrec M., Boulègue J. and Boudou J.P. (1995). Major and trace element and Sr isotope constraints on fluid circulations in the Barbados accretionary complex. Part 1: fluid origin. *Earth and Planetary Science Letters* **134**, 69-85.
- Diez S., Gràcia E., Gutscher M.A., Matias L.M., Mulder T., Terrinha P., Somoza L., Zitellini N., De Alteriis G., Henriot J.P. and Dañobeitia J.J. (2005). Bathymetric map of the Gulf of Cadiz, NE Atlantic Ocean: the SWIM multibeam compilation. *250th anniversary of the Lisbon earthquake*.
- Elderfield H. and Gieskes J.M. (1982). Sr isotopes in interstitial waters of marine sediments from Deep Sea Drilling Project cores. *Nature* **300**, 493-497.
- Elderfield H. and Schultz A. (1996). Mid-ocean ridge hydrothermal fluxes and the chemical composition of the ocean. *Annual Review of Earth and Planetary Sciences* **24**, 191-224.
- Elderfield H., Wheat C.G., Mottl M.J., Monnin C. and Spiro B. (1999). Fluid and geochemical transport through oceanic crust: a transect across the eastern flank of the Juan de Fuca Ridge. *Earth and Planetary Science Letters* **172**, 151-165.

- Evans R. (1978). Origin and significance of evaporites in basins around Atlantic margin. *The American Association of Petroleum Geologists Bulletin* **62**, 223-234.
- Fehn U., Snyder G.T. and Muramatsu Y. (2007). Iodine as a tracer of organic material: ¹²⁹I results from gas hydrate systems and fore arc fluids. *Journal of Geochemical Exploration* **95**, 66-80.
- Fontes J.C. and Matray J.M. (1993). Geochemistry and origin of formation brines from the Paris Basin, France: 1. brines associated with Triassic salts. *Chemical Geology* **109**, 149-175.
- Gehre M. and Strauch G. (2003). High-temperature elemental analysis and pyrolysis techniques for stable isotope analysis. *Rapid Communications in Mass Spectrometry* **17**, 1497-1503.
- Gieskes J., Mahn C., Day S., Martin J.B., Greinert J., Rathburn T. and McAdoo B. (2005). A study of the chemistry of pore fluids and authigenic carbonates in methane seep environments: Kodiak Trench, Hydrate Ridge, Monterey Bay, and Eel River Basin. *Chemical Geology* **220**, 329-345.
- Grasshoff K., Erhardt M. and Kremling K. (2002). *Methods of seawater analysis*. Wiley-VCH, Weinheim.
- Grevenmeyer I., Kaul N. and Kopf A.J. (2009). Heat flow anomalies in the Gulf of Cadiz and off Cape San Vicente, Portugal. *Marine and Petroleum Geology* **26**, 795-804.
- Haese R.R., Hensen C. and De Lange G.J. (2006). Pore water geochemistry of eastern Mediterranean mud volcanoes: implications for fluid transport and fluid origin. *Marine Geology* **225**, 191-208.
- Hanor J.S. (1994). Origin of saline fluids in sedimentary basins. In: *Geological Society Special Publication* **78** (ed. Parnell J.), 151-174, Geological Society, London.
- Hayes D.E., Pimm A.C., Benson W.E., Berger W.H. and Rad U.V. (1972). Site 135. *Initial Reports of the Deep Sea Drilling Program* **14**, 15-48.
- Hensen C., Wallmann K., Schmidt M., Ranero C.R. and Suess E. (2004). Fluid expulsion related to mud extrusion off Costa Rica - a window to the subducting slab. *Geology* **32**, 201-204.
- Hensen C., Nuzzo M., Hornibrook E., Pinheiro L.M., Bock B., Magalhães V.H. and Brückmann W. (2007). Sources of mud volcano fluids in the Gulf of Cadiz - indications for hydrothermal imprint. *Geochimica et Cosmochimica Acta* **71**, 1232-1248.
- Hoefs J. and Sywall M. (1997). Lithium isotope composition of quaternary and tertiary biogene carbonates and a global lithium isotope balance. *Geochimica et Cosmochimica Acta* **61**, 2679-2690.
- Holser E.S., Saltzman E.S. and Brookins D.G. (1983). Geochemistry and petrology of evaporites cored from a deep-sea diapir at Site 546 offshore Morocco. *Initial Reports of the Deep Sea Drilling Program* **79** (eds. Hinz K., Winterer E.L. and Party D.L.S.), 509-540.
- Huh Y., Chan L.H., Zhang L. and Edmond J.M. (1998). Lithium and its isotopes in major world rivers: implications for weathering and the oceanic budget. *Geochimica et Cosmochimica Acta* **62**, 2039-2051.
- James R.H. and Palmer M.R. (2000). Marine geochemical cycles of the alkali elements and boron: the role of sediments. *Geochimica et Cosmochimica Acta* **64**, 3111-3122.
- James R.H., Rudnicki M.D. and Palmer M.R. (1999). The alkali element and boron geochemistry of the Escanaba Trough sediment-hosted hydrothermal system. *Earth and Planetary Science Letters* **171**, 157-169.
- James R.H., Allen D.E. and Seyfried W.E. (2003). An experimental study of alteration of oceanic crust and terrigenous sediments at moderate temperatures (51 to 350°C): insights as to chemical processes in near-shore ridge-flank hydrothermal systems. *Geochimica et Cosmochimica Acta* **67**, 681-691.
- Kastner M., Elderfield H. and Martin J.B. (1991). Fluids in convergent margins: what do we know about their composition, origin, role in diagenesis and importance for oceanic chemical fluxes. *Philosophical Transactions of the Royal Society of London: Physical Sciences and Engineering* **335**, 243-259.
- Kopf A.J. (2002). Significance of mud volcanism. *Reviews on Geophysics* **40**, 1005, doi:10.1029/2000RG000093.

- Luff R. and Wallmann K. (2003). Fluid flow, methane fluxes, carbonate precipitation and biogeochemical turnover in gas hydrate-bearing sediments at Hydrate Ridge, Cascadia Margin: numerical modeling and mass balances. *Geochimica et Cosmochimica Acta* **67**, 3403-3421.
- Maldonado A., Somoza L. and Pallares L. (1999). The Betic orogen and the Iberian-African boundary in the Gulf of Cadiz: geological evolution (central North Atlantic). *Marine Geology* **155**, 9-43.
- Martin J.B., Kastner M. and Elderfield H. (1991). Lithium: sources in pore fluids of Peru slope sediments and implications for oceanic fluxes. *Marine Geology* **102**, 281-292.
- Martin J.B., Gieskes J.M., Torres M. and Kastner M. (1993). Bromine and iodine in Peru margin sediments and pore fluids: implications for fluid origins. *Geochimica et Cosmochimica Acta* **57**, 4377-4389.
- McArthur J.M. and Howarth R.J. (2004). Strontium isotope stratigraphy: the Phanerozoic $^{87}\text{Sr}/^{86}\text{Sr}$ -curve and explanatory notes. In: *A geological timescale* (eds. Gradstein F.M., Ogg J.G. and Smith A.G.), 96-105. Cambridge University Press, Cambridge, NJ.
- Medialdea T., Vegas R., Somoza L., Vázquez J.T., Maldonado A., Díaz-del-Río V., Maestro A., Córdoba D. and Fernández-Puga M.C. (2004). Structure and evolution of the "Olistostrome" complex of the Gibraltar Arc in the Gulf of Cadiz (eastern Central Atlantic): evidence from two long seismic cross-sections. *Marine Geology* **209**, 173-198.
- Milkov A.V. (2000). Worldwide distribution of submarine mud volcanoes and associated gas hydrates. *Marine Geology* **167**, 29-42.
- Milkov A.V., Sassen R., Apanasovich T.V. and Dadashev F.G. (2003). Global gas flux from mud volcanoes: a significant source of fossil methane in the atmosphere and the ocean. *Geophysical Research Letters* **30**, doi:10.1029/2002GL016358.
- Millot R., Guerrot C. and Vigier N. (2004). Accurate and high-precision measurement of lithium isotopes in two reference materials by MC-ICP-MS. *Geostandards and Geoanalytical Research* **28**, 153-159.
- Niemann H., Duarte J., Hensen C., Omorigie E., Magalhães V.H., Elvert M., Pinheiro L.M., Kopf A.J. and Boetius A. (2006). Microbial methane turnover at mud volcanoes of the Gulf of Cadiz. *Geochimica et Cosmochimica Acta* **70**, 5336-5355.
- Nuzzo M., Hornibrook E.R.C., Hensen C., Parkes R.J., Cragg B.A., Rinna J., Von Deimling J.S., Sommer S., Magalhães V.H., Reitz A., Brückmann W. and Pinheiro L.M. (2008). Shallow microbial recycling of deep-sourced carbon in Gulf of Cadiz mud volcanoes. *Geomicrobiology Journal* **25**, 283-295.
- Ohnuki T., Murakami T., Sato T. and Isobe H. (1994). Redistribution of strontium and cesium during alteration of smectite to illite. *Radiochimica Acta* **66/67**, 323-326.
- Olsher U., Izatt R.M., Bradshaw J.S. and Dalley N.K. (1991). Coordination chemistry of lithium ion - a crystal and molecular-structure review. *Chemical Reviews* **91**, 137-164.
- Palmer M.R. and Edmond J.M. (1989). The strontium isotope budget of the modern ocean. *Earth and Planetary Science Letters* **92**, 11-26.
- Pinheiro L.M., Ivanov M.K., Sautkin A., Akhmanov G., Magalhães V.H., Volkonskaya A., Monteiro J.H., Somoza L., Gardner J., Hamouni N. and Cunha M.R. (2003). Mud volcanism in the Gulf of Cadiz: results from the TTR-10 cruise. *Marine Geology* **195**, 131-151.
- Pinheiro L.M., Ivanov M., Kenyon N., Magalhães V., Somoza L., Gardner J., Kopf A.J., Van Rensbergen P., Monteiro J.H. and the Euromargins Team (2005). Structural control of mud volcanism and hydrocarbon-rich fluid seepage in the Gulf of Cadiz: results from TTR-15 and previous cruises. *CIESM Workshop Monographs* **29**, 53-58.
- Reitz A., Haeckel M., Wallmann K., Hensen C. and Heeschen K. (2007). Origin of salt-enriched pore fluids in the northern Gulf of Mexico. *Earth and Planetary Science Letters* **259**, 266-282.

- Rovere M., Ranero C.R., Sartori R., Torelli L. and Zitellini N. (2004). Seismic images and magnetic signature of the Late Jurassic to Early Cretaceous Africa-Eurasia plate boundary off SW Iberia. *Geophysical Journal International* **158**, 554-568.
- Saffer D.M. and Screatton E.J. (2003). Fluid flow at the toe of convergent margins: interpretation of sharp pore-water geochemical gradients. *Earth and Planetary Science Letters* **213**, 261-270.
- Sartori R., Torelli L., Zitellini N., Peis D. and Lodolo E. (1994). Eastern Segment of the Azores-Gibraltar Line (Central-Eastern Atlantic): an oceanic plate boundary with diffuse compressional deformation. *Geology* **22**, 555-558.
- Sheppard S.M.F. and Gilg H.A. (1996). Stable isotope geochemistry of clay minerals. *Clay Minerals* **31**, 1-24.
- Sonnenfeld P. (1984). *Brines and evaporites*. Academic Press, New York, NY.
- Śródoń J. (1999). Nature of mixed-layer clays and mechanisms of their formation and alteration. *Annual Review of Earth and Planetary Sciences* **27**, 19-53.
- Stadnitskaia A., Ivanov M.K., Blinova V., Kreulen R. and Van Weering T.C.E. (2006). Molecular and carbon isotopic variability of hydrocarbon gases from mud volcanoes in the Gulf of Cadiz, NE Atlantic. *Marine and Petroleum Geology* **23**, 281-296.
- Stadnitskaia A., Ivanov M.K. and Sinninghe Damsté J.S. (2008). Application of lipid biomarkers to detect sources of organic matter in mud volcano deposits and post-eruptional methanotrophic processes in the Gulf of Cadiz, NE Atlantic. *Marine Geology* **255**, 1-14.
- Stoffyn-Egli P. (1982). Conservative behaviour of dissolved lithium in estuarine waters. *Estuarine, Coastal and Shelf Science* **14**, 577-587.
- Teichert B.M.A., Torres M.E., Bohrmann G. and Eisenhauer A. (2005). Fluid sources, fluid pathways and diagenetic reactions across an accretionary prism revealed by Sr and B geochemistry. *Earth and Planetary Science Letters* **239**, 106-121.
- Teng F.Z., McDonough W.F., Rudnick R.L., Dalpe C., Tomascak P.B., Chappell B.W. and Gao S. (2004). Lithium isotopic composition and concentration of the upper continental crust. *Geochimica et Cosmochimica Acta* **68**, 4167-4178.
- Thiebot E. and Gutscher M.A. (2006). The Gibraltar Arc seismogenic zone (part 1): constraints on a shallow east dipping fault plane source for the 1755 Lisbon earthquake provided by seismic data, gravity and thermal modeling. *Tectonophysics* **426**, 135-152.
- Tomaru H., Lu Z., Snyder G.T., Fehn U., Hiruta A. and Matsumoto R. (2007). Origin and age of pore waters in an actively venting gas hydrate field near Sado Island, Japan Sea: interpretation of halogen and ¹²⁹I distributions. *Chemical Geology* **236**, 350-366.
- Tomascak P.B. (2004). Developments in the understanding and application of lithium isotopes in the earth and planetary sciences. In: *Geochemistry of non-traditional stable isotopes. Reviews in Mineralogy and Geochemistry* **55** (eds. Johnson C.M., Beard C.L. and Albarède F.) 153-195. Mineralogical Society of America, Washington D.C.
- Tomascak P.B., Carlson R.W. and Shirey S.B. (1999). Accurate and precise determination of Li isotopic compositions by multi-collector sector ICP-MS. *Chemical Geology* **158**, 145-154.
- Tomascak P.B., Langmuir C.H., Le Roux P.J. and Shirey S.B. (2008). Lithium isotopes in global mid-ocean ridge basalts. *Geochimica et Cosmochimica Acta* **72**, 1626-1637.
- Torres M.E., Teichert B.M.A., Trehu A.M., Borowski W. and Tomaru H. (2004). Relationship of pore water freshening to accretionary processes in the Cascadia margin: fluid sources and gas hydrate abundance. *Geophysical Research Letters* **31**, doi:10.1029/2004GL021219.

- Usdowski E. (1973). Geochemical properties of strontium during genesis of Ca-carbonates and Ca-sulfates (in German). *Contributions to Mineralogy and Petrology* **38**, 177-195.
- Wheat C.G., Elderfield H., Mottl M.J. and Monnin C. (2000). Chemical composition of basement fluids within an oceanic ridge flank: implications for along-strike and across-strike hydrothermal circulation. *Journal of Geophysical Research* **105**, 13437-13447.
- Williams L.B. and Hervig R.L. (2005). Lithium and boron isotopes in illite-smectite: the importance of crystal size. *Geochimica et Cosmochimica Acta* **69**, 5705-5716.
- Wunder B., Meixner A., Romer R.L. and Heinrich W. (2006). Temperature-dependent isotopic fractionation of lithium between clinopyroxene and high-pressure hydrous fluids. *Contributions to Mineralogy and Petrology* **151**, 112-120.
- Wunder B., Meixner A., Romer R.L., Feenstra A., Schettler G. and Heinrich W. (2007). Lithium isotope fractionation between Li-bearing staurolite, Li-mica and aqueous fluids: an experimental study. *Chemical Geology* **238**, 277-290.
- You C.F., Chan L.H., Spivack A.J. and Gieskes J.M. (1995). Lithium, boron, and their isotopes in sediments and pore waters of Ocean Drilling Program Site 808, Nankai Trough: implications for fluid expulsion in accretionary prisms. *Geology* **23**, 37-40.
- You C.F., Chan L.H., Gieskes J.M. and Klinkhammer G.P. (2003). Seawater intrusion through the oceanic crust and carbonate sediment in the Equatorial Pacific: lithium abundance and isotopic evidence. *Geophysical Research Letters* **30**, doi:10.1029/2003GL018412.
- You C.F., Gieskes J.M., Lee T., Yui T.F. and Chen H.W. (2004). Geochemistry of mud volcano fluids in the Taiwan accretionary prism. *Applied Geochemistry* **19**, 695-707.
- Zhang L., Chan L.H. and Gieskes J.M. (1998). Lithium isotope geochemistry of pore waters from Ocean Drilling Program Sites 918 and 919, Irminger Basin. *Geochimica et Cosmochimica Acta* **62**, 2437-2450.

Tracing organic and inorganic sources to deep-seated marine interstitial fluids: iodine and $^{129}\text{I}/\text{I}$ systematics in the Gulf of Cadiz

Florian Scholz^{a,*}, Christian Hensen^a, Zunli Lu^{b,†} and Udo Fehn^b

^a*Leibniz Institute of Marine Sciences, IFM-GEOMAR, Wischhofstraße 1-3, D-24148 Kiel, Germany*

^b*Department of Earth and Environmental Sciences, University of Rochester, Rochester, NY, USA*

Submitted to Earth and Planetary Science Letters

Abstract

Iodine and its radioisotope, ^{129}I , are powerful tracers for the age and origin of pore waters in submarine mud volcanoes and cold seeps because of their close association with organic material in deeply buried sediments. We report here iodine concentrations and $^{129}\text{I}/\text{I}$ ratios for fluids from five mud volcanoes sampled along an E-W transect through the Gulf of Cadiz. Iodine concentrations increase consistently seaward from 44 to 180 μM , accompanied by a decrease in $^{129}\text{I}/\text{I}$ ratios from 6490×10^{-15} to 660×10^{-15} . The exceptionally high $^{129}\text{I}/\text{I}$ ratios reflect the addition of fissiogenic ^{129}I , produced by spontaneous fission of ^{238}U in terrigenous sediments from the surrounding continental margins. The observed trends, together with similar changes in $^{87}\text{Sr}/^{86}\text{Sr}$ ratios, indicate a progressive seaward transition from organic-poor/continental to organic-rich/marine fluid sources. Age estimates based on $^{129}\text{I}/\text{I}$ ratios

* Corresponding author: Florian Scholz; e-mail address: fscholz@ifm-geomar.de.

† Present address: Department of Earth Science, University of Oxford, Oxford, United Kingdom.

and mass balance calculations suggest that most organic iodine in pore fluids is derived from source formations with minimum ages in the early Miocene.

Comparison of our results with literature data for varying geological settings reveals a general relationship between fissiogenic ^{129}I , radiogenic ^{87}Sr and the lithology or provenance of rocks and sediments, respectively. While iodine isotopes in oceanic settings or volcanogenic sediments reflect release from organic matter diagenesis, ^{129}I systematics in continental rock-hosted aquifers and terrigenous sedimentary systems are dominated by fissiogenic ^{129}I . The Gulf of Cadiz represents the full transition between these continental and marine $^{129}\text{I}/\text{I}$ and $^{87}\text{Sr}/^{86}\text{Sr}$ end members. This is the first systematic investigation of the controls on fissiogenic ^{129}I production in marine sedimentary environments.

III.1. Introduction

III.1.1. Scientific objective

Submarine mud volcanoes (MVs) and cold seeps represent shortcuts in geochemical cycles connecting deeply buried sediments or basement rocks with the global ocean reservoir. Numerous articles have been published about the origin and diagenetic evolution of deep-sourced interstitial waters seeping through continental margin sediments (e.g. Elderfield et al., 1990; Dia et al., 1995; Martin et al., 1996; Aloisi et al., 2004; Hensen et al., 2004). Nonetheless, the overall relationship between tectonic setting, sediment thickness, provenance and/or composition of ambient sediments or rocks and the geochemical signals in the rising fluids is still poorly constrained.

The Gulf of Cadiz is a prime location to study varying controls on fluid chemistry. Mud volcanism and other phenomena related to fluid expulsion are widespread in this area, occurring from the Iberian and Moroccan shelf to almost 4000 m water depth. In a recent study, Scholz et al. (2009) investigated the lateral variability of geochemical signals in deep-sourced MV fluids in the Gulf of Cadiz. Based on strontium and lithium isotope systematics, the authors demonstrated a systematic pattern of fluid sources and deep-seated diagenetic processes across the continental margin. At the near-shore locations fluids are primarily influenced by interactions with fine-grained, terrigenous sediments. By contrast, at the deep-sea sites this sediment-diagenetic signature is less pronounced due to admixing of a basement-derived fluid component (Scholz et al., 2009). Because of the well-defined controls

on fluid chemistry, deep-sourced pore fluids in the Gulf of Cadiz may provide insights into how other diagenetic tracers respond to lateral changes in sediment thickness, lithology and diagenetic conditions.

Iodine is commonly associated with organic matter in marine sedimentary environments. As a consequence, dissolved concentrations of iodine and its radioisotope ^{129}I are commonly applied as tracers for the origin of hydrocarbon gases and the age of organic matter in deep subsurface sediments (e.g. Fehn et al., 2000, 2003; Lu et al., 2007, 2008a,b; Tomaru et al., 2007). In the Gulf of Cadiz, however, pore fluids are additionally affected by in situ production of ^{129}I within terrigenous sediments. Common trends in ^{129}I concentrations and other geochemical tracers across the margin provide insights into the factors controlling in situ production of ^{129}I in marine sedimentary environments. Finally, the presented results and literature data are used to derive a general relationship between tectonic or geological setting and iodine isotope systematics in interstitial water.

III.1.2. Geochemistry of iodine in marine sediments

Due to its strong biophilic character, iodine is assimilated by phytoplankton in surface waters (Elderfield and Truesdale, 1980; Harvey, 1980) and reaches the sediment surface associated with sinking organic matter (Price and Calvert, 1973, 1977). A considerable amount of the delivered iodine is released into the pore water during early diagenesis and undergoes shallow recycling in the surficial sediments (Kennedy and Elderfield, 1987a,b). Another portion, however, is buried to greater depth (Martin et al., 1993), especially on continental margins where high organic matter fluxes lead to long-term storage of organic carbon and associated compounds in deeply buried sediments. In such environments, on-going microbial or thermal decomposition of organic matter produces high iodine concentrations in deep interstitial fluids, often exceeding $1000\ \mu\text{M}$ (e.g. Fehn et al., 2000, 2007; Lu et al., 2007; Gieskes and Mahn, 2007). Under the strongly reducing conditions that prevail in deeply buried sediments, iodide (hereafter referred to as I^-) is the stable species of iodine in pore water. Because of its little affinity for interactions with ambient sediments, I^- travels over large distances in overpressured sedimentary environments (Martin et al., 1993; Fehn et al., 2000; Lu et al., 2008a).

Iodine has one stable isotope, ^{127}I , and one long-lived radioisotope, ^{129}I , which decays to ^{129}Xe with a half-life of 15.7 Ma. The major, natural production mechanisms of ^{129}I are spallation of Xe isotopes in the atmosphere by cosmic rays and spontaneous fission of ^{238}U in the earth

crust. Both of these mechanisms contribute equal amounts of ^{129}I to surface reservoirs (Fabryka-Martin et al., 1985). Because of its long residence time (300 ka), the ocean is well mixed with respect to iodine and has an iodine concentration of $0.44 \mu\text{M}$ and a $^{129}\text{I}/\text{I}$ ratio of 1500×10^{-15} (Broecker and Peng, 1982; Fehn et al., 2007a). Once iodine is removed from the well-mixed surface reservoir, e.g. through sedimentation and burial of organic matter, the initial $^{129}\text{I}/\text{I}$ ratio will decrease due to continuous decay of ^{129}I . Therefore, iodine released into deep interstitial waters carries an age signal which may be deciphered by determining $^{129}\text{I}/\text{I}$ ratios by accelerator mass spectrometry (AMS) (Elmore et al., 1980). Since I^- has a similar diffusion coefficient and thus migration behavior as methane, $^{129}\text{I}/\text{I}$ ratios in rising pore waters have been used to constrain sources and age of, respectively, hydrocarbons and organic matter in subduction zones, gas hydrate fields and related settings (Fehn et al., 2000, 2003; Lu et al., 2007, 2008a, 2008b; Tomaru et al., 2007).

The iodine age signal in pore water may be altered by addition of ^{129}I from other sources than decomposition of deeply buried organic matter. Especially the $^{129}\text{I}/\text{I}$ ratio of near-surface reservoirs has been increased up to several orders of magnitude through addition of anthropogenic ^{129}I from nuclear weapon tests and reprocessing facilities (e.g. Schink et al., 1995; Wagner et al., 1996). In marine sediments, however, this anthropogenic iodine has not penetrated beyond the depth of bioturbation (Moran et al., 1998). Potentially of greater relevance for deep-seated fluids is ^{129}I produced in ambient sediments or rocks through spontaneous fission of ^{238}U . Although this fissiogenic ^{129}I has been found to be of minor importance in marine settings hitherto investigated (Fehn et al., 2000, 2003; Lu et al., 2007, 2008a,b; Tomaru et al., 2007), it may govern the $^{129}\text{I}/\text{I}$ ratio of groundwaters or crustal fluids in uranium-rich rock formations (Fabryka-Martin et al., 1989; Bottomley et al., 2002; Fehn and Snyder, 2005).

III.1.3. Geological setting

The Gulf of Cadiz is located at the eastern end of the Azores-Gibraltar transform, the transpressional plate boundary between Africa and Eurasia (inlet in Figure III.1). The area has a complex geological history comprising several phases of rifting, convergence and strike-slip motion since the Triassic (Maldonado et al., 1999). At present time, slow plate convergence (4 mm a^{-1} ; Argus et al., 1989) is accommodated over a broad and diffuse deformation zone (Zitellini et al., 2009) with maximal compressional stress in WNW-ESE direction (Sartori et al., 1994). The transition from continental to oceanic crust is concealed

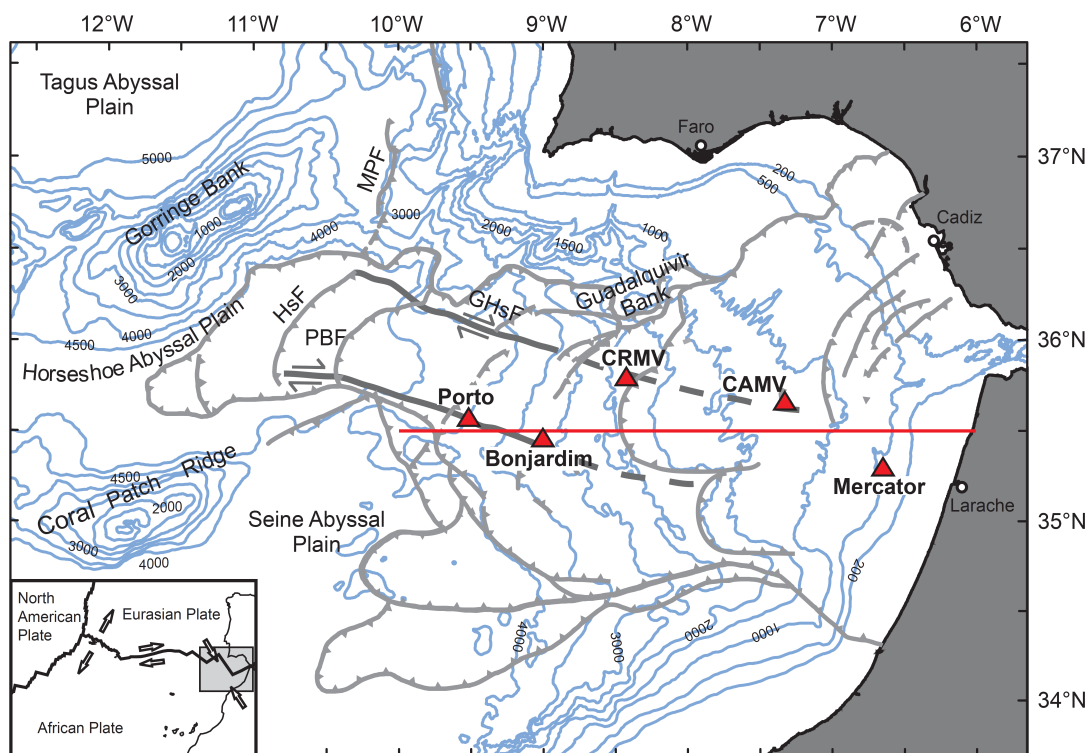


Figure III.1. Structural and bathymetrical map of the Gulf of Cadiz within the NE Atlantic Ocean (inlet at lower left side). The major tectonic features (after Medialdea et al., 2004; bathymetry from Diez et al., 2005) are the Marques de Pombal (MPF) and Horseshoe (HsF) thrust faults, the Porto-Bonjardim (PBF) and Goringe-Horseshoe (GHsF) strike-slip faults as well as the basement highs Goringe Bank, Guadalquivir Bank and Coral Patch Ridge. Large triangles represent the five MVs investigated within this study (Table III.1). The horizontal red line stretching parallel to 35.5 °N depicts the transect across the continental margin shown in Figure III.3.

beneath up to 13 km thick (Thiebot and Gutscher, 2007), mostly terrigenous sediments which have been supplied from the Iberian and N African margins (Maldonado and Nelson, 1999; Medialdea et al., 2004). Seismic cross-sections of the area show basement rocks under comparably undisturbed Mesozoic and Paleogene strata, overlain by a westward thinning wedge of intensely faulted Miocene and Plio-Quaternary sediments (Gutscher et al., 2002; Medialdea et al., 2004). Both tectonic and gravitational mechanisms have been invoked to explain the accumulation and westward emplacement of this sedimentary unit extending from the Iberian and N African margins to the Horseshoe and Seine abyssal plains (e.g. Torelli et al., 1997; Gutscher et al., 2002; Medialdea et al., 2004; Thiebot and Gutscher, 2007).

In the Gulf of Cadiz, the upward transport of fluids and solid matter follows pre-dominantly tectonic control (Medialdea et al., 2009). This is demonstrated by the observation that MVs and related fluid escape structures are mostly located on deep-seated strike-slip and thrust faults which are associated with the transpressional African-Eurasian plate boundary

(Pineiro et al., 2005; Medialdea et al., 2009). Strike-slip motion and thrusting along these faults has been proposed as the most likely mechanism by which basement fluids are injected into the sedimentary cover (Scholz et al., 2009). Transport/reaction modeling of pore water profiles has revealed moderate upwelling rates and a strong spatial and, most likely, temporal variability of fluid flow in the Gulf of Cadiz (advection rates of $<0.01 - 15 \text{ cm a}^{-1}$; Hensen et al., 2007)

The five MVs studied here are aligned on an E-W transect stretching roughly parallel to 36.5°N (Figure III.1). Geographical coordinates and water depths of the sampling locations are summarized in Table III.1. The retrieved gravity cores are composed of greenish to dark gray, fine-grained sediments, mostly overlain by a thin layer of brownish hemipelagic material. Finely dispersed gas hydrates were recovered at all sampling sites except for those at Mercator MV. Most of the cores contain mm- to cm-sized rock clasts composed of fine-grained, terrigenous material. Following a previously made classification (Scholz et al., 2009) which is based on geographical and geochemical conformities, the sampling sites will be sub-grouped in proximal (Mercator MV and Captain Arutyunov MV (CAMV)) and distal MVs (Carlos Ribeiro MV, Bonjardim MV and Porto MV) in the following sections.

III.2. Sampling and analytical methods

Sediment samples were obtained during the MSM1-3 cruise of *RV Maria S. Merian* in 2006 using a 6 m long gravity corer (GC) equipped with plastic liners. Upon recovery, GCs were sectioned into 1 m segments and then cut lengthwise into work and archive halves. Subsequent sampling was carried out in a cooled laboratory close to in situ (i.e. seafloor) temperature. Sediment subsamples were taken from the work halves at intervals of 10 - 30 cm. A sediment squeezer operated with argon gas at a pressure of 1 - 5 bar was used

Table III.1. Geographical coordinates and water depth of the sampling locations. The MVs are order from E to W according to increasing water depth.

Sampling location	Gravity core	Latitude N	Longitude W	Water depth [m]
Mercator MV	239-GC20	35°17.917'	6°38.700'	353
	263-GC28	35°17.866'	6°38.797'	351
Captain Arutyunov MV (CAMV)	174-GC9	35°39.736'	7°19.959'	1322
Carlos Ribeiro MV (CRMV)	154-GC5	35°47.257'	8°25.357'	2198
Bonjardim MV	130-GC1	35°27.817'	9°00.136'	3049
Porto MV	143-GC3	35°33.703'	9°30.439'	3860

for pore water recovery. The extruded pore water was filtered through 0.2 μm cellulose acetate membrane filters. Pore water subsamples for shore-based analyses and archive core halves were kept frozen or cooled until further processing after the cruise.

Cl and I⁻ concentrations were measured by Ion Exchange Chromatography (IC, IC-Compact, Metrohm). The chlorinity of brine samples was additionally checked by titration with 0.01 N AgNO_3 (Grasshoff et al., 2002). Analytical precision based on duplicate measurements of samples and standards was found to be <1 % for Cl and <5 % for I⁻.

About 0.5 mg of iodine is needed for measurement in the AMS. The amount of pore water obtained during the cruise was, in most cases, below the required volume of $\sim 15 - 100 \mu\text{l}$. Therefore, additional pore water was recovered from archive core halves in shore based laboratories at IFM-GEOMAR. Sediment samples were taken from the lower core end where I⁻ concentrations are highest and essentially uniform with depth. The I⁻ concentrations of the additional pore water samples were similar to those measured on the original samples from the same sediment depth. This demonstrates that cooled storage of sediment cores for about 14 months does not change the interstitial I⁻ concentrations. For the determination of $^{129}\text{I}/\text{I}$ ratios, AMS targets were prepared at the Rochester Cosmogenic Isotope Laboratory following established methods (Fehn et al., 1992). In brief, iodine was extracted into chloroform, back-extracted using sodium bi-sulfite and precipitated as AgI by addition of AgNO_3 . The AMS measurements were carried out at IsoTrace Laboratory, University of Toronto. Error ranges for individual analyses are listed in Table III.2.

In order to estimate the amount of fissiogenic ^{129}I derived from decay of ^{238}U in deeply buried sediments, three rock clasts from archive core halves were analyzed for their uranium content. The dried and ground clasts were digested with concentrated HNO_3 , HClO_4 (both sub-boiled distilled) and HF (suprapure) following a standard protocol described in Garbe-Schönberg (1993). The uranium analyses were carried out by Inductively Coupled Plasma Mass Spectrometry (ICP-MS, AGILENT 7500cs) at the ICP-MS laboratory, University of Kiel (Garbe-Schönberg, 1993). Accuracy and analytical precision, based on duplicate digestion and analysis of samples and reference standards (AGV-2, BVHO-2, SDO-1; USGS; Govindaraju, 1994), were found to be <10 % and <2 %, respectively.

Table III.2. Iodide concentrations and ¹²⁹I/I and ⁸⁷Sr/⁸⁶Sr ratios in deep fluids of MVs in the Gulf of Cadiz. See text for details on the calculation of excess ¹²⁹I.

Sampling location	Gravity core	Sediment depth [cm]	I ⁻ [μM]	¹²⁹ I/I x 10 ⁻¹⁵	¹²⁹ I x 10 ⁷ [atoms L ⁻¹]	¹²⁹ I x 10 ⁷ (18.5 Ma) [atoms L ⁻¹]	Excess ¹²⁹ I x 10 ⁷ [atoms L ⁻¹]	⁸⁷ Sr/ ⁸⁶ Sr ^a
Mercator MV	239-GC20	150-175	44.1	6490 ± 400	17.2	1.76	15.5	0.7106
		175-195	63.3	4650 ± 260	17.7	2.53	15.2	
		100-120	97.5	1290 ± 69	7.55	3.89	3.66	0.7106
CAMV	174-GC9	120-140	94.5	1600 ± 85	9.09	3.77	5.32	
		205-225	81.6	4880 ± 400	24.0	3.26	20.7	0.7099
CRMV	154-GC5	240-260	82.5	5840 ± 610	29.0	3.29	25.7	
		162-187	130	2150 ± 180	16.8	5.19	11.6	0.7083
		197-228	128	2100 ± 240	16.1	5.09	11.0	
Bonjardim MV	130-GC1	220-245	118	3370 ± 660	24.0	4.72	19.3	0.7087
		245-265	132	2710 ± 260	21.5	5.26	16.2	
Porto MV	143-GC3	80-100	182	898 ± 45	9.85	7.27	2.58	0.7075
		100-120	181	663 ± 40	7.23	7.23	0.00	
Seawater			0.44 ^b	1500 ± 150 ^c				0.7092 ^d

^a Scholz et al. (2009).^b Broecker and Peng (1982).^c Fehn et al. (2007).^d Banner (2004).

III.3. Results

Concentration-depth profiles of Cl and I⁻ for all stations are shown in Figure III.2. All pore water profiles show a progressive downward decrease or increase from normal seawater concentration (Cl: 545 mM; I⁻: 0.44 μM) towards a near-constant value in the lower core section. Following previous studies (Hensen et al., 2007; Scholz et al., 2009), pore waters from below the depth where mixing with bottom water occurs will be termed ‘deep fluid’ in the following sections.

Deep fluids of the proximal MVs are enriched in Cl with the highest concentrations measured in core 263-GC28 of Mercator MV. By contrast, deep fluids of the distal MVs are depleted in Cl with respect to seawater. The lowest Cl concentration were detected in core 154-GC5 of CRMV (as low as 199 μM). All deep fluids are enriched in I⁻ by more than two orders of magnitude over seawater with the highest concentrations measured in core 143-GC3 of Porto MV (up to 161 μM). The I⁻ concentrations in deep fluids decrease in the order Porto MV > CRMV > Bonjardim MV > CAMV > Mercator MV.

Iodine isotope ratios for deep fluids are listed in Table III.2. The only station where $^{129}\text{I}/\text{I}$ ratios are clearly below that of natural seawater (i.e. seawater free from anthropogenic ^{129}I ;

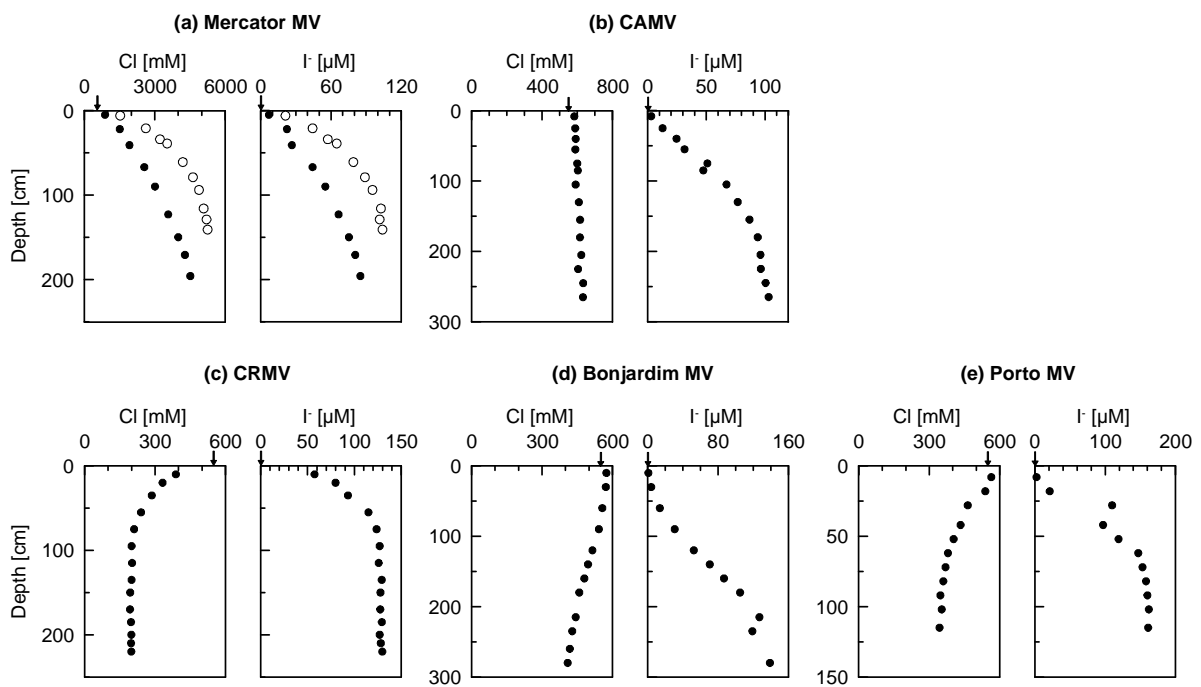


Figure III.2. Pore water profiles of Cl and I⁻ for (a) cores 239-GC20 (closed circles) and 263-GC28 (open circles) of Mercator MV, (b) 174-GC9 of CAMV, (c) 154-GC5 of CRMV, (d) 130-GC3 of Bonjardim MV and (e) 143-GC3 of Porto MV. Vertical arrows on x-axis represent normal seawater values.

$^{129}\text{I}/\text{I}$: 1500×10^{-15} ; Fehn et al., 2007a) is Porto MV where the lowest $^{129}\text{I}/\text{I}$ ratio measured is 663×10^{-15} . At the other MVs, deep fluids show $^{129}\text{I}/\text{I}$ ratios similar to (263-GC28 of Mercator MV) or considerably above that of natural seawater (up to 6490×10^{-15} in core 239-GC20 of Mercator MV). The $^{129}\text{I}/\text{I}$ ratios increase in the order Porto MV > Mercator MV (263-GC28) > CRMV > Bonjardim MV > CAMV > Mercator MV (239-GC20).

III.4. Discussion

III.4.1. Diagenetic controls on iodide in pore waters

The curved shape of the pore water profiles of Cl and I⁻ at all sampling locations (Figure III.2) indicates active upward-directed transport of fluids that are chemically distinct from seawater. Hensen et al. (2007) and Scholz et al. (2009) inferred from inversely correlated hydrogen and oxygen isotope values that the inorganic geochemistry of deep fluids in the Gulf of Cadiz is dominated by clay mineral transformation and dehydration processes (e.g. smectite to illite conversion). The resulting trend of pore water freshening (Cl profiles in Figure 2c and e) is overprinted at the proximal locations by dissolution of Triassic evaporites (mainly halite, NaCl). As a result, deep fluids at CAMV and especially Mercator MV have higher Cl concentrations than modern seawater (Cl profiles in Figure III.2a and b) and display Na/Cl ratios of unity (Scholz et al., 2009). It is common practice in studies on freshened pore fluids to compare element/Cl ratios in order to compensate for dilution effects related to clay dehydration or dissociation of gas hydrates (Gieskes and Mahn, 2007). However, given the non-conservative behavior of Cl at the near-shore locations, this is not possible in the present case. Therefore, minor uncertainties due to varying dilution at the various sites have to be taken into account in the interpretation of the I⁻ profiles. Strong I⁻ enrichments in MV fluids in the Gulf of Cadiz are consistent with other indicators for organic matter decomposition in the subsurface, such as the presence of thermogenic methane and heavier hydrocarbons (Stadnitskaia et al., 2006; Niemann et al., 2007; Nuzzo et al., 2009). The detected I⁻ concentrations are in the same order of magnitude as those observed at other deep-sourced fluid escape structures. For comparison, Lu et al. (2007) reported I⁻ concentrations between 90 and 650 μM in deep fluids of cold seeps on the Central American convergent margin. Considerably higher I⁻ concentrations, sometimes reaching values up to several mM, have been measured in pore fluids recovered by means of deep-sea drilling in subduction zones

(e.g. Peru Margin; Fehn et al., 2007b; Cascadia Margin; Lu et al., 2008a) and deep-seated gas hydrate settings (e.g. Blake Ridge; Egeberg and Dickens, 1999). The comparably low I- concentrations in the pore fluids studied here may be attributed to less intense organic matter diagenesis but also to dilution with clay-derived water and to lateral admixing of pristine pore water during upward transport (Hensen et al., 2007).

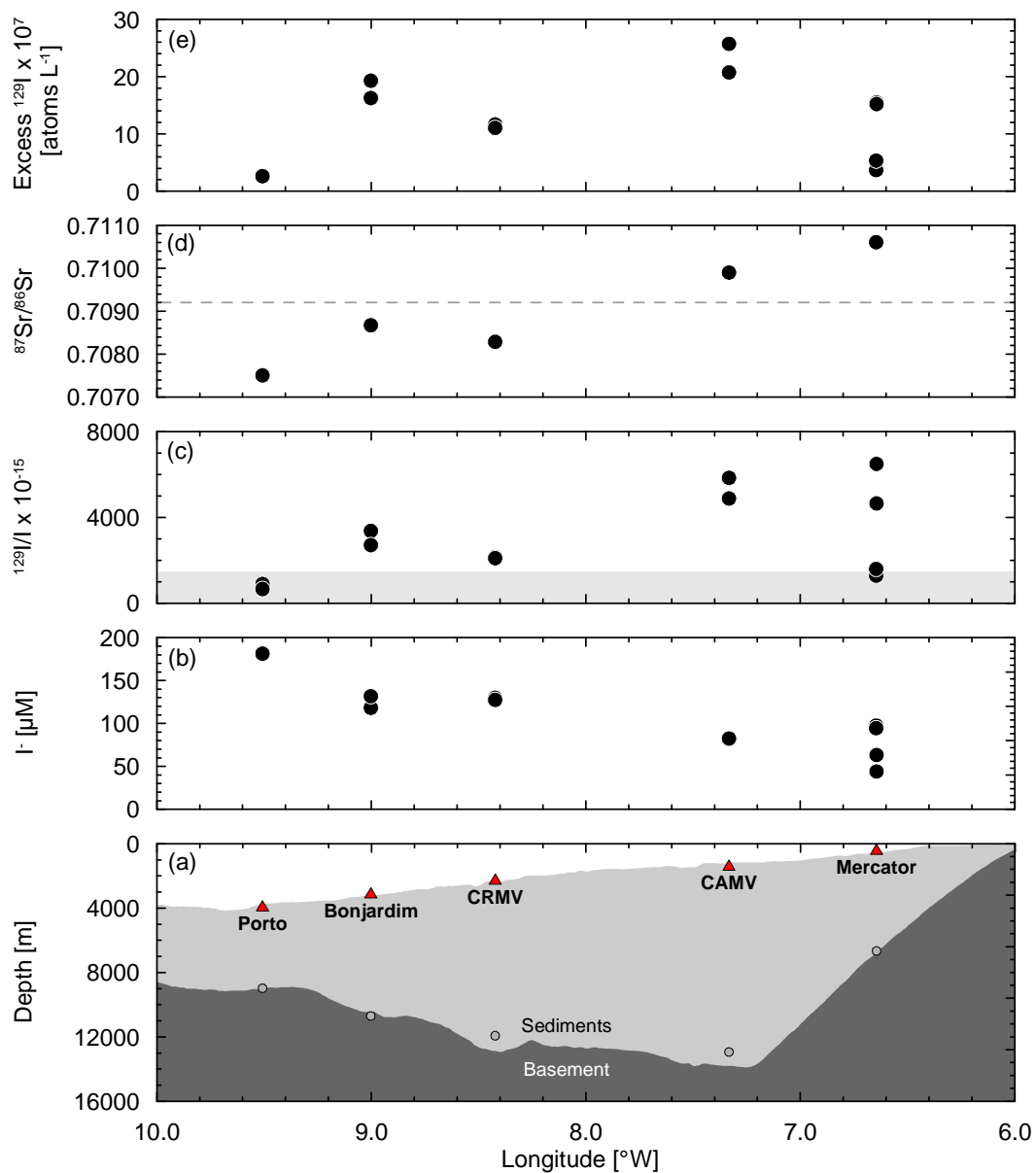


Figure III.3. Geological and geochemical cross section over the Gulf of Cadiz continental margin (see Figure III.1 for location). (a) Sampling locations (red triangles), bathymetry and depth to basement (data from GEBCO 2008 data base and Thiebot and Gutscher, 2006; gray circles depict the depth to basement at the exact location of the MVs), (b) I^- concentrations, (c) $^{129}\text{I}/\text{I}$ ratios (gray array encompasses $^{129}\text{I}/\text{I}$ ratio \leq natural seawater value), (d) $^{87}\text{Sr}/^{86}\text{Sr}$ ratios (dashed line represents $^{87}\text{Sr}/^{86}\text{Sr}$ of modern ocean) and (e) excess ^{129}I in deep fluids of the MVs.

Iodide concentrations in deep fluids increase in westward direction and with increasing water depth of the MVs (Figure III.3a and c). This might be related to a steadily increasing intensity of thermal organic matter diagenesis across the margin. However, Scholz et al. (2009) presented isotopic evidence for strongly varying formation temperatures at the various locations suggesting that reaction temperature does not control I⁻ concentrations in upwelling fluids. Alternatively, varying amounts of organic matter in the subsurface could be responsible for the I⁻ trend observed. Most of the Cenozoic sedimentary cover in the Gulf of Cadiz consists of a westward thinning wedge of terrigenous sediments (Figure III.3a) which have been supplied from the Iberian and N African margins through mass wasting and turbidity flows (Maldonado and Nelson, 1999; Medialdea et al., 2004). Considering fairly uniform fluxes of organic matter to the sediments throughout the Gulf of Cadiz and westward decreasing accumulation rates of terrigenous detrital material, the eventual organic matter content of the sediments should increase across the margin. In a similar way, dilution with terrigenous matter has been invoked to explain lower organic matter contents of modern sediments in the Chilean upwelling area with respect to those in the Peruvian upwelling area (Böning et al., 2005). The ability of such a scenario to explain seaward decreasing organic matter contents and thus iodine concentration in interstitial fluids will be further substantiated in a later section.

III.4.2. Iodine isotope systematics

III.4.2.1. Sources of old iodine

The only site where pore water samples have ¹²⁹I/I ratios below natural seawater is Porto MV (Table III.2). At all other locations, ¹²⁹I/I ratios above the natural seawater value indicate the addition of ¹²⁹I from another source than organic matter diagenesis (hereafter referred to as excess ¹²⁹I) (Table III.2). Iodine isotope ratios and I⁻ concentrations are negatively correlated in most cores. Extending the correlation trend depicted in Figure III.4a to the x-axis suggests that the pure organic I⁻ source has a ¹²⁹I/I ratio ≤ Porto MV and an I⁻ concentration of 180 - 200 μM. The corresponding iodine ages may be calculated using the standard decay equation:

$$R_{SA} = R_0 \cdot \exp(-\lambda_{129} \cdot t) \quad (III.1)$$

where R_{SA} and R_0 are the ¹²⁹I/I ratios of samples and initial seawater and λ_{129} is the decay constant of ¹²⁹I ($4.41 \times 10^{-8} \text{ a}^{-1}$). The resulting age of the lowermost sample of core 143-GC3 is 18.5 Ma or lower Miocene (Figure III.5). In general, ages obtained by this method have to be

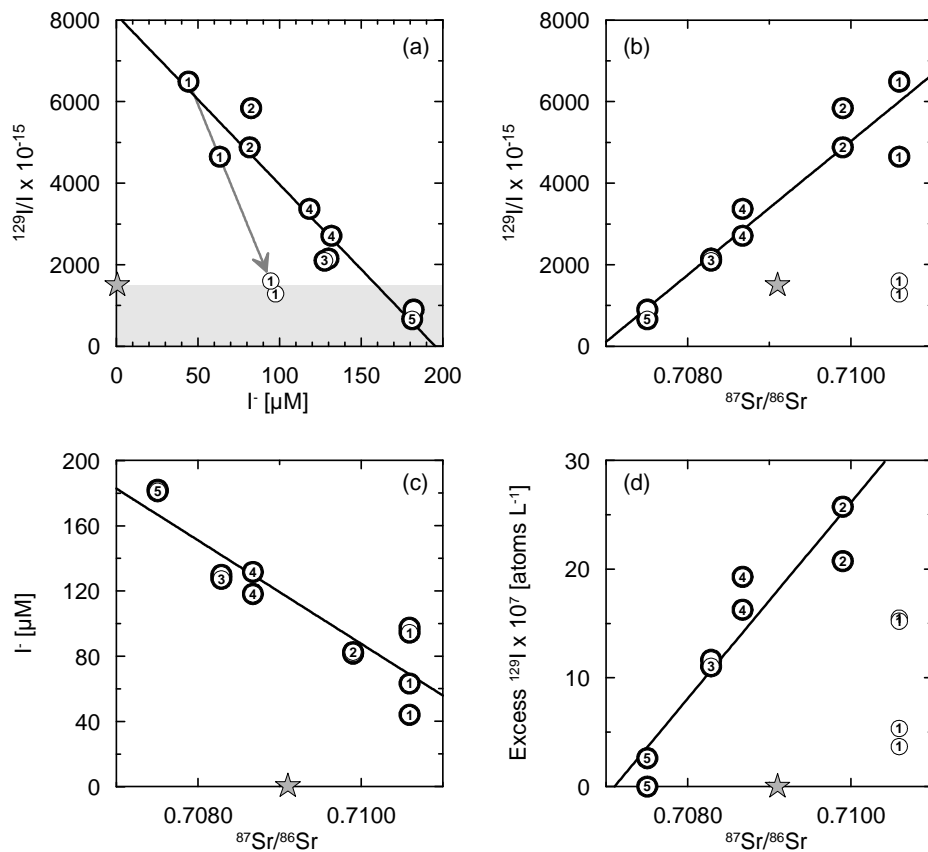


Figure III.4. Plots of (a) $^{129}\text{I}/\text{I}$ versus I^- , (b) $^{129}\text{I}/\text{I}$ versus $^{87}\text{Sr}/^{86}\text{Sr}$, (c) I^- versus $^{87}\text{Sr}/^{86}\text{Sr}$ and (d) excess ^{129}I versus $^{87}\text{Sr}/^{86}\text{Sr}$ in deep fluids of (1) Mercator MV, (2) CAMV, (3) CRMV, (4) Bonjardim MV and (5) Porto MV. Gray stars represent natural seawater values. Black lines depict the major correlation trends. Only bold circles are considered in the linear regression (deviating symbols in (a) and (b) represent core 263-GC28 of Mercator MV). The gray arrow in (a) indicates mixing with shallower pore water at Mercator MV.

interpreted as minimum ages because of the potential presence of anthropogenic or fissiogenic ^{129}I . This is of particular importance in the present case given the anomalously high $^{129}\text{I}/\text{I}$ ratios in most cores.

Most deep-seated marine settings investigated so far revealed considerably lower $^{129}\text{I}/\text{I}$ ratios than Porto MV (horizontal bars in Figure III.5). Roughly similar ages have been found for cold seep fluids from the Central American Margin (20 – 40 Ma; Lu et al., 2007). Pore waters recovered at shallow sediment depth in MVs and cold seeps may have migrated over large vertical distances. During this transport, admixing of shallower and thus younger pore water is likely to have shifted the initially low isotope ratio to higher values. This kind of mixing is particularly important in core 263-GC28 of Mercator MV which plots separately from the general trend between the highest ratios of core 239-GC20 and a $^{129}\text{I}/\text{I}$ ratio and I^- concentration intermediate between seawater and Porto MV (Figure III.5a). Admixing of an

exceptionally high portion of shallower pore water in this core is consistent with a lower thermal maturity of dissolved hydrocarbon gases with respect to 239-GC20 (Nuzzo et al., 2009). In general, mixing of shallower and deep-sourced organic components of at least lower Miocene age is in agreement with several other studies focusing on biomarkers and the isotopic composition of hydrocarbon gases (Stadnitskaia et al., 2006, 2008; Nuzzo et al., 2009). A more detailed recognition of the source strata is inhibited by the poorly defined stratigraphic framework in the area and by the presence of excess ^{129}I in most fluids.

III.4.2.2. Sources of excess ^{129}I

Input of either anthropogenic or fissiogenic ^{129}I could be the reason for anomalously high $^{129}\text{I}/\text{I}$ ratios in pore fluids of the Gulf of Cadiz. All samples which have been subjected to iodine isotope measurement are derived from below the depth of pore water irrigation and bioturbation. An in situ contamination of the pore fluids with anthropogenic ^{129}I is therefore excluded (Moran et al., 1998). Because of the low iodine concentrations in meteoric waters, contamination of samples during lab work is also unlikely. In the present case, between 25 % and 70 % of the sample volume would have to be derived from contaminated meteoric water (I^- : 8 μM ; $^{129}\text{I}/\text{I}$: 1×10^{-7} ; Fehn et al., 2007a) to produce the $^{129}\text{I}/\text{I}$ ratio and I^- concentration observed. Iodine isotope ratios show a pronounced E-W decrease across the continental margin (Figure III.3c) and are positively correlated with $^{87}\text{Sr}/^{86}\text{Sr}$ ratios (Figure III.4b). The correlation of $^{129}\text{I}/\text{I}$ with geometric properties (Figure III.3a and c) and other isotopic

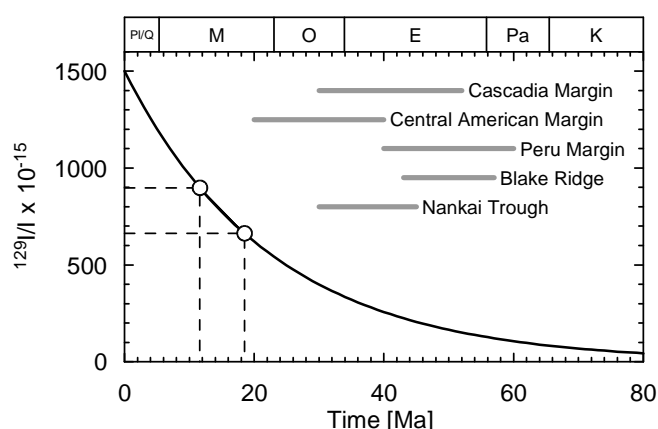


Figure III.5. Decay curve illustrating decreasing concentrations of cosmogenic ^{129}I after isolation from the active surface reservoir. Open circles and dashed lines depict the relationship between measured $^{129}\text{I}/\text{I}$ ratios and iodine ages in core 143-GC3 of Porto MV. A stratigraphic bar encompassing ages from Cretaceous to present is shown on the upper axis. The horizontal gray bars represent age ranges found for fluids in other deep-seated marine settings (data from Fehn et al., 2000, 2007; Lu et al., 2007, 2008a,b; Tomaru et al., 2007).

parameters, that are independent from anthropogenic inputs, suggest that the excess ¹²⁹I has a natural, i.e. fissiogenic origin within the underlying sediments or rocks.

Assuming that the iodine age at Porto MV applies to all sampling locations studied here, the amount of excess ¹²⁹I may be estimated by subtracting the number of ¹²⁹I atoms L⁻¹ after 18.5 Ma (at the given I⁻ concentration) from the actually measured concentration of ¹²⁹I (Table III.2). Interestingly, concentrations of both total and excess ¹²⁹I in the pore fluids (Table III.2) are in good agreement with those reported for brines in the Canadian Shield (total number of ¹²⁹I atoms L⁻¹: 3.0 – 34 x 10⁻⁷, I⁻: 140 μM) which have gained their ¹²⁹I/I signature through interaction with organic matter-rich marine sediments and basement rocks (Bottomley et al., 1999, 2002). Fabryka and Martin (1989) developed the following equation to describe the concentration of fissiogenic ¹²⁹I in crystalline rocks (N_{129} in atoms g⁻¹) as a function of time:

$$N_{129} = N_{238} \cdot \lambda_{sf} \cdot Y_{129} \cdot \left(\frac{1 - \exp(-\lambda_{129} \cdot t)}{-\lambda_{129}} \right) \quad (\text{III.2})$$

where N_{238} = ²³⁸U atoms g⁻¹ rock, λ_{sf} = spontaneous fission decay constant for ²³⁸U (8.5 x 10⁻¹⁷ a⁻¹, Decarvalho et al., 1982), Y_{129} = spontaneous fission yield of ²³⁸U at mass 129 (3 x 10⁻⁴; Sabu, 1971), λ_{129} = decay constant of ¹²⁹I (4.41 x 10⁻⁸ a⁻¹) and t = residence time of uranium in the rock. The concentration of ¹²⁹I in the ambient groundwater (C_{129} in atoms L⁻¹) was estimated by multiplying N_{129} by the ratio of rock density (ρ) and escape efficiency (ϵ , value of 1 implies total release of ¹²⁹I into the water) to effective porosity (ϕ) (Fabryka and Martin, 1989):

$$C_{129} = N_{129} \cdot \frac{\rho \cdot \epsilon}{\phi} \quad (\text{III.3})$$

In the present case, however, the production and release mechanism of fissiogenic ¹²⁹I most likely differs from that in a rock-hosted groundwater aquifer. Much of the rising pore fluids are produced through transformation of terrigenous clay minerals in deeply buried sediment and compacted shale (Hensen et al., 2007; Scholz et al., 2009). During this mineral replacement and liquefaction process, all mineral-bound ¹²⁹I is likely transferred into the pore water (i.e. $\epsilon = 1$). The final concentration of ¹²⁹I in the fluid is thus a function of the weight of the rock (ρV_R) to the volume of water (V_W) (Katz and Starinsky, 2003). Accordingly, concentrations of ¹²⁹I in deep-sourced pore waters are calculated as follows:

$$C_{129} = N_{129} \cdot \frac{\rho \cdot V_R}{V_W} \quad (\text{III.4})$$

Uranium concentrations in three shale clasts from cores 130-GC1, 174-GC9 and 239-GC20 range between 1.6 and 2.7 mg kg⁻¹ which is within the range typical for fine-grained terrigenous sediments and shale (1.5 – 8 mg kg⁻¹ U; Wedepohl, 1978). Applying a range of 1.5 – 3 mg kg⁻¹ uranium, a grain density of 2.65 g cm⁻³, a V_R/V_W ratio of 20 (corresponding to a porosity of ~5 % at a burial depth of ~5 km; Baldwin and Butler, 1985) and a residence time of 18.5 Ma (iodine age at Porto MV) yields concentrations of excess ^{129}I of 7×10^7 – 13×10^7 atoms L⁻¹. This range covers most of the excess ^{129}I concentrations listed in Table III.4. Moreover, it has to be considered that the adopted residence time is a minimum estimate. A slightly modified combination of input values, e.g. a higher residence time and/or uranium concentration, would yield excess ^{129}I concentrations fitting the whole range of data observed. It is therefore concluded that release of fissiogenic ^{129}I during clay mineral

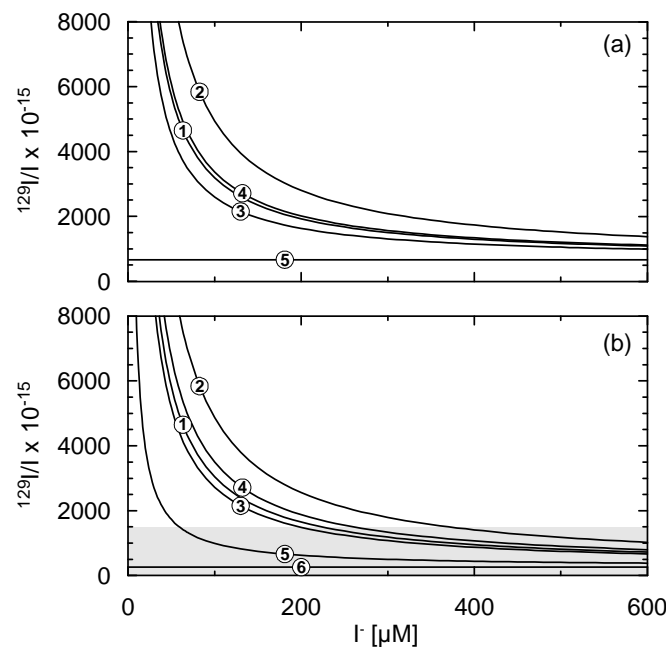


Figure III.6. $^{129}\text{I}/\text{I}$ ratios as a function of excess ^{129}I and I^- concentrations. The $^{129}\text{I}/\text{I}$ ratios (black lines) were calculated by dividing ^{129}I concentrations by the total number of iodine atoms in solution at 0 – 600 μM . The ^{129}I concentrations were calculated by combining cosmogenic ^{129}I with excess ^{129}I (excess ^{129}I = measured ^{129}I – cosmogenic ^{129}I). Cosmogenic ^{129}I was calculated applying (a) the iodine age estimated for Porto MV (18.5 Ma) and (b) an iodine age of 40 Ma, i.e. the average age found for other deep-seated marine settings (see Figure III.5). Circles represent the actually measured $^{129}\text{I}/\text{I}$ ratios and I^- concentrations of the deepest samples of cores (1) 239-GC20 of Mercator MV, (2) 174-GC9 of CAMV, (3) 154-GC5 of CRMV, (4) 130-GC1 of Bonjardim MV and (5) 143-GC3 of Porto MV. An I^- concentration of 200 μM for the theoretical end member (6) in (b) (iodine age of 40 Ma) was chosen according to the correlation trend in Figure III.4a. Gray arrays encompass $^{129}\text{I}/\text{I}$ ratio \leq natural seawater value.

alteration processes within deeply buried sediments and shale is the most likely reason for anomalously high $^{129}\text{I}/\text{I}$ ratios in deep-sourced interstitial fluids in the Gulf of Cadiz.

III.4.2.3. Controls on fissiogenic ^{129}I in deep-seated marine interstitial fluids

The influence of in situ-produced fissiogenic ^{129}I on the $^{129}\text{I}/\text{I}$ ratio is most significant at low I⁻ concentrations, since the fissiogenic production is independent of the amount of stable iodine in solution (Snyder and Fabryka-Martin, 2007). Iodide concentrations in deep-sourced interstitial fluids in the Gulf of Cadiz decrease across the continental margin (Figure III.3b) and are inversely correlated with $^{87}\text{Sr}/^{86}\text{Sr}$ ratios (Figure III.4c). The seaward decrease in $^{87}\text{Sr}/^{86}\text{Sr}$ (Figure III.3d) has been attributed to admixing of a basement-derived fluid component carrying an isotopic signature from interaction with the basaltic crust (Scholz et al., 2009). In any case, non-radiogenic $^{87}\text{Sr}/^{86}\text{Sr}$ ratios at the distal locations indicate less intense interaction with terrigenous sediments. This is in accordance with reduced dilution of buried organics with detrital matter and, thus, with higher amounts of organic matter-derived I⁻ in interstitial fluids (see Section III.4.1). Because of, in general, much lower iodine concentrations of terrestrial organic material (e.g. Muramatsu and Wedepohl, 1998) possible inputs of land-derived organic matter at the proximal locations cannot compensate for this dilution effect.

The effect of varying I⁻ concentrations on the $^{129}\text{I}/\text{I}$ ratio of fluids containing fissiogenic ^{129}I is highlighted in Figure III.6. The impact of fissiogenic ^{129}I on $^{129}\text{I}/\text{I}$ decreases with increasing I⁻ concentration and, consequently, in seaward direction across the Gulf of Cadiz continental margin. Potentially present excess ^{129}I in fluids of Porto MV has therefore a smaller influence on $^{129}\text{I}/\text{I}$ compared to the other sites. The $^{129}\text{I}/\text{I}$ ratios in Figure III.6b were calculated assuming that the pure organic iodine source (theoretical end member) has an iodine age of 40 Ma. Even in that case, I⁻ concentrations would have to be <60 μM to shift the $^{129}\text{I}/\text{I}$ ratio of Porto MV above the normal marine value. If, in turn, all fluids had a common I⁻ concentration of 180 μM (i.e. like fluids of Porto MV), $^{129}\text{I}/\text{I}$ ratios of the other locations would still be higher than the normal marine value. Hence, comparably low I⁻ concentrations are one important, but not the only reason for anomalously high $^{129}\text{I}/\text{I}$ ratios at most mud volcanoes in the Gulf of Cadiz.

Excess ^{129}I concentrations (calculated with respect to Porto MV, Table III.2) are plotted vs. $^{87}\text{Sr}/^{86}\text{Sr}$ ratios in Figure III.4d. Most sampling locations plot on a trend line corresponding to concomitantly increasing amounts of fissiogenic ^{129}I and radiogenic ^{87}Sr in the fluids. Both of

these isotopes are produced through radioactive decay within ambient sediments and rocks. The parent isotopes are ^{238}U and ^{87}Rb , respectively. The coupled trend in interstitial fluids may be explained with the similar behavior of uranium and rubidium during the formation of primary rocks. Both elements become enriched during magma differentiation resulting in one to two orders of magnitude higher concentrations in felsic rocks compared to mafic rocks (Wedepohl, 1978). Terrigenous sediments in the Gulf of Cadiz are derived from the Iberian and N African margins where the Variscan basement consists of felsic metamorphic rocks (Weijermars, 1991; Maldonado et al., 1999). These sediments have accumulated considerable amounts of ^{87}Sr ($^{87}\text{Sr}/^{86}\text{Sr}$ up to 0.7150; Scholz et al., 2009) and ^{129}I (see Section III.4.2.2) which are transferred into pore fluids during clay mineral diagenesis. By contrast, the underlying oceanic basement in the outer reaches of the Gulf of Cadiz has low uranium and rubidium concentrations. Decreasing $^{87}\text{Sr}/^{86}\text{Sr}$ ratios due to admixing of basement fluid are therefore accompanied by a decrease in excess ^{129}I (Figure III.3d and e, Figure III.4d). Deviating values of Mercator MV might be related to the thinner sediment coverage (Figure III.3a) or to admixing of shallower pore water (Section III.4.2.1, Figure III.4a). In the least radiogenic pore fluids of Porto MV, excess ^{129}I is virtually absent so that $^{129}\text{I}/\text{I}$ ratios are governed by cosmogenic ^{129}I from sediment organic matter.

Table III.3 compares $^{129}\text{I}/\text{I}$ and $^{87}\text{Sr}/^{86}\text{Sr}$ ratios of this study with data from other studies carried out in different geological settings. In most other marine systems, where iodine isotope dating has been carried out, interstitial $^{87}\text{Sr}/^{86}\text{Sr}$ ratios are less radiogenic than

Table III.3. Compilation of $^{129}\text{I}/\text{I}$ and $^{87}\text{Sr}/^{86}\text{Sr}$ data for different geological settings.

Location	$^{129}\text{I}/\text{I} \times 10^{-15}$ ^a	Γ ^b [μM]	$^{87}\text{Sr}/^{86}\text{Sr}$ ^c
Cascadia Margin ^d	111/760	510/640	0.7072 - 0.7092
Central American Margin ^e	80/790	242/84	0.7075 - 0.7092
Peru Margin ^f	140/990	1171/325	0.7092 - 0.7099
Nankai Trough ^g	181/1490	230/100	0.7070 - 0.7087
Yellowknife, Canadian Shield ^h	≤ 4000	≤ 140	≤ 0.7140
Gulf of Cadiz	663/6490	181/44.1	0.7075 - 0.7106

^a Highest/lowest $^{129}\text{I}/\text{I}$ reported.

^b Γ concentrations corresponding to highest/lowest $^{129}\text{I}/\text{I}$.

^c Range of $^{87}\text{Sr}/^{86}\text{Sr}$ reported.

^d ODP Leg 204, Sites 1244 - 1252 (Lu et al., 2008b; Teichert et al., 2005).

^e Cold seeps and ODP Leg 205, Site 1253 - 1255 (Lu et al., 2007; Kastner et al., 2006).

^f ODP Leg 201, Site 1230 and ODP Leg 112, Site 685 (Fehn et al., 2007; Elderfield et al., 1990).

^g BH-1 and ODP Leg 131, Site 808 (Fehn et al., 2003; Kastner et al., 1993).

^h $^{129}\text{I}/\text{I}$ was calculated using the ^{129}I and Γ concentrations reported (Bottomley et al., 1999, 2002).

seawater. The only case where $^{87}\text{Sr}/^{86}\text{Sr}$ ratios slightly more radiogenic than seawater are coupled to $^{129}\text{I}/\text{I}$ ratios below natural seawater are ODP pore fluids from the Peru Margin. Because of the very high concentrations of old iodine ($>1000 \mu\text{M}$), however, potentially present fissiogenic ^{129}I is most likely not perceptible. A meaningful analog to the fissiogenic ^{129}I -rich pore fluids presented here is the Yellowknife brine in the Canadian Shield. In that case, interaction with basement rocks have produced $^{129}\text{I}/\text{I}$ and $^{87}\text{Sr}/^{86}\text{Sr}$ ratios above natural seawater. Most of the other studies listed in Table III.3 have been carried out in subduction zone settings where sediments mostly consist of andesitic volcanic matter from the volcanic arc. Because of the comparably low uranium and rubidium contents of these sediments, $^{129}\text{I}/\text{I}$ ratios are generally governed by ^{129}I from organic matter diagenesis. The Gulf of Cadiz represents a transition between the Yellowknife and subduction zone cases. At the near-shore locations, $^{129}\text{I}/\text{I}$ ratios are dominated by fissiogenic ^{129}I that has been produced within terrigenous, clay-rich sediments. With increasing distance from shore, however, reduced interaction with terrigenous matter results in an almost pure iodine age signal at the most distal location.

III.5. Summary and conclusions

Iodide and iodine isotope systematics have been successfully used to track the age and origin of organic components in deep-sourced marine interstitial fluids. In the Gulf of Cadiz, in situ production of ^{129}I within deeply buried sediments and shale complicates iodine dating, but yet provides additional information on the inorganic sources to the fluids. This particular situation is due to a complex interplay of tectonic, sedimentological and geochemical factors. Terrigenous sediments in the Gulf of Cadiz are derived from uranium-rich, Paleozoic basement rocks on the Iberian and N African margins. Spontaneous fission of ^{238}U produces ^{129}I which is released into pore water during fluid/sediment and fluid/rock interactions. With the westward thinning of terrigenous sediments, the proportion of fissiogenic ^{129}I and thus $^{129}\text{I}/\text{I}$ ratios decrease across the margin. This trend is further amplified by increasing concentrations of stable iodine from organic matter diagenesis, which, in turn, is attributed to the reduced dilution of buried organics with terrigenous matter. A similar lateral trend is observed in the $^{87}\text{Sr}/^{86}\text{Sr}$ systematics of the pore fluids. At the proximal locations, $^{87}\text{Sr}/^{86}\text{Sr}$ ratios are more radiogenic than seawater reflecting high Rb/Sr ratios typical for terrigenous material. In contrast, fluids in the outer reaches of the Gulf of Cadiz show non-radiogenic

$^{87}\text{Sr}/^{86}\text{Sr}$ ratios derived from alteration processes within the oceanic basement. Our results reveal a close coupling between $^{129}\text{I}/\text{I}$ and $^{87}\text{Sr}/^{86}\text{Sr}$ ratios, which is related to the common enrichment of the parent isotope elements, uranium and rubidium, during differentiation of primary rocks.

At the farthest off-shore MV, $^{129}\text{I}/\text{I}$ ratios are lower than the natural seawater value, indicating that the isotopic composition is dominated by ^{129}I from organic matter diagenesis. Isotopic dating of these fluids reveals a mixture of shallow and deep-sourced organic components, the latter produced within sediments with minimum ages in the lower Miocene (i.e. older than 18.5 Ma). This source age is compatible with results from other cold seep and gas hydrate settings, although at the younger end of the overall age range observed in previous studies.

Comparison of the results presented here with literature data demonstrates a general relationship between iodine isotope systematics and the lithology and provenance of rocks and sediments, respectively. In continental rock-hosted groundwater aquifers and terrigenous sedimentary systems iodine isotope systematics are dominated by in situ-produced fissiogenic ^{129}I . In contrast, in uranium-poor, e.g. volcanogenic sediments with mafic to intermediate composition, iodine isotope systematics are governed by ^{129}I from organic matter diagenesis. The Gulf of Cadiz represents the full transition between these continental and oceanic/volcanic end members.

Acknowledgements

We wish to thank the officers and crew of *RV Maria S. Merian* for excellent technical support at sea and A. Bleyer, B. Domeyer and R. Surberg for manifold help in ship-board and shore-based laboratories. We also thank X. Zhao and the group at the IsoTrace Laboratory for ^{129}I determinations. This is publication No. 181 of the Sonderforschungsbereich 574 “Volatiles and Fluids in Subduction Zones” at Kiel University and publication No. GEOTECH-1296 of the R&D program GEOTECHNOLOGIEN. Financial support was obtained by RWE-Dea through R&D project West Nile Delta (WND), by the Federal Ministry of Education and Research (BMBF) (COMET, Grant No. 03G0600D) and from the National Science Foundation (NSF) (Grant OCE-550122).

References

- Aloisi G., Drews M., Wallmann K. and Bohrmann G. (2004). Fluid expulsion from the Dvurechenskii mud volcano (Black Sea) Part I. Fluid sources and relevance to Li, B, Sr, I and dissolved inorganic nitrogen cycles. *Earth and Planetary Science Letters* **225**, 347-363.
- Argus D.F., Gordon R.G., Demets C. and Stein S. (1989). Closure of the Africa Eurasia North America Plate Motion Circuit and Tectonics of the Gloria Fault. *Journal of Geophysical Research-Solid Earth and Planets* **94**, 5585-5602.
- Baldwin B. and Butler C. (1985). Compaction curves. *AAPG Bulletin* **69**, 622-626.
- Böning P., Cuypers S., Grunwald M., Schnetger B. and Brumsack H.J. (2005). Geochemical characteristics of Chilean upwelling sediments at ~36° S. *Marine Geology* **220**, 1-21.
- Bottomley D.J., Katz A., Chan L.H., Starinsky A., Douglas M., Clark I.D. and Raven K.G. (1999). The origin and evolution of Canadian Shield brines: evaporation or freezing of seawater? New lithium isotope and geochemical evidence from the Slave craton. *Chemical Geology* **155**, 295-320.
- Bottomley D.J., Renaud R., Kotzer T. and Clark I.D. (2002). Iodine-129 constraints on residence times of deep marine brines in the Canadian Shield. *Geology* **30**, 587-590.
- Broecker W.S. and Peng T.H. (1982). *Tracers in the sea*. Eldegio Press, Palisades, NY.
- Decarvalho H.G., Martins J.B., Medeiros E.L. and Tavares O.A.P. (1982). Decay constant for spontaneous-fission process in ²³⁸U. *Nuclear Instrumentation and Methods in Physics Research* **197**, 417-426.
- Dia A.N., Castrec M., Boulègue J. and Boudou J.P. (1995). Major and trace element and Sr isotope constraints on fluid circulations in the Barbados accretionary complex. Part 1: fluid origin. *Earth and Planetary Science Letters* **134**, 69-85.
- Diez S., Gràcia E., Gutscher M.A., Matias L.M., Mulder T., Terrinha P., Somoza L., Zitellini N., De Alteriis G., Henriët J.P. and Dañoibeitia J.J. (2005). Bathymetric map of the Gulf of Cadiz, NE Atlantic Ocean: the SWIM multibeam compilation. *250th anniversary of the Lisbon earthquake*.
- Egeberg P.K. and Dickens G.R. (1999). Thermodynamic and pore water halogen constraints on gas hydrate distribution at ODP Site 997 (Blake Ridge). *Chemical Geology* **153**, 53-79.
- Elderfield H. and Truesdale V.W. (1980). On the biophilic nature of iodine in seawater. *Earth and Planetary Science Letters* **50**, 105-114.
- Elderfield H., Kastner M. and Martin J.B. (1990). Compositions and Sources of Fluids in Sediments of the Peru Subduction Zone. *Journal of Geophysical Research* **95**, 8819-8827.
- Elmore D., Gove H.E., Ferraro R., Kilius L.R., Lee H.W., Chang K.H., Beukens R.P., Litherland A.E., Russo C.J., Purser K.H., Murrell M.T. and Finkel R.C. (1980). Determination of ¹²⁹I using tandem accelerator mass spectrometry. *Nature* **286**, 138-140.
- Fehn U. and Snyder G.T. (2005). Residence times and source ages of deep crustal fluids: interpretation of ¹²⁹I and ³⁶Cl results from the KTB-VB drill site, Germany. *Geofluids* **5**, 42-51.
- Fehn U., Peters E.K., Tullai-Fitzpatrick S., Kubik P.W., Sharma P., Teng R.T.D., Gove H.E. and Elmore D. (1992). ¹²⁹I and ³⁶Cl concentrations in waters of the eastern Clear Lake area, California: residence times and source ages of hydrothermal fluids. *Geochimica et Cosmochimica Acta* **56**, 2069-2079.
- Fehn U., Snyder, G., Egeberg, P.K. (2000). Dating of Pore Waters with ¹²⁹I: relevance for the Origin of Marine Gas Hydrates. *Science* **289**, 2332-2335.
- Fehn U., Snyder G.T., Matsumoto R., Muramatsu Y. and Tomaru H. (2003). Iodine dating of pore waters associated with gas hydrates in the Nankai area, Japan. *Geology* **31**, 521-524.

- Fehn U., Moran J.E., Snyder G.T. and Muramatsu Y. (2007a). The initial ¹²⁹I/I ratio and the presence of 'old' iodine in continental margins. *Nuclear Instruments and Methods in Physics Research Section B: Beam Interactions with Materials and Atoms* **259**, 496-502.
- Fehn U., Snyder G.T. and Muramatsu Y. (2007b). Iodine as a tracer of organic material: ¹²⁹I results from gas hydrate systems and fore arc fluids. *Journal of Geochemical Exploration* **95**, 66-80.
- Garbe-Schönberg C.-D. (1993). Simultaneous determination of 37 trace elements in 28 international rock standards by ICP-MS. *Geostandards and Geoanalytical Research* **17**, 81-97.
- Gieskes J.M. and Mahn C. (2007). Halide systematics in interstitial waters of ocean drilling sediment cores. *Applied Geochemistry* **22**, 515-533.
- Govindaraju K. (1994). Compilation of working values and sample description for 383 geostandards. *Geostandards Newsletter* **18**, 1-158.
- Grasshoff K., Erhard M. and Kremling K. (2002). *Methods of seawater analysis*. Wiley-VCH, Weinheim.
- Harvey G.R. (1980). A study of the chemistry of iodine and bromine in marine sediments. *Marine Chemistry* **8**, 327-332.
- Hebeda E.H., Schulz L. and Freundel M. (1987). Radiogenic, fissiogenic, and nucleogenic noble-gases in zircons. *Earth and Planetary Science Letters* **85**, 79-90.
- Hensen C., Wallmann K., Schmidt M., Ranero C.R. and Suess E. (2004). Fluid expulsion related to mud extrusion off Costa Rica - a window to the subducting slab. *Geology* **32**, 201-204.
- Hensen C., Nuzzo M., Hornibrook E., Pinheiro L.M., Bock B., Magalhaes V.H. and Brückmann W. (2007). Sources of mud volcano fluids in the Gulf of Cadiz - indications for hydrothermal imprint. *Geochimica et Cosmochimica Acta* **71**, 1232-1248.
- Kastner M., Elderfield H., Jenkins W.J., Gieskes J.M. and Gamo T. (1993). 32. Geochemical and isotopic evidence for fluid flow in the western Nankai subduction zone, Japan. *Proceedings of the Ocean Drilling Program Scientific Results* **131** (eds. Hill I.A., Taira A. and Firth J.V.), 397-413.
- Kastner M., Solomon E., Wei W., Chan L.H. and Saether O.M. (2006). 5. Data report: Chemical and isotopic composition of pore fluids and sediments from across the middle America trench, offshore Costa Rica. *Proceedings of the Ocean Drilling Program Scientific Results* **205** (eds. Morris J.D., Villinger H.W. and Klaus A.), 397-413.
- Katz A. and Starinsky A. (2003). Iodine-129 constraints on residence times of deep marine brines in the Canadian Shield: comment and reply. *Geology* **31**, 93-94.
- Kennedy H.A. and Elderfield H. (1987a). Iodine diagenesis in non-pelagic deep-sea sediments. *Geochimica et Cosmochimica Acta* **51**, 2505-2514.
- Kennedy H.A. and Elderfield H. (1987b). Iodine diagenesis in pelagic deep-sea sediments. *Geochimica et Cosmochimica Acta* **51**, 2489-2504.
- Lu Z., Hensen C., Fehn U. and Wallmann K. (2007). Old iodine in fluids venting along the Central American convergent margin. *Geophysical Research Letters* **34**, 1-7.
- Lu Z., Hensen C., Fehn U. and Wallmann K. (2008a). Halogen and ¹²⁹I systematics in gas hydrate fields at the northern Cascadia margin (IODP Expedition 311): insights from numerical modeling. *Geochemistry Geophysics Geosystems* **9**, 1-18.
- Lu Z., Tomaru H. and Fehn U. (2008b). Iodine ages of pore waters at Hydrate Ridge (ODP Leg 204), Cascadia Margin: implications for sources of methane in gas hydrates. *Earth and Planetary Science Letters* **267**, 654-665.
- Maldonado A., Somoza L. and Pallares L. (1999). The Betic orogen and the Iberian-African boundary in the Gulf of Cadiz: geological evolution (central North Atlantic). *Marine Geology* **155**, 9-43.

- Martin J.B., Gieskes J.M., Torres M. and Kastner M. (1993). Bromine and iodine in Peru margin sediments and pore fluids: implications for fluid origins. *Geochimica et Cosmochimica Acta* **57**, 4377-4389.
- Martin J.B., Kastner M., Henry P., Le Pichon X. and Lallement S. (1996). Chemical and isotopic evidence for sources of fluids in a mud volcano field seaward of the Barbados accretionary wedge. *Journal of Geophysical Research* **101**, 20325-20345.
- Medialdea T., Somoza L., Pinheiro L.M., Fernández-Puga M.C., Vázquez J.T., León R., Ivanov M.K., Magalhaes V., Díaz-del-Río V. and Vegas R. (2009). Tectonics and mud volcano development in the Gulf of Cádiz. *Marine Geology* **261**, 48-63.
- Moran J.E., Fehn U. and Teng R.T.D. (1998). Variations in ratios in recent marine sediments: evidence for a fossil organic component. *Chemical Geology* **152**, 193-203.
- Muramatsu Y. and Wedepohl K.H. (1998). The distribution of iodine in the earth's crust. *Chemical Geology* **147**, 201-216.
- Niemann H., Duarte J., Hensen C., Omoregie E., Magalhães V.H., Elvert M., Pinheiro L.M., Kopf A.J. and Boetius A. (2006). Microbial methane turnover at mud volcanoes of the Gulf of Cadiz. *Geochimica et Cosmochimica Acta* **70**, 5336-5355.
- Nuzzo M., Hornibrook E.R.C., Gill F., Hensen C., Pancost R.D., Haeckel M., Reitz A., Scholz F., Magalhães V.H., Brückmann W. and Pinheiro L.M. (2009). Origin of light volatile hydrocarbon gases in mud volcano fluids, Gulf of Cadiz - evidence for multiple sources and transport mechanisms in active sedimentary wedges. *Chemical Geology* **266**, 359-372.
- Pinheiro L.M., Ivanov M., Kenyon N., Magalhães V., Somoza L., Gardner J., Kopf A.J., Van Rensbergen P., Monteiro J.H. and the Euromargins Team (2005). Structural control of mud volcanism and hydrocarbon-rich fluid seepage in the Gulf of Cadiz: results from TTR-15 and previous cruises. *CIESM Workshop Monographs* **29**, 53-58.
- Price N.B. and Calvert S.E. (1973). The geochemistry of iodine in oxidised and reduced recent marine sediments. *Geochimica et Cosmochimica Acta* **37**, 2149-2158.
- Price N.B. and Calvert S.E. (1977). The contrasting geochemical behaviours of iodine and bromine in recent sediments from the Namibian shelf. *Geochimica et Cosmochimica Acta* **41**, 1769-1775.
- Sabu D.D. (1971). On mass-yield of xenon and krypton isotopes in the spontaneous fission of uranium. *Journal of Inorganic and Nuclear Chemistry* **33**, 1509-1531.
- Sartori R., Torelli L., Zitellini N., Peis D. and Lodolo E. (1994). Eastern Segment of the Azores-Gibraltar Line (Central-Eastern Atlantic): an oceanic plate boundary with diffuse compressional deformation. *Geology* **22**, 555-558.
- Scholz F., Hensen C., Reitz A., Romer R.L., Liebetrau V., Meixner A., Weise S.M. and Haeckel M. (2009). Isotopic evidence (⁸⁷Sr/⁸⁶Sr, δ⁷Li) for alteration of the oceanic crust at deep-rooted mud volcanoes in the Gulf of Cadiz, NE Atlantic Ocean. *Geochimica et Cosmochimica Acta* **73**, 5444-5459.
- Snyder G.T. and Fabryka-Martin J.T. (2007). ¹²⁹I and ³⁶Cl in dilute hydrocarbon waters: marine-cosmogenic, in situ, and anthropogenic sources. *Applied Geochemistry* **22**, 692-714.
- Stadnitskaia A., Ivanov M.K., Blinova V., Kreulen R. and Van Weering T.C.E. (2006). Molecular and carbon isotopic variability of hydrocarbon gases from mud volcanoes in the Gulf of Cadiz, NE Atlantic. *Marine and Petroleum Geology* **23**, 281-296.
- Stadnitskaia A., Ivanov M.K. and Sinninghe Damsté J.S. (2008). Application of lipid biomarkers to detect sources of organic matter in mud volcano deposits and post-eruptional methanotrophic processes in the Gulf of Cadiz, NE Atlantic. *Marine Geology* **255**, 1-14.
- Teichert B.M.A., Torres M.E., Bohrmann G. and Eisenhauer A. (2005). Fluid sources, fluid pathways and diagenetic reactions across an accretionary prism revealed by Sr and B geochemistry. *Earth and Planetary Science Letters* **239**, 106-121.

- Thiebot E. and Gutscher M. A. (2006). The Gibraltar Arc seismogenic zone (part 1): constraints on a shallow east dipping fault plane source for the 1755 Lisbon earthquake provided by seismic data, gravity and thermal modeling. *Tectonophysics* **426**, 135-152.
- Tomaru H., Lu Z., Fehn U., Muramatsu Y. and Matsumoto R. (2007). Age variation of pore water iodine in the eastern Nankai Trough, Japan: evidence for different methane sources in a large gas hydrate field. *Geology* **35**, 1015-1018.
- Wagner M.J.M., Dittrich-Hannen B., Synal H.A., Suter M. and Schotterer U. (1996). Increase of ¹²⁹I in the environment. *Nuclear Instruments and Methods in Physics Research Section B: Beam Interactions with Materials and Atoms* **113**, 490-494.
- Wedepohl K.H. (1978). *Handbook of geochemistry II*, Springer Verlag, Heidelberg.
- Weijermars R. (1991). Geology and tectonics of the Betic Zone, SE Spain. *Earth-Science Reviews* **31**, 153-236.
- Zitellini N., Gràcia E., Matias L., Terrinha P., Abreu M.A., De Alteriis G., Henriët J.P., Dañobeitia J.J., Masson D.G., Mulder T., Ramella R., Somoza L. and Diez S. (2009). The quest for the Africa-Eurasia plate boundary west of the Strait of Gibraltar. *Earth and Planetary Science Letters* **280**, 13-50.

Lithium isotope geochemistry of marine pore waters – insights from cold seep fluids

Florian Scholz^{a,*}, Christian Hensen^a, Gert J. De Lange^b, Matthias Haeckel^a, Volker Liebetrau^a,
Anette Meixner^c, Anja Reitz^a and Rolf L. Romer^c

^a*Leibniz Institute of Marine Sciences, IFM-GEOMAR, Wischhofstraße 1-3, D-24148 Kiel*

^b*Utrecht University, Faculty of Geosciences, Department of Earth Sciences - Geochemistry, P.O. Box 80021,
3508 TA Utrecht, The Netherlands*

^c*Deutsches GeoForschungsZentrum, GFZ, Telegrafenberg, D-14473 Potsdam, Germany*

Submitted to *Geochimica et Cosmochimica Acta*

Abstract

Lithium concentration and isotope data ($\delta^7\text{Li}$) were collected for pore fluids from 18 cold seep locations and reference fluids from shallow marine sediments, a sediment-hosted hydrothermal system and two Mediterranean brine basins. The new reference data and literature data of hydrothermal fluids and pore fluids from the Ocean Drilling Program follow an empirical relationship between Li concentration and $\delta^7\text{Li}$ ($\delta^7\text{Li} = -6.0(\pm 0.3) \cdot \ln[\text{Li}] + 51(\pm 1.2)$) reflecting Li release from sediment or rocks and/or uptake of Li during mineral authigenesis. Cold seep fluids display $\delta^7\text{Li}$ values between +7.5 ‰ and +45.7 ‰, mostly in agreement with this general relationship. Ubiquitous diagenetic signals of clay dehydration in all cold seep fluids indicate that authigenic smectite-illite is the major sink for light pore water Li in deeply buried continental margin sediments. Deviations from the general

* Corresponding author: Florian Scholz; e-mail address: fscholz@ifm-geomar.de.

relationship are attributed to the varying provenance and composition of sediments or to transport-related fractionation trends: Pore fluids on passive margins receive disproportionately high amounts of Li from intensely weathered and transported terrigenous matter. By contrast, on convergent margins and in other settings with strong volcanogenic input, Li concentrations in pore water are lower because of intense Li uptake by alteration minerals and, most notably, adsorption of Li onto smectite. The latter process is not accompanied by isotope fractionation, as revealed from a separate study on shallow sediments. A numerical transport-reaction model was applied to simulate Li isotope fractionation during upwelling of pore fluids. It is demonstrated that slow pore water advection (order of mm a^{-1}) suffices to convey much of the deep-seated diagenetic Li signal into shallow sediments. If cautiously applied, Li isotope systematics may, thus, provide a valuable record of fluid/mineral interaction that has been inherited several hundreds or thousands of meters below the actual seafloor fluid escape structure.

IV.1. Introduction

In the past two decades, the behavior of Li isotopes has been studied in various marine systems, including mid-ocean ridge and sediment-hosted hydrothermal systems (Chan et al., 1993; Chan et al., 1994; James et al., 1999), subduction zone settings (You et al., 1995; Chan and Kastner, 2000) and normal coastal and deep-sea sediments recovered by means of deep-sea drilling (Zhang et al., 1998; James and Palmer, 2000). Major processes identified to cause deviations from the seawater isotopic composition are adsorption/desorption reactions (Zhang et al., 1998; James and Palmer, 2000), formation and transformation of silicate minerals (Chan and Kastner, 2000; Williams and Hervig, 2005) and leaching of Li from sediments or underlying crust at high temperature (Chan et al., 1993, Chan et al., 1994; James et al., 1999). As a result of the accomplished work, Li isotopes are considered a promising tracer for the diagenetic evolution and provenance of pore fluids in overpressured sedimentary environments.

The Li isotopic composition of seawater ($\delta^7\text{Li}$: +31 ‰; Millot et al., 2004) is distinct from mid-ocean ridge basalt (MORB) ($\delta^7\text{Li}$: $+3.4 \pm 1.4$ ‰; Tomascak et al., 2008) and clastic, marine sediments ($\delta^7\text{Li}$: -1.5 - +5 ‰; Chan et al., 2006) and the direction of Li exchange among these reservoirs is temperature-dependent. Under normal seafloor conditions, seawater Li is sequestered by authigenic clay minerals. Since the light isotope, ^6Li , is

preferentially taken up, the remaining Li-depleted fluids become isotopically heavier during this process. By contrast, at elevated temperatures, simultaneous leaching of Li from primary minerals and uptake into secondary minerals shifts the Li isotope value of fluids between that of seawater and the initial solid (e.g. Chan et al., 1993, 1994; Zhang et al., 1998; James et al., 2003). Since both the distribution coefficient between solid and fluid and the extent of isotope fractionation during mineral authigenesis are a function of temperature (Berger et al., 1988; Chan et al., 1994), mobile fluids in porous media may undergo multiple stages of Li uptake and loss. The complex Li isotope signature resulting from this bears a valuable record of fluid/mineral interaction that is, however, challenging to unravel.

To better constrain the Li isotope signature of advecting pore fluids in continental margin sediments, pore water samples from 18 cold seep locations in varying geological settings were analyzed for their Li concentration and isotopic composition. Literature data of hydrothermal fluids and pore waters from the Ocean Drilling Program (ODP) were compiled in order to establish a frame of reference for Li isotope exchange between fluids and solids in related marine systems. Comparison of the presented results with that reference frame yields insights into the provenance and diagenetic evolution of cold seep fluids. Two evolutionary distinct Messinian brines from the Mediterranean Sea were included in this study to test whether hypersaline pore fluids are subject to individual fractionation mechanisms. Eventually, a transport-reaction model is used to retrace fractionation trends during upwelling of fluids to the seafloor. Besides being of relevance to studies on the origin and evolution of cold seep fluids, this article reviews general principles for the interpretation of Li isotope variations in the context of diagenesis and pore water/mineral interaction in marine sediments.

IV.2. Samples

The following section gives a brief overview about the geological characteristics of the studied seepage areas (Figure IV.1) and major processes affecting the composition of pore fluids. More detailed information may be obtained from the references cited in the text. The geographical position and water depth of the sampling locations are summarized in Table IV.1.

IV.2.1. Regional settings

Upward movement of overpressured fluids is often associated with compressional tectonics and subduction related processes (Hyndman and Davis, 1992). Mound 11, Mud Pie and Mound Ridge are cold seeps on the Central American margin (map 1 in Figure IV.1) where the Cocos plate is subducted beneath the Caribbean plate (Ranero and Von Huene, 2000; Hensen et al., 2004). Fluid seepage and mud volcanism on the Mediterranean Ridge is related to subduction of the African plate beneath the Eurasian plate (Camerlenghi et al., 1992; Robertson et al., 1996; Robertson and Kopf, 1998). The major mud volcano (MV) areas on the Mediterranean Ridge are the Olimpi Field on the accretionary prism south of Crete (Napoli Dome) and, further east, the Anaximander Mountains (Kazan and Amsterdam MVs) located at the junction of the Hellenic and Cyprus Arcs (map 4 in Figure IV.1; Zitter et al., 2005). Although not directly related to subduction, mud volcanism in the Black Sea

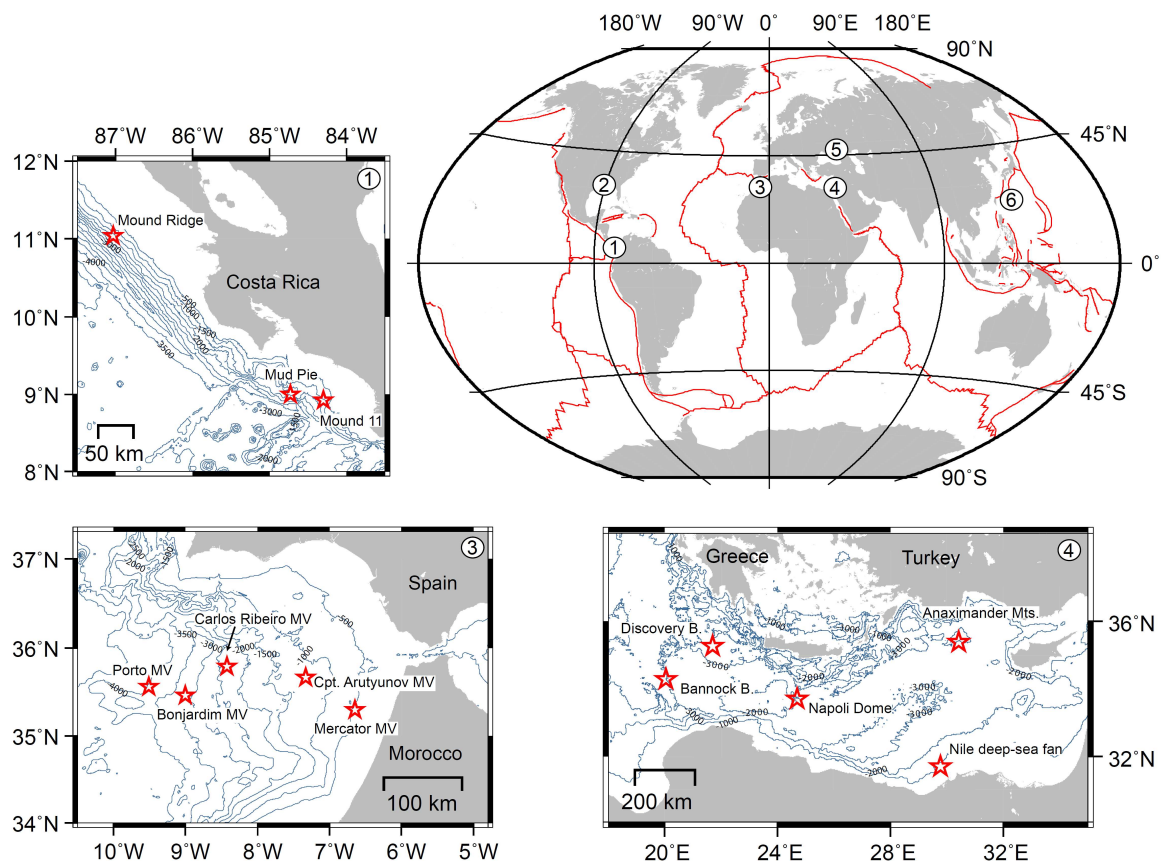


Figure IV.1. Global map showing the study areas: (1) Central American margin, (2) Gulf of Mexico, (3) Gulf of Cadiz, (4) Eastern Mediterranean Sea, (5) Black Sea and (6) Okinawa Trough. Major tectonic plate boundaries are represented by red lines. Detailed maps with bathymetric information are shown for (1), (3) and (4). Stars indicate the position of sampling sites or sub-regions. See Table IV.1 for geographical positions and water depths.

(Dvurechenskii MV and Pechori Mound) occurs likewise in the tectonic context of plate convergence between Africa and Eurasia (Limonov et al., 1997; Bohrmann et al., 2003; Nikishin et al., 2003). By contrast, in the northern Gulf of Mexico (Green Canyon Bush Hill and 415 East) and on the Nile deep-sea fan (Giza and North Alex MVs) in the eastern Mediterranean Sea (Roberts and Carney, 1997; Loncke et al., 2004; Loncke et al., 2006), fluid seepage and mud volcanism are caused by thin-skinned tectonic processes. In these areas, huge sediment accumulation rates and actively moving salt bodies in the subsurface create faults along which fluids, gas and mud are transported to the seafloor. In the Gulf of Cadiz, mud volcanisms and related phenomena are concentrated along deeply cutting thrust and strike-slip faults that are associated to the boundary between the African and Eurasian plates (Pinheiro et al., 2005; Medialdea et al., 2009). In a recent study, Scholz et al. (2009) investigated five MVs located on an E-W transect across the Gulf of Cadiz (map 3 in Figure IV.1). Deep-sourced pore fluids from this transect reflect a consistent transition from continental-sedimentary to oceanic-crustal fluid sources. Scholz et al. (2009) inferred from Sr and Li isotope systematics that deep-seated faults serve as conduits for fluids originating in the underlying oceanic basement and drew parallels to ridge flank hydrothermal systems.

IV.2.2. Diagenetic characterization of pore fluids

Deeply buried sediments on continental margins are strongly reducing environments. Accordingly, deep-sourced pore fluids are, in most cases, devoid of SO_4^{2-} but strongly enriched in reduced components such as NH_4^+ , I^- and CH_4 (e.g. Aloisi et al., 2004; Wallmann et al., 2006a; Fehn et al., 2007; Gieskes and Mahn, 2007). Most of the pore fluids investigated here have lower salinities than normal seawater. Although dissociation of gas hydrates has been identified in a few cases (Suess et al., 1999), dehydration of clay minerals in the deep subsurface is commonly regarded as the major reason for pore water freshening (Moore and Vrolijk, 1992; Dählmann and De Lange, 2003; Hensen et al., 2004; Hensen et al., 2007). Clay mineral dehydration processes such as the conversion of smectite to illite chiefly occur at temperatures between 60 and 150 °C and are accompanied by K consumption and the release of Na, Li and B into the ambient pore water (Ishikawa and Nakamura, 1993; Środoń, 1999; Chan and Kastner, 2000). The release of mobile cations from sediments continues at temperatures beyond the typical range for clay diagenesis leading to very high B and Li concentrations in décollement fluids at subduction zones and in fluids of sediment-hosted hydrothermal systems (Butterfield et al., 1994; You et al., 1996; James et al., 1999;

Table IV.1. General characteristics of the sampling sites and sediment cores.

Area	Location	Cruise	Station/ sampling device ^b	Latitude	Longitude	Water depth [m]
<i>Reference sites</i>						
Gulf of Cadiz	Reference core	MSM1-3	139-MUC2	35°27.56' N	8°59.88' W	3054
Nile deep-sea fan (E Mediterranean Sea)	Reference core	POS362-2	MUC28	31°41.58' N	29°46.07' E	725
Black Sea	Reference core	POS362-2	GC2	31°41.63' N	29°46.10' E	722
	Reference core	M72-3	GeoB11905 (MIC)	41°57.43' N	41°16.80' E	877
	Reference core	M72-3	GeoB11974 (GC)	41°57.43' N	41°16.80' E	884
Okinawa Trough (NW Pacific Ocean)	Abyss Vent ^a	S0196	95MUC28	24°50.78' N	122°42.03' E	1394
	Abyss Vent ^a	S0196	44PC33	24°50.78' N	122°42.03' E	~1390
E Mediterranean Sea	Swallow chimney ^a	S0196	34GC1	24°50.84' N	122°42.00' E	1382
	Discovery brine	PaleoPass04	28CT (rosette)	35°16.62' N	21°41.45' E	
	Bannock brine	PaleoPass04	09CT (rosette)	34°17.99' N	20°01.72' E	
<i>Seep sites</i>						
Central American margin (E equatorial Pacific)	Mound 11	S0173	TVMUC127	8°55.31' N	84°18.22' W	1012
	Mud Pie	M66	108/78/27 (PC)	8°59.60' N	84°43.68' W	1917
	Mound Ridge	M66	GC219	11°02.45' N	87°02.16' W	1710
Gulf of Mexico, Green Canyon	415 East	S0174	TGC3	27°32.61' N	90°59.55' W	353
	Bush Hill	S0174	GC8	27°46.98' N	91°30.47' W	553
Gulf of Cadiz (NE Atlantic Ocean)	Porto MV	MSM1-3	143GC3	35°33.70' N	9°30.44' W	3860
	Bonjardim MV	MSM1-3	130GC1	35°27.82' N	9°00.14' W	3049
	Carlos Ribeiro MV	MSM1-3	154GC5	35°47.26' N	8°25.36' W	2198
	Captain Arutyunov MV	MSM1-3	174GC9	35°39.74' N	7°19.96' W	1322
	Captain Arutyunov MV	MSM1-3	205GC13	35°39.70' N	7°20.08' W	1326
	Mercator MV	MSM1-3	239GC20	35°17.92' N	6°38.70' W	353
	Mercator MV	MSM1-3	263GC28	35°17.87' N	6°38.80' W	351

continued on next page

^a Sediment cores were retrieved in the vicinity of the identically named hydrothermal vent structures.^b MUC = multi corer; PC = push core; GC = gravity corer; PiC = piston corer; MIC = mini corer.

Table IV.1. Continued.

Area	Location	Cruise	Station/ sampling device ^b	Latitude	Longitude	Water depth [m]
E Mediterranean Sea	Napoli Dome	MD69	KC11 (PiC)	33°43.28' N	24°41.27' E	1925
	Kazan MV	Aegeo04	18GC1	35°25.91' N	30°33.71' E	1696
	Kazan MV	MIMES04	07GT (GC)	35°25.92' N	30°33.71' E	1663
	Amsterdam MV	Aegeo04	02AP2 (GC)	35°20.00' N	30°16.28' E	2030
	Amsterdam MV	Aegeo04	02AP3 (GC)	35°20.00' N	30°16.24' E	2022
	Giza MV	POS362-2	GC5	31°40.51' N	29°45.00' E	666
	Giza MV	POS362-2	GC34	31°40.54' N	29°45.24' E	671
	North Alex MV	POS362-2	GC100	31°58.16' N	30°08.16' E	483
	Dvurechenskii MV	M72-3	GeoB11977 (MIC)	44°16.89' N	34°58.91' E	2052
	Dvurechenskii MV	M72-3	GeoB11978 (MIC)	44°16.94' N	34°58.90' E	2050
Black Sea	Pechori Mound	M72-3	GeoB11955 (GC)	41°58.96' N	41°07.54' E	1012

^a Sediment cores were retrieved in the vicinity of the identically named hydrothermal vent structures.

^b MUC = multi corer; PC = push core; GC = gravity corer; PiC = piston corer; MIC = mini corer.

Kastner and Rudnicki, 2004). In some cases (e.g. Green Canyon 415 East in the Gulf of Mexico, Napoli Dome in the Mediterranean Sea, Dvurechenskii MV in the Black Sea), the clay mineral diagenetic signal of pore water dilution is overprinted by admixing of evaporated seawater or by dissolution of evaporite minerals (e.g. Dählmann and De Lange, 2003; Aloisi et al., 2004; Reitz et al., 2007). In order to investigate the above-described processes independently from each other, reference fluids with a less complex geochemical evolution have been included in this study. Shallow pore waters from the Nile deep-sea fan and the eastern Black Sea show downcore decreasing Li concentrations indicating Li uptake by sediments during early diagenesis (Zhang et al., 1998; James et al., 2000). Lithium-rich pore fluids from sediments in the Okinawa Trough hydrothermal system are formed through interaction of seawater with andesitic volcanic rocks and terrigenous sediments at temperatures above 300 °C (Glasby and Notsu, 2003; Konno et al., 2006). Brine samples have been obtained from two evolutionary distinct brine basins in the eastern Mediterranean Sea. While Bannock brine has evolved through twelve fold evaporation of seawater and subsequent burial (Vengosh et al., 1998), Discovery brine has formed through dissolution of late stage evaporite minerals (mainly bischofite, $\text{MgCl}_2 \cdot 6 \text{H}_2\text{O}$) by sediment pore waters (Wallmann et al., 1997).

IV.3. Methods

IV.3.1. Sediment sampling and pore water recovery

Pore water samples for this study were obtained on several cruises using piston and gravity corers equipped with PVC or tube foil liners, multi or mini corers and ROV-guided push cores (Table IV.1). Brine samples were collected with Niskin bottles mounted on a CTD/rosette (De Lange et al., 1990). Upon recovery, core liners were sectioned, sealed and transferred into a cooled laboratory to assure subsampling under in-situ (i.e. seafloor) temperature. Subsamples were taken within regular distance from the lengthwise-cut sediment cores. Multi and mini cores were stepwise extruded from the liners and cut into 1 - 3 cm thick slices. Pore water recovery was done by pressure filtration (argon gas at 2 - 5 bar) or by centrifuging (4000 rpm for 20 min). Pore waters were filtered through 0.2 µm cellulose-acetate membrane filters and then divided into aliquots for ship-board and shore-based analyses. Aliquots for cation analyses were acidified (HCl or HNO_3 , suprapur) to prevent any mineral precipitation or adsorption. For the same purpose, brine samples were additionally

diluted 1:3 with bi-distilled water. Pore water and brine samples were stored cooled until further processing on land.

IV.3.2. Laboratory analyses

Chlorinity measurements were carried out on-board by Ion Chromatography (761 IC-Compact, Metrohm) or titration with 0.01 N AgNO₃ (Grasshoff et al., 2002). Lithium was analyzed by Inductively Coupled Plasma Optical Emission Spectrometry (ICP-OES, JY 170 Ultrace, Jobin Yvon). The analytical precision based on repeated analysis of IAPSO seawater standard is <1 % for Cl and <5 % for Li. Further information about these routine methods may be obtained from the IFM-GEOMAR web page.

Lithium isotope analyses were carried out by Multi Collector Inductively Coupled Plasma Mass Spectrometry (MC ICP-MS, NEPTUNE, ThermoFisher Scientific) after chromatographical Li separation following a modified protocol after Tomascak et al. (1999). For ion exchange chromatography, a sample aliquot containing 0.5 µg Li was evaporated and re-dissolved in 1 N HNO₃ and 80 % methanol. Samples with an unfavorable molar Li to Na proportion (Na/Li > ~2 x 10⁵) were subjected to a second or third chromatographical step using 0.5 N HCl and 80 % methanol as solvent (modified after Jeffcoate et al., 2004). Lithium concentrations before and after the actual Li eluate were typically less than 0.1 % of the total Li in the sample and, therefore, did not cause a detectable isotopic shift due to sample purification. Further details on the ion chromatographic and mass spectrometric procedures are given in Wunder et al. (2006; 2007). The Li standard NIST SRM 8545 (L-SVEC) and seawater were repeatedly included in the chromatographic separation to check the accuracy of the procedure. The resulting Li isotope values are given relative to the standard NIST SRM 8545 according to $\delta^7\text{Li} = ((^7\text{Li}/^6\text{Li})_{\text{sample}}/(^7\text{Li}/^6\text{Li})_{\text{standard}} - 1) \times 1000$. Repeated analysis of seawater during this study yielded a $\delta^7\text{Li}$ of $+30.9 \pm 0.3 \text{ ‰}$ (2σ , $n = 9$).

Strontium isotope ratios were determined by Thermal Ionization Mass Spectrometry (TIMS, TRITON, ThermoFisher Scientific) after chemical separation via cation exchange chromatography using a Sr-specific resin (Eichrom). All isotope ratios were internally normalized to an ⁸⁶Sr/⁸⁸Sr ratio of 0.1194. Repeated analysis of the standard NIST SRM 987 over the course of this study yielded an average value of 0.710220 ± 17 (2σ , $n = 12$). For comparison with literature values all ⁸⁷Sr/⁸⁶Sr were normalized to a value of 0.710248 for the NIST SRM 987.

IV.3.3. Transport-reaction modeling

A one-dimensional, numerical transport-reaction model was developed to simulate Li isotope fractionation during upward advection of pore fluids. Partial differential equations for solutes follow the classical approach of Berner (1980):

$$\phi \cdot \frac{\partial [C]}{\partial t} = \frac{\partial \left(\phi \cdot D_s \cdot \frac{\partial [C]}{\partial x} \right)}{\partial x} - \frac{\partial (\phi \cdot v \cdot [C])}{\partial x} + \phi \cdot R \quad (\text{IV.1})$$

where [C] is the concentration of dissolved species in pore water, x is depth, t is time, ϕ is porosity, D_s is the molecular diffusion coefficient in sediments, v is the vertical advection velocity of the pore water and R defines all reactions occurring in the simulated sediment domain. The model calculates the concentration-depth profiles of three dissolved species (total dissolved Li, ^7Li and ^6Li) considering the decrease in porosity with sediment depth, molecular diffusion, advective transport of solutes via sediment burial, steady state compaction and pressure-driven flow as well as the temperature-dependent precipitation of Li and the related isotope fractionation.

Sediment porosity decreases with depth due to sediment compaction. Assuming steady-state compaction, the profile can be approximated by:

$$\phi = (\phi_{TOP} - \phi_{BOT}) \cdot \exp(-const \cdot x) + \phi_{BOT} \quad (\text{IV.2})$$

where ϕ_{BOT} and ϕ_{TOP} are the porosity at the lower and upper boundary and const is the attenuation coefficient for the exponential decrease of porosity with depth. The burial velocity of solids is expressed as steady-state compaction with:

$$\omega(x) = \frac{1 - \phi_{BOT}}{1 - \phi(x)} \omega_{BOT} \quad (\text{IV.3})$$

where $\omega(x)$ represents the depth-dependent burial velocity and ω_{BOT} is the sediment burial velocity at the base of the model domain. The upward directed pore water velocity through sediments is composed of the downward burial component modified by compaction and the upward fluid advection:

$$v(x) = \frac{\omega_{BOT} \cdot \phi_{BOT} - v_{TOP} \cdot \phi_{TOP}}{\phi(x)} \quad (\text{IV.4})$$

where v(x) represents the depth-dependent fluid velocity and v_{TOP} is the upward fluid advection velocity at the sediment surface.

Temperature-dependent molecular diffusion coefficients of Li were calculated after Boudreau et al. (1997) and corrected for tortuosity using the following relationship (Boudreau, 1996):

$$D_s(x) = \frac{D_M(x)}{1 - \ln(\phi(x))^2} \quad (\text{IV.5})$$

where D_M is the molecular diffusion coefficient in seawater. The same value of D_M was used for both Li isotopes. Temperature variations from bottom water to the lower boundary of the simulated sediment column were also considered in a depth-dependency of D_M .

The rate law for Li precipitation and isotope fractionation as well as the boundary conditions and fitting parameters for the model runs are specified in Section IV.5.2. The model was run to steady state from arbitrary initial conditions. Finite difference techniques (the method-of-lines code) were applied to solve the partial differential equations (PDEs). A set of three PDEs (one for each species) is converted into 200 ordinary differential equations (ODE) giving the temporal change of species concentration at each depth interval. The ODE system was set up on an uneven grid with higher resolution at the surface and solved using the NDSolve object of MATHEMATICA Version 7.0 (cf. Hensen and Wallmann, 2005; Wallmann et al., 2006a, 2008).

IV.4. Results

Depth profiles for dissolved Li concentrations and molar Li/Cl ratios are plotted in Figure IV.2. Ratios of Li/Cl highlight deviations from the general salinity trend, i.e. denote consumption or release of Li during chemical reactions. A compilation of $\delta^7\text{Li}$, $^{87}\text{Sr}/^{86}\text{Sr}$ as well as Cl and Li concentration data is given in Table IV.2. Lithium isotope data of MVs in the Gulf of Cadiz have previously been published by Scholz et al. (2009).

Hemipelagic reference cores are characterized by downcore decreasing Li/Cl ratios but seawater-like $\delta^7\text{Li}$ values (Figure IV.2a and b, Table IV.2). Hydrothermal fluids from the Okinawa Trough are considerably enriched in Li and show comparably light $\delta^7\text{Li}$ values between -0.7 and +5.8 ‰. The $\delta^7\text{Li}$ of brine samples varies over a narrow range from +24.3 to +25.1 ‰.

Most pore water profiles of cold seeps display a mixing relationship between bottom water concentrations at the top and an almost uniform concentration in the lower core section.

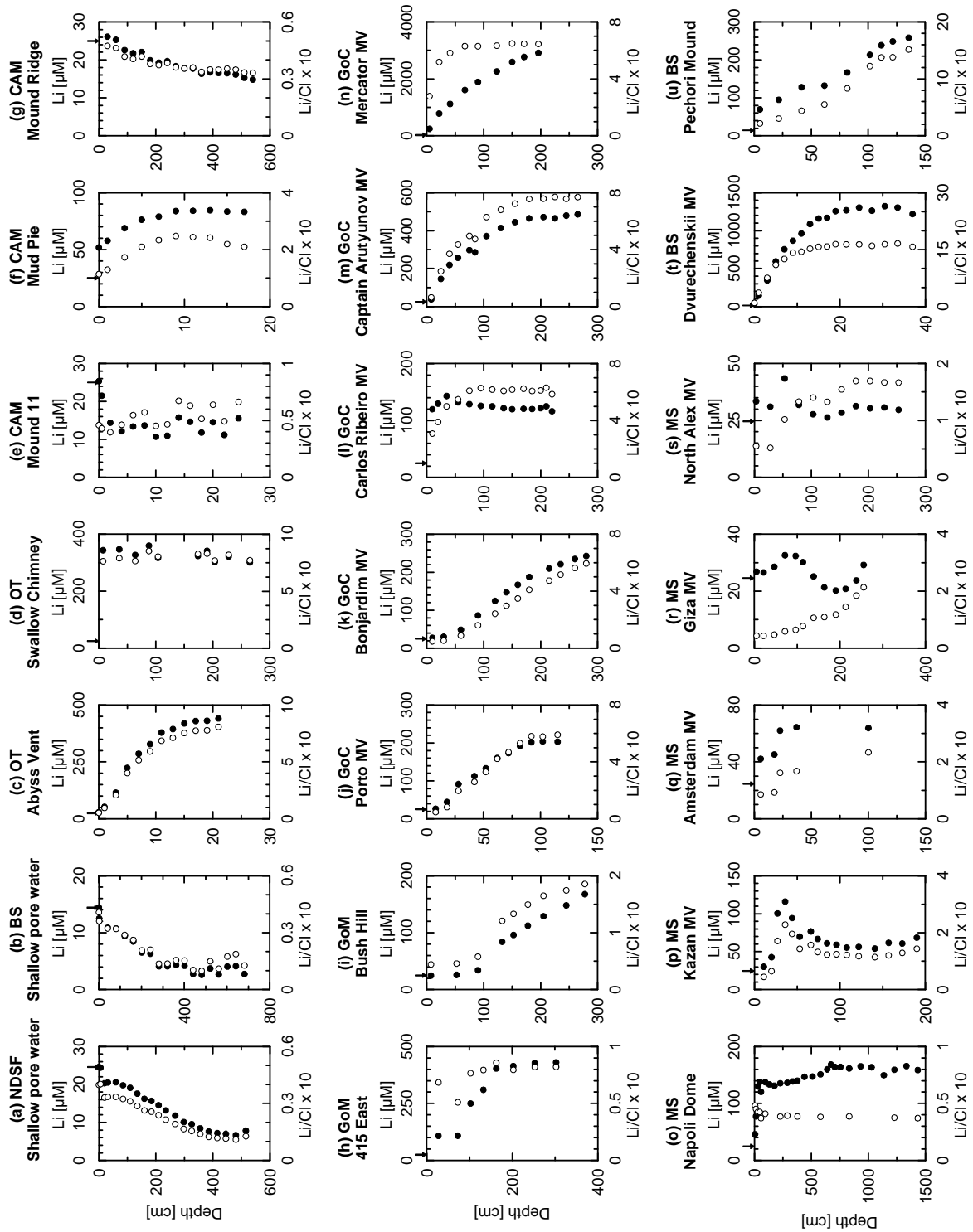


Figure IV.2. Pore water profiles of Li concentration (black circles) and Li/Cl ratio (open circles) for all studied sediment cores. Arrows on upper axis indicate normal seawater Li concentration ($26 \mu\text{M}$). Pore water profiles of different cores from the same site are similar to each other. Therefore, only one profile per site is shown ((l) 174-GC9, (n) 239-GC20, (p) AX18GC1, (q) AX02AP2, (r) GC5, (t) GeoB11977). Abbreviations for study areas are as follows: NDSF = Nile deep sea fan; BS = Black Sea; OT = Okinawa Trough; CAM = Central American margin; GoM = Gulf of Mexico; GoC = Gulf of Cadiz; MS = Mediterranean Sea.

Table IV.2. Pore water and bottom water (BW) data for Cl, Li, $\delta^7\text{Li}$ and $^{87}\text{Sr}/^{86}\text{Sr}$.

Area	Location	Core	Depth [cm]	Cl [mM]	Li [μM]	$\delta^7\text{Li}$ [‰]	$^{87}\text{Sr}/^{86}\text{Sr}$
<i>Reference sites</i>							
Gulf of Cadiz		139-MUC2	BW	559	24.0	30.9	0.709179
Nile deep-sea fan		MUC28	BW	618	24.6	30.9	0.709200
		GC2	109.5	615	19.1	29.1	
			297.5	610	10.1	30.9	0.709130 ^d
			415.5	609	7.2	29.6	0.709100 ^d
Black Sea		GeoB11905	1.0	353	14.4	32.3	0.709136 ^d
		GeoB11974	301.5	300	4.1	31.9	
Okinawa Trough	Abyss Vent	MUC28	21.0	546	204	5.8	0.709323
		44PC33	21.0	553	441	2.7	0.709483
	Swallow Chimney	34GC1	36.0	441	347	1.1	0.709788
Mediterranean Sea	Discovery brine	PP28CT ^c	265.0	392	301	-0.7	0.709829
			3672.0	9550	310	25.0	
			3677.0	9550	310	25.1	0.708961
	Bannock brine	PP09CT ^c	I-3460	5300	270	24.5	
			I-3505	5320	280	24.8	0.708650
			II-3612	5350	300	24.3	0.708629
<i>Seep sites</i>							
Central American margin	Mound 11	TVMUC127	19.0	230	13.2	29.6	
			23.5	230	13.4	29.9	0.708699
	Mud Pie	108/78/27	9.0	339	83.9	23.7	0.707320
			11.0	345	84.1	24.4	
			510.0	445	11.2	27.6	
Gulf of Mexico ^a	Mound Ridge	GC219	540.0	424	11.0	27.2	0.709126
			202.5	5200	414	45.7	0.708629
			252.5	5210	428	45.4	
	GC 415 East	TGC3	302.5	5240	430	44.8	0.708625
			302.5-r			44.7	
			245.0	849	148	23.3	
Gulf of Cadiz ^b	Porto MV	143-GC3	277.5	903	168	23.6	0.708663
			18.0	539	44	24.2	0.708676
			62.0	380	160	15.3	0.707668
	Bonjardim MV	130-GC1	102.0	353	204	12.1	0.707534
			115.0	344	203	12.2	0.707536
Carlos Ribeiro MV	154GC5	160.0	480	167	19.6	0.708694	
		180.0	458	188	19.5		
		200.0	199	122	19.7	0.708208	
			220.0	199	116	20.0	0.708208

continued on next page

^a $^{87}\text{Sr}/^{86}\text{Sr}$ data from Reitz et al. (2007).^b Data from Scholz et al. (2009).^c Water depth in meter below sea surface.^d Measured on samples from neighboring depth interval.

Table IV.2. Continued.

Area	Location	Core	Depth [cm]	Cl [mM]	Li [μM]	$\delta^7\text{Li}$ [‰]	$^{87}\text{Sr}/^{86}\text{Sr}$
Gulf of Cadiz ^b	Captain Arutyunov MV	174-GC9	245.0	633	479	16.3	0.709922
		205-GC13	270.0	623	503	17.2	0.709910 ^d
	Mercator MV	239-GC20	171.0	4280	2770	12.5	0.710626
		263-GC28	196.0	4510	2910	12.5	0.710613
Mediterranean Sea	Napoli Dome	KC11	116.0	5080	3270	11.9	0.710628
			832.0	4190	162	17.1	
			1228.0	4190	159	17.2	
	Kazan MV	AX18GC1	1433.0	4190	159	17.7	0.708407
			46.0	254	57.3	16.6	
			62.5	198	68.0	16.6	0.707938
			11.0	672	30.1	30.9	
	Amsterdam MV	AX02AP2	36.0	508	116	14.7	0.707932
			173.0	470	60.7	22.7	
			37.0	383	64.4	22.0	
	Giza MV	GC5	100.0	273	63.8	20.6	
			55.0	299	66.8	22.2	
			76.0	246	65.6	22.1	0.708550
			96.5	506	32.4	23.0	
North Alex MV	GC100	190.5	172	20.2	22.8		
		255.5	137	29.2	20.7	0.707820	
		219.5	165	29.1	21.9	0.707642 ^d	
		53.0	427	43.5	20.6	0.706590 ^d	
		128.0	199	26.3	21.9	0.706587 ^d	
Black Sea	Dvurechenskii MV	GeoB11977	203.0	179	30.3	19.6	
			30.5	805	1322	7.5	0.708310
			33.5	784	1300	7.7	
	Pechori Mound	GeoB11978	30.5	786	1240	7.5	
			33.5	789	1230	7.6	
			121.5	180	249	14.0	0.707890
			135.5	170	258	14.1	

^a $^{87}\text{Sr}/^{86}\text{Sr}$ data from Reitz et al. (2007).

^b Data from Scholz et al. (2009).

^c Water depth in meter below sea surface.

^d Measured on samples from neighboring depth interval.

In accordance with previous studies (e.g. Hensen et al., 2007; Scholz et al., 2009), pore waters from below the mixing zone between seawater and upwelling fluid will be referred to as ‘deep fluid’ in the following sections. Most deep fluids display Cl concentrations below local bottom water values (Table IV.2), which indicates that they have been affected by clay mineral dewatering (cf. Dählmann and De Lange, 2003; Hensen et al., 2004, 2007; Haese et al., 2006). Chloride concentrations above seawater at a few locations are related to dissolution of evaporite minerals (e.g. Green Canyon 415 East, Reitz et al., 2007; Mercator MV, Scholz et al.,

2009; Napoli Dome, Dählmann and De Lange, 2003; Dvurechenskii MV, Aloisi et al., 2004). Lithium enrichments above local bottom water values or elevated Li/Cl ratios in most cores indicate release of Li from sediments or rocks during diagenetic processes. Exceptions are two sites at the Central American margin (Mound 11, Mound Ridge; Figure IV.2e and g) where Li concentrations and Li/Cl ratios are constant or even decrease with depth. The $\delta^7\text{Li}$ of deep fluids varies over a broad range from +7.5 ‰ at Dvurechenskii MV in the Black Sea to +45.7 ‰ at Green Canyon 415 East in the Gulf of Mexico (Table IV.2).

IV.5. Discussion

IV.5.1. Controls on the lithium isotope composition of marine pore fluids

Most of the cold seep fluids investigated here originate from much greater sediment depths than may be reached by conventional coring techniques. A general concept of the controls on their Li isotope signature may be obtained by comparing the presented results with reference data that have been collected in related marine settings. Figure IV.3a presents a compilation of Li concentration and $\delta^7\text{Li}$ data of vent and pore fluids from normal ridge crest and sediment-hosted hydrothermal systems and of deep-seated interstitial fluids from the ODP (see Appendix A for table of data and references). The interstitial fluids are grouped into low-temperature and high-temperature diagenetic pore fluids according to the original data interpretation. Processes referred to as low-temperature diagenesis are cation-exchange and Li uptake by authigenic clay minerals in shallow sediments (e.g. Zhang et al., 1998; James and Palmer, 2000). In contrast, Li release from primary minerals at elevated temperatures ($>\sim 50\text{ }^\circ\text{C}$) (You et al., 1995; Chan and Kastner, 2000) coupled to uptake of Li by secondary minerals (James and Palmer, 2000) represents the major high-temperature diagenetic process. The reference data plotted in Figure IV.3a show a pronounced negative correlation between $\delta^7\text{Li}$ and Li concentration. This general trend may be expressed by the following empirical relationship:

$$\delta^7\text{Li} = -6.0(\pm 0.3) \cdot \ln[\text{Li}] + 51(\pm 1.2) \quad (\text{IV.6})$$

The different fluid types define distinct Li and $\delta^7\text{Li}$ ranges which are ordered according to increasing reaction temperature within the respective geological systems (low-temperature diagenetic – high-temperature diagenetic – hydrothermal). This general sequence is also

confirmed by the new reference data of pore waters from shallow, hemipelagic sediments and hydrothermal pore fluids from the Okinawa Trough (Figure IV.3a).

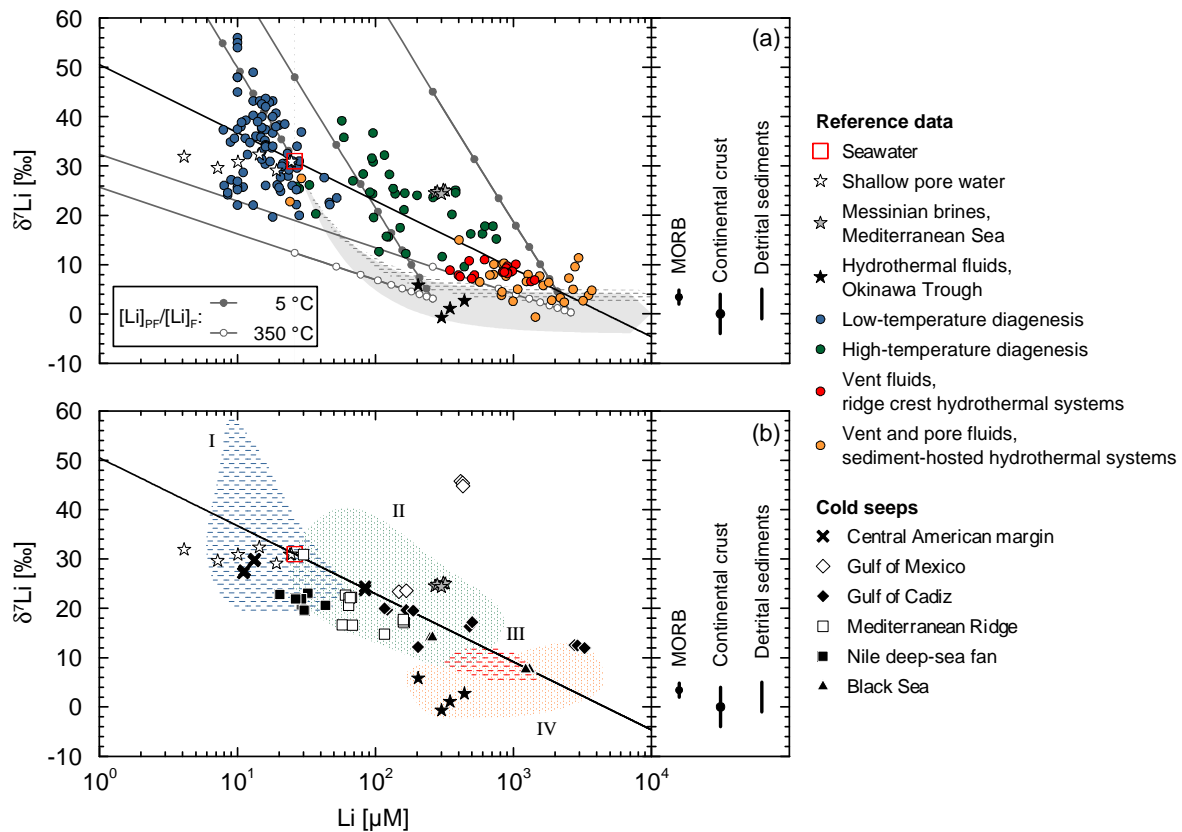


Figure IV.3. Plots of $\delta^7\text{Li}$ versus Li concentration for reference data (a) and cold seep fluids (b). Note logarithmic scale of x-axis. Reference data are grouped into low-temperature diagenetic fluids, high-temperature diagenetic fluids, vent fluids from ridge crest hydrothermal systems and vent and pore fluids from sediment-hosted hydrothermal systems (Chan et al., 1993, 1994; You et al., 1995; Zhang et al., 1998; James et al., 1999; Chan and Kastner, 2000; James and Palmer, 2000; You et al., 2003; Foustoukos et al., 2004). A table including all literature data is given in Appendix A. Vertical bars in the inlet on the right-hand side depict the average isotopic composition of MORB (Tomascak et al., 2008), upper continental crust (Teng et al., 2004) and detrital marine sediments (Chan et al., 2006). Thick black lines in both diagrams represent the logarithmic regression through all reference data ($\delta^7\text{Li} = -6.0(\pm 0.3) \cdot \ln[\text{Li}] + 51(\pm 1.2)$; $R^2 = 0.76$). Shaded arrays in (a) indicate mixing between seawater Li and Li from fresh MORB (upper array) and the upper continental crust (lower array). The gray lines in (a) have been calculated using a Rayleigh fractionation model in order to exemplify the evolution of pore fluids during progressive Li uptake by authigenic clay minerals at 5 and 350 °C. Nodes on the gray lines depict the fraction of initial Li (26, 260 and 2600 μM) remaining in the fluid ($[\text{Li}]_{\text{PF}}/[\text{Li}]_{\text{F}} = 1.0 - 0.1$). Colored domains in (b) encompass the Li concentration and $\delta^7\text{Li}$ ranges of reference fluid types: I = low-temperature diagenesis; II = high-temperature diagenesis; III = ridge-crest hydrothermal systems; IV = sediment-hosted hydrothermal systems. See text for further explanation.

IV.5.1.1. Hydrothermal fluids

Fluids from hydrothermal systems plot close to or within the average range of $\delta^7\text{Li}$ values reported for MORB and detrital sediment, respectively (bars on right-hand side of Figure IV.3a). A straightforward explanation for this isotopic composition could be simple leaching of Li from minerals without any further reaction. The $\delta^7\text{Li}$ of a fluid (subscript F) resulting from binary mixing between seawater Li (subscript SW) and solid phase Li (subscript SP) can be written as follows:

$$\delta^7 Li_F = \frac{[Li]_{SW}}{[Li]_F} \cdot \delta^7 Li_{SW} + \frac{[Li]_{SP}}{[Li]_F} \cdot \delta^7 Li_{SP} \quad (\text{IV.7})$$

The shaded mixing arrays in Figure IV.3 were calculated applying a $\delta^7\text{Li}_{SW}$ of +31 ‰ (Millet et al., 2004) and recently reported $\delta^7\text{Li}$ ranges reported for MORB ($+3.4 \pm 1.4$ ‰; Tomascak et al., 2008) and for upper continental crust (0.0 ± 1.4 ‰; Teng et al., 2004). The average $\delta^7\text{Li}$ of the upper continental crust by Teng et al. (2004) is based on a variety of shales, loess, granites and other crustal composites. This average value is considered the best estimate of the isotopic composition of terrigenous sediments prior to interaction with fluids in diagenetic or near-shore hydrothermal environments.

Some of the fluids from sediment-hosted hydrothermal systems (e.g. those from the Okinawa Trough) plot within the mixing array between seawater and the upper continental crust (Figure IV.3a) suggesting that their $\delta^7\text{Li}$ is dominated by simple Li release from minerals. Most of the hydrothermal fluids, however, show a distinct offset from the mixing arrays towards heavier $\delta^7\text{Li}$ values. Since isotope fractionation during incongruent mineral dissolution was found to be negligible (Pistiner and Henderson, 2003), this offset is commonly attributed to subsequent incorporation of isotopically light Li into secondary clay minerals (e.g. Chan et al., 1993; James et al., 1999). The average $\delta^7\text{Li}$ of hydrothermal fluids is $+8.6 \pm 1.3$ ‰ for sediment-free systems and $+5.7 \pm 3.1$ ‰ for sediment-hosted systems (the shallowest three samples from ODP Site 1038 in the Escabana Trough have not been considered in this calculation because of their disproportionately high content of pristine seawater; cf. James et al., 1999). Interestingly, the isotopic offset between fluids from sediment-free systems and MORB (5.2 ‰) and fluids from sediment-hosted systems and the upper continental crust (5.7 ‰) are in remarkable agreement. Differences in $\delta^7\text{Li}$ between the two fluid types reflect the isotopic difference between the upper continental crust and the upper mantle, which, in turn, has been attributed to preferential retention of the light Li

isotope during weathering of crustal material (Teng et al., 2004). Preservation of this primary signal in hydrothermal fluids is remarkable, considering the extent of alteration occurring subsequently to the release of Li in the hydrothermal reaction zone. Higher Li concentrations in fluids from sediment-hosted hydrothermal systems are attributed to higher Li concentrations in clastic marine sediment with respect to MORB (Chan et al., 2006; Tomascak et al., 2008) and, in addition, to the higher extraction efficiency of Li from sediments (James et al., 2003).

IV.5.1.2. Sediment interstitial fluids

In conformity with pore fluids of sediment-hosted hydrothermal systems, high-temperature diagenetic pore fluids are affected by Li release from sediments. Because of the lower temperatures prevailing in diagenetic environments, however, less Li is extracted from primary minerals and relatively more Li is sequestered by secondary minerals (Berger et al., 1988; James and Palmer, 1999; James et al., 2003). As a consequence, the pore fluids' Li concentrations are lower and their $\delta^7\text{Li}$ values are heavier compared to hydrothermal fluids (Figure IV.3a).

Depending on factors such as concentration-depth gradient, pore pressure and heat flow, Li in interstitial fluids undergoes advective and diffusive transport. In either case, pore water Li is unlikely to remain in contact with alteration products. As a consequence, the $\delta^7\text{Li}$ of the remaining pore fluid (subscript PF) can be approximated by a Rayleigh-type equation:

$$\delta^7 Li_{PF} = \left(\frac{[Li]_{PF}}{[Li]_F} \right)^{(\alpha-1)} \cdot (\delta^7 Li_F + 10^3) - 10^3 \quad (\text{IV.8})$$

The Li concentration and $\delta^7\text{Li}$ evolution of fluids during progressive Li loss to authigenic clay minerals is illustrated in Figure IV.3a. Starting values lie on the mixing line between seawater Li and Li derived from sediments at hundred-fold, ten-fold and normal seawater concentration. Fractionation factors between authigenic clay minerals and pore fluids for low and high temperature end members were taken from Chan et al. (1994): $\alpha_{\text{mineral-fluid}} = 0.981$ for 5 °C and $\alpha_{\text{mineral-fluid}} = 0.996$ for 350 °C.

Most pore water Li data that have been published so far for diagenetic environments may be explained with a combination of mixing with Li from sediments or rocks (see Section IV.4.1.1) and Raleigh fractionation during formation of secondary minerals (Figure IV.3b). The increasing distance of the general trend from the mixing arrays towards lower Li

concentrations reflects the enhanced isotope fractionation at lower temperatures (Chan et al., 1994). Fluids from low-temperature diagenetic environments are characterized by lower Li concentrations than seawater. Most of the fluids in this category display heavier $\delta^7\text{Li}$ values than seawater and plot close to the Rayleigh distillation line corresponding to Li uptake by secondary minerals at 5 °C (Figure IV.3a). Other low-temperature diagenetic fluids, however, show $\delta^7\text{Li}$ values equal to or even below seawater. Likewise, new Li data of pore waters from surficial hemipelagic sediments on the Nile deep-sea fan and in the eastern Black Sea show seawater-like $\delta^7\text{Li}$ values throughout the core (Table IV.2) although downward decreasing Li concentrations within the upper four meters indicate shallow Li removal (Figure IV.2a and b). This combination of $\delta^7\text{Li}$ and Li concentration cannot be produced through isotope fractionation during incorporation of seawater Li into secondary minerals at low temperature. Instead, another Li-consuming process, involving less or no isotope fractionation, has to be considered.

In the crystal lattice of clay minerals, Li either replaces Mg in the structural, octahedral sites or it occupies the interlayers as adsorbed cation. While structural incorporation produces a significant isotope fractionation, this is not necessarily the case for Li adsorption (Vigier et al., 2008). For instance, sorption experiments with vermiculite and kaolinite resulted in a significant Li isotope fractionation ($\alpha_{\text{mineral-fluid}}$ up to 0.971 (Zhang et al., 1998)). By contrast, Pistiner and Henderson (2003) and Vigier et al. (2008) observed no isotope fractionation during Li adsorption onto smectite. Smectite is the predominant clay mineral on the Nile deep-sea fan and in the eastern Black Sea (Venkatarathnam and Ryan, 1971; Stoffers and Müller, 1978). Accordingly, the downcore Li decrease in pore water at these sites is attributed to adsorption rather than structural incorporation. The large scattering of the low-temperature diagenetic fluids around seawater values suggests that adsorption onto smectite, or other mechanisms involving no or little isotope fractionation, play an important role in shallow marine sediments.

IV.5.1.3. Cold seep fluids

The overall pattern of processes identified in the previous section may be used as a general frame of reference for Li isotope exchange between fluids and silicate minerals in marine systems. Comparing signatures of the cold seep fluids with that reference frame is anticipated to reveal information about their origin and diagenetic evolution.

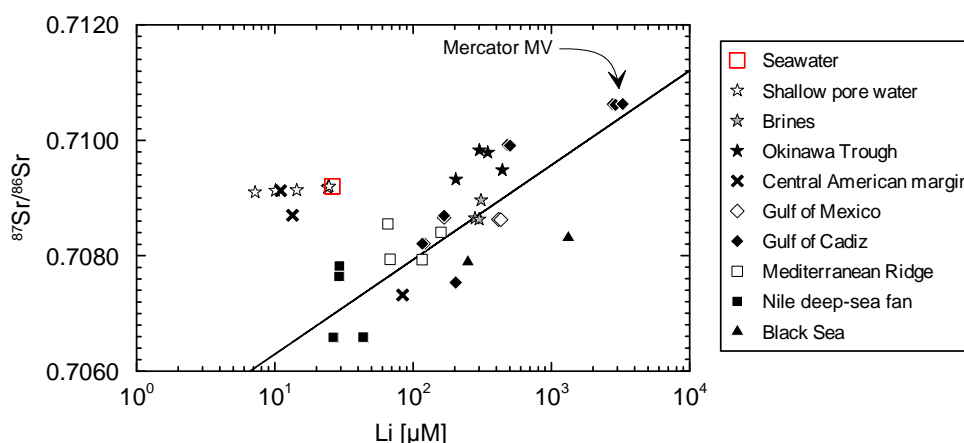


Figure IV.4. Plot of $^{87}\text{Sr}/^{86}\text{Sr}$ versus Li concentration for cold seep fluids. Note logarithmic scale of x-axis. The black line represents a logarithmic regressions through the cold seep data ($R^2 = 0.72$; fluids of Mound 11 and Mound Ridge have been excluded since they show little evidence for exchange with sediments).

Figure IV.3b shows the Li concentration and $\delta^7\text{Li}$ data of deep fluids from cold seeps along with the compositional ranges of reference fluids (cf. Figure IV.3a). Most of the cold seep fluids plot within the domain characteristic for high-temperature diagenetic environments. Many of the reference samples in this domain are décollement fluids whose Li isotopic composition has been explained with sediment dehydration reactions deep within subduction zones. Laboratory experiments conducted by Williams and Hervig (2005) revealed extensive uptake of isotopically light Li from solution during illitization of smectite. Release of Li from sediments at temperatures $>60^\circ\text{C}$ and incorporation into authigenic smectite-illite is in excellent agreement with the ubiquitous diagenetic signal of pore water freshening and other indicators for high-temperature fluid/sediment interactions at all seep locations investigated (Table IV.2; Dählmann and De Lange, 2003; Aloisi et al., 2004; Hensen et al., 2004; Haese et al., 2006; Hensen et al., 2007; Reitz et al., 2007). However, some of the cold seep fluids plot within other domains (e.g. hydrothermal or low-temperature diagenetic) suggesting a differing or more diverse combination of processes or influencing factors.

Pore fluids of two seep locations on the Central American margin, Mound 11 and Mound Ridge, display comparably heavy isotopic compositions close to seawater. At these sites, little downcore deviation from the Li/Cl ratio of seawater indicates that Li has not been involved in chemical reactions to a significant extent (Figure IV.2e and f).

Two seep sites, Dvurechenskii MV in the Black Sea and Mercator MV in the Gulf of Cadiz, plot within the domain of sediment-hosted hydrothermal systems. The fluid composition of Dvurechenskii MV is in excellent agreement with the empirical relationship between $\delta^7\text{Li}$ and Li concentration in marine systems (Figure IV.3b). Therefore, it is reasonable to anticipate

fluid-sediment interactions at temperatures beyond the range typical for clay mineral diagenesis (>150 °C) at this location. In case of Mercator MV, however, fluids have disproportionately high Li concentrations compared to their $\delta^7\text{Li}$ value (Figure IV.3b). Scholz et al. (2009) attributed the exceptionally high Li content of deep-sourced pore fluids in the Gulf of Cadiz to the terrigenous/continental provenance of sediments in this area. Felsic continental rocks are moderately enriched in Li compared to mafic material (Wedepohl, 1978). During chemical weathering, Li is retained in minerals and additional Li is taken up during transport of eroded solids into the ocean (Rudnick et al., 2004; Kısakürek et al., 2005). As a result, terrigenous sediments and sedimentary rocks have very high Li concentrations, sometimes exceeding 100 mg kg⁻¹ (Teng et al., 2004; Chan et al., 2006). The influence of the provenance and/or composition of marine sediments on the Li concentration of adjacent pore fluids is further illustrated in a plot of $^{87}\text{Sr}/^{86}\text{Sr}$ versus Li concentration in Figure IV.4. All cold seep fluids which have undergone appreciable interaction with sediments or rocks show a positive correlation between $^{87}\text{Sr}/^{86}\text{Sr}$ and Li concentration. Pore fluids of Mercator MV, the shallowest seep site in the Gulf of Cadiz (map 3 in Figure IV.1), have the most radiogenic $^{87}\text{Sr}/^{86}\text{Sr}$ ratios and the highest Li concentrations (Table IV.2). Accordingly, they are considered the terrigenous/continental deep fluid end member.

In contrast to that, pore fluids of Mud Pie on the Central American margin and seep locations on the Nile deep-sea fan display the least radiogenic $^{87}\text{Sr}/^{86}\text{Sr}$ ratios and the lowest Li concentrations (Table IV.2, Figure IV.4). Siliciclastic sediments in these areas are derived from Cenozoic, mostly mafic volcanic rocks in the Central American Arc (Kimura et al., 1997) and the Ethiopian highlands (Ryan et al., 1973; Foucault and Stanley, 1989), respectively. Such pristine, volcanogenic material contains little readily leachable Li compared to the extensively weathered and transported terrigenous matter of the Gulf of Cadiz. Moreover, alteration of labile volcanic minerals and ash particles to smectite and zeolites may further deplete ambient pore fluids in Li (Kastner and Rudnicki, 2004). Therefore, non-radiogenic $^{87}\text{Sr}/^{86}\text{Sr}$ ratios are coupled to lower dissolved Li concentrations in these areas. Owing to intense alteration of volcanic matter, smectite is a major constituent of sediments on both the Nile deep-sea fan and the Central American margin (Venkatarathnam and Ryan, 1971; Spinelli and Underwood, 2004). It was shown in Section IV.4.1.2 that adsorption of Li onto smectite may remove a considerable portion of dissolved Li from pore water, without causing any isotope fractionation. Due to this process, seep fluids of the Nile deep-sea fan display disproportionately low Li concentrations compared to their $\delta^7\text{Li}$ values and plot in the transition area between the high-temperature and the low-temperature diagenetic domains

in Figure IV.3b. Smectite has the largest cation exchange capacity of the common clay minerals in marine sediments (Stumm and Morgan, 1995) and is most abundant on convergent margins and in other volcanogenic settings (Griffin et al., 1968). In addition to alteration of ash, Li adsorption is likely to limit pore water Li concentrations in such areas. As a consequence, seep fluids with the least-radiogenic $^{87}\text{Sr}/^{86}\text{Sr}$ ratios and low Li concentrations in Figure IV.4 are considered the volcanogenic deep fluid end member.

Pore fluids of the cold seep Green Canyon 415 East in the Gulf of Mexico display particularly high Li concentrations and $\delta^7\text{Li}$ values beyond any of the reference domains (Figure IV.3b). Comparison with the Rayleigh distillation lines in Figure IV.3a demonstrates that near-complete scavenging of Li during transport at low temperature could have produced this fluid composition. Alternatively, anomalously high $\delta^7\text{Li}$ values and Li concentrations could be related to the strongly increased salinity of the fluids (Cl >5000 mM; Table IV.2), i.e. to individual fractionation mechanisms during brine formation.

IV.5.1.4. Marine brines

Evaporite beds and local occurrences of evaporated and infiltrated seawater, also referred to as primary brines, are common features in deeply buried continental margin sediments. Interaction of pore fluids with evaporite minerals or mixing with a primary brine can lead to a significant alteration of the original diagenetic signal. In general, coinciding enrichment of Li, Cl and Na in many deep-seated interstitial fluids (Figure IV.5; e.g. Bernasconi, 1999; Aloisi et al., 2004; Reitz et al., 2007; Scholz et al., 2009) calls for a systematic investigation of Li isotopes in hypersaline, sedimentary environments. Figure IV.5a shows Na and Cl data for all cold seep fluids with elevated salinity as well as for the Discovery and Bannock brines. The evaporation pathway of seawater and a line denoting Na/Cl ratios of unity are shown for comparison. All hypersaline pore fluids contain equimolar proportions of Na and Cl which indicates that dissolution of halite (NaCl) is the most common reason for elevated pore water salinities at cold seeps. Proportions of Li to Cl, however, strongly diverge from each other (Figure IV.5b) suggesting that the Li enrichments are not related to halite dissolution. This inference is corroborated by the chemical composition of Discovery brine which has evolved through dissolution of late-stage evaporite minerals (mainly bischofite; Wallmann et al., 1997). Although late-stage evaporite minerals are by far more enriched in Li than halite (Sonnenfeld, 1984), Li concentrations of the Discovery brine fail to reach those measured in pore fluids.

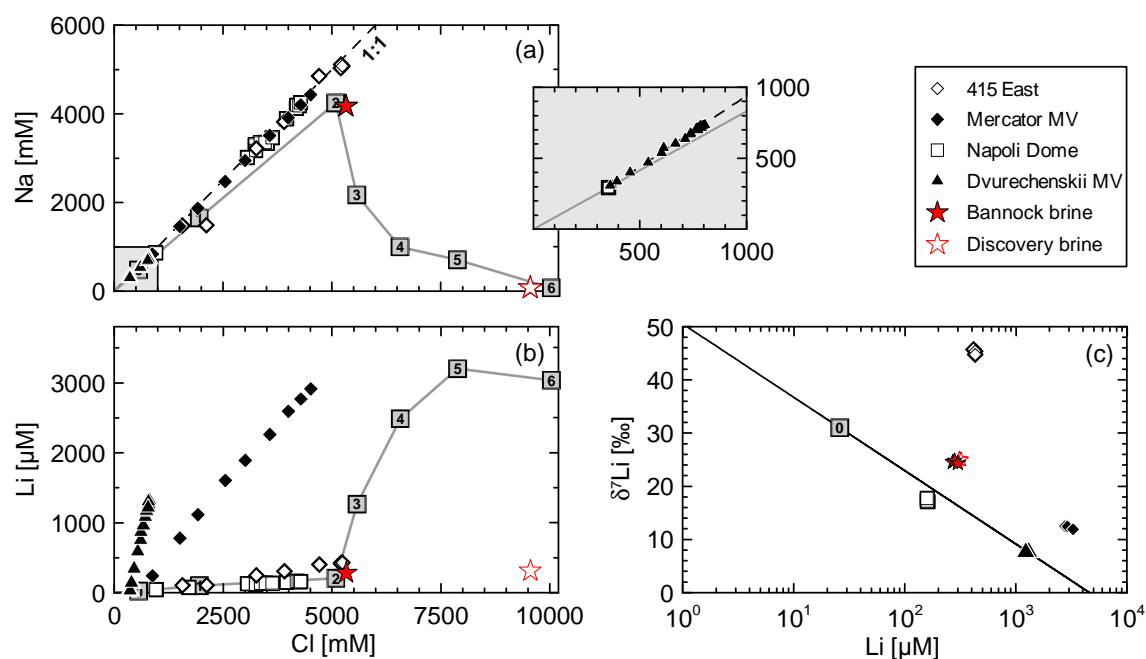


Figure IV.5. Plots of Na versus Cl (a), Li versus Cl (b) and $\delta^7\text{Li}$ versus Li (c) for hypersaline cold seep fluids as well as the Bannock and Discovery brines. Pore water profiles of different cores from the same site resemble each other. Therefore, only one core per site is shown (cf. Figure IV.2). Gray lines and squares in (a) and (b) depict the chemical evolution of seawater during progressive evaporation and precipitation of evaporite minerals: 0 = seawater, 1 = gypsum, 2 = halite, 3 = epsomite, 4 = sylvite, 5 = carnallite and 6 = bischofite (from Fontes and Matray, 1993). The dashed line in (a) depicts Na/Cl ratios of unity. Due to the reduced salinity in the Black Sea, Na and Cl data of Dvurechenskii MV are shown in a separate plot with adapted scale. The black line in (c) represents the empirical relationship between $\delta^7\text{Li}$ value and Li concentration in marine systems (cf. Figure IV.3a). Note logarithmic scale of x-axis in (c).

Since Li contributions from evaporite minerals are minor, significant effects on the $\delta^7\text{Li}$ of pore fluids are only to be expected if the isotopic composition of the evaporite-derived Li strongly diverges from that of the fluids. The $\delta^7\text{Li}$ of pore fluids and brines is plotted versus Li concentrations in Figure IV.5c. Most of the samples, including the Bannock and Discovery brines, plot close to the general relationship between $\delta^7\text{Li}$ and Li concentration in marine systems (cf. Figure IV.3a). The isotopic compositions of the Bannock and Discovery brines are almost indistinguishable, although their chemical evolution is entirely different. This clearly shows that the offset in $\delta^7\text{Li}$ from seawater in both cases has not been produced during evaporation or precipitation of evaporite minerals. Two studies have addressed the Li isotopic composition of brines so far. Bottomley et al. (1999) analyzed brines of the Canadian Shield and inferred a marine origin based on $\delta^7\text{Li}$ values close to modern seawater. In contrast, Chan et al. (2002) found $\delta^7\text{Li}$ values lighter than seawater ($\delta^7\text{Li}$: +18.2 – +27.0 ‰) in Messinian oil field brines in Israel and attributed this to Li release from ambient sediments. This explanation is somewhat problematic in the present case, since Li concentrations of the

Bannock brine are in good agreement with its evolution through twelve-fold evaporation of seawater ($\text{Cl} = \sim 5300 \text{ mM}$; Table IV.2).

Another possible, but yet unexplored, reason for isotopic differences between brines and modern seawater are temporal changes in basin chemistry due to prolonged isolation from the global ocean. Müller and Mueller (1991) reported a shift of $^{87}\text{Sr}/^{86}\text{Sr}$ ratios below that of Messinian seawater in Mediterranean evaporites of upper Messinian age ($^{87}\text{Sr}/^{86}\text{Sr}$ decrease from 0.7089 to 0.7086). The authors attributed this trend to the increasing proportion of Sr derived from the Nile river ($^{87}\text{Sr}/^{86}\text{Sr} = 0.7076$; Müller and Mueller, 1991) in the isolated Mediterranean basin. In general, Li dissolved in river water has an isotopic composition intermediate between seawater and the catchment rocks (mean $\delta^7\text{Li}$ of major world rivers: +23.4 ‰; Huh et al., 1998). Consequently, a temporal shift towards less radiogenic $^{87}\text{Sr}/^{86}\text{Sr}$ ratios in the isolated Mediterranean basin should have been accompanied by a decrease in $\delta^7\text{Li}$ as well. The $^{87}\text{Sr}/^{86}\text{Sr}$ ratio of the Bannock brine is in agreement with the decreased Mediterranean seawater ratio during the late Messinian ($^{87}\text{Sr}/^{86}\text{Sr} = \sim 0.7086$; Table IV.2) and, thus, with an offset in $\delta^7\text{Li}$ from the world ocean. By contrast, the $^{87}\text{Sr}/^{86}\text{Sr}$ ratio of the Discovery brine is equal to the global Messinian ratio ($^{87}\text{Sr}/^{86}\text{Sr} = \sim 0.7089$; Table IV.2). Therefore, temporal changes in basin chemistry towards the upper Messinian could explain for differences in $\delta^7\text{Li}$ among the two brines (0.5 ‰ on average). The overall isotopic offset from global seawater (≥ 6 ‰), however, must be caused by a different mechanism.

The above discussion has demonstrated that the Li isotope signature of brines is entirely independent from the actual brine formation. Instead, isotopic exchange with ambient sediments during burial or upward transport must have transferred isotopically light Li into the saline solutions. The Li isotope signature resulting therefrom follows the empirical relationship between $\delta^7\text{Li}$ and Li concentration in marine systems (Figure IV.5c). It is therefore deduced that Li isotope systematics of marine brines does not underlie individual fractionation mechanisms.

IV.5.2. Lithium isotope fractionation during fluid advection

Lithium isotope constraints on the origin and evolution of pore fluids from comparison with reference fluids are limited by the differing modes of transport in the respective geological systems. In bare ridge-crest and most sediment-hosted hydrothermal systems, fluids are rapidly transferred to the seafloor through vigorous convection within the oceanic crust or

overlying sediments (Fisher, 2004). In non-advective interstitial waters of hemipelagic sediments, Li moves slowly along a concentration-depth gradient through molecular diffusion. In either case, most of the Li isotope fractionation recorded in the $\delta^7\text{Li}$ of fluids is likely to have occurred in a relatively narrow temperature range. This is an important prerequisite for the validity of the Rayleigh distillation approach outlined in Section IV.4.1.2. Compared to hydrothermal systems, fluid advection at cold seeps is much slower and subject to strong temporal fluctuations (e.g. Castec et al., 1995; Haese et al., 2006; Hensen et al., 2007). Pore fluids leach Li from deeply buried sediments at a depth of several km below seafloor and at temperatures between 50 °C and ~200 °C. Because of slow Darcy velocities, fluids may cool down during upward transport and Li exchange due to mineral authigenesis is likely to occur at multiple temperatures. Consequently, the accompanying isotope fractionation cannot be approximated with a single fractionation factor and the aforementioned Rayleigh approach is not applicable anymore.

In order to evaluate the influence of varying transport modes on the extent of Li isotope fractionation, we applied a transport-reaction model to simulate the ascent of deep-seated pore fluids to the seafloor. The height of the modeled sediment column and the boundary conditions were chosen to embrace as much of the heterogeneity encountered at the various seep and reference sites as possible. Although such a generalized model scenario cannot explain specific pore water profiles at single sites, it may well be used to retrace the major fractionation trends identified in Figure IV.3. The adopted sediment thickness of 2 km represents an intermediate value between typical fluid mobilization depths at cold seeps (~2 – >5 km; Kopf, 2002) and basement depths at sediment-hosted or ridge-flank

Table IV.3. Properties and boundary conditions applied in the numerical transport-reaction model.

Parameter	Value
Column length	2000 m
Temperature, sediment surface, T_{TOP}	5 °C
Temperature, lower boundary, T_{BOT}	65 °C
Porosity, sediment surface, ϕ_{TOP}	0.8
Porosity, lower boundary, ϕ_{BOT}	0.2
Attenuation coefficient, const	$1 \times 10^{-5} \text{ cm}^{-1}$
Sediment burial velocity, lower boundary, ω_{BOT}	0.01 cm a^{-1}
Upward fluid velocity, v_{TOP}	$0 - 0.3 \text{ cm a}^{-1}$
Rate constant for Li precipitation, k_{PPT}	$1 \times 10^{-4} \text{ a}^{-1}$
Li concentration, sediment surface, $[\text{Li}]_{\text{TOP}}$	26 μM
Li concentration, lower boundary, $[\text{Li}]_{\text{BOT}}$	2600 μM
$\delta^7\text{Li}$, sediment surface	+31 ‰
$\delta^7\text{Li}$, lower boundary	+0.3 ‰

hydrothermal systems ($\sim 0.1 - >1$ km; e.g. Davis et al., 1997; Fouquet et al., 1998). The Li concentration and $\delta^7\text{Li}$ value at the upper boundary correspond to average seawater values. The $\delta^7\text{Li}$ value at the lower boundary has been calculated from the mixing relationship between seawater and continental crust (Equation IV.7) assuming a Li concentration hundred times that of seawater (i.e. $2600 \mu\text{M}$). This concentration is in the upper range of values observed for cold seep and hydrothermal fluids (Figure IV.3a). Concentrations of ^6Li and ^7Li were calculated from $\delta^7\text{Li}$ values assuming a $^7\text{Li}/^6\text{Li}$ ratio of 12.02 for the NIST-SRM 8545 (Flesch et al., 1973).

It is known from laboratory experiments that the Li distribution coefficient between secondary minerals and fluids increases exponentially with decreasing temperature (Berger et al., 1988). However, the actual amount of Li sequestered by different minerals at a given temperature turned out to be strongly variable (Berger et al., 1988). For the present transport-reaction model, we have to consider a wide variety of mineral assemblages. Moreover, the amount of secondary minerals formed at the various sites is essentially unknown. For that reason, the following function was applied as a first order rate law for Li removal into secondary minerals:

$$R_{\text{Li}_{\text{PPT}}}(x, t) = k_{\text{PPT}} \cdot \exp(-0.5 \cdot T) \cdot [\text{Li}]_{\text{PF}}(x, t) \quad (\text{IV.9})$$

In agreement with Berger et al. (1988), the amount of Li precipitated (subscript PPT) depends on the Li concentration in the fluid and increases exponentially with decreasing temperature (T). The coefficient in the exponent was determined by adjusting the model to the general relationship between Li concentration and $\delta^7\text{Li}$ depicted in Figure IV.3. The rate constant for Li precipitation, k_{PPT} , characterizes the ability of different sediment types to form authigenic clay minerals. A k_{PPT} of $1 \times 10^{-4} \text{ a}^{-1}$ has proven to fit most of the variance in the data set. Temperature-dependent Li fractionation factors for Li uptake by authigenic minerals were calculated according to the empirical relationship by Chan et al. (1994) ($\alpha_{\text{PPT-PF}} = -1 \cdot 10^{-7} \cdot T^2 + 8 \cdot 10^{-5} \cdot T + 0.981$; T in $^{\circ}\text{C}$). The amount of ^6Li and ^7Li precipitated was obtained from the general equation defining the isotope fractionation factor:

$$\alpha_{\text{PPT-PF}} = \frac{\left[\frac{^7\text{Li}}{^6\text{Li}} \right]_{\text{PPT}}}{\left[\frac{^7\text{Li}}{^6\text{Li}} \right]_{\text{PF}}} \quad (\text{IV.10})$$

by substituting $[^7\text{Li}]_{\text{PPT}}$ with $[\text{Li}]_{\text{PPT}} - [^6\text{Li}]_{\text{PPT}}$:

$$[{}^6\text{Li}]_{PPT} = \frac{[Li]_{PPT}}{(\alpha_{PPT-PF} \cdot \left[\frac{{}^7\text{Li}}{{}^6\text{Li}} \right]_{PF} + 1)} \quad (\text{IV.11})$$

Note that ongoing leaching of Li during transport is not considered in the model. All parameters used to produce the model curves are summarized in Table IV.3 and in the caption of Figure IV.6.

Model scenarios 1 to 4 (lines in Figure IV.6 and IV.7) simulate transport of deep-seated fluids through sediments at a common rate constant, k_{PPT} , but varying upward fluid advection rates. Fluid advection rates were chosen to represent regional averages for sedimentary settings that are influenced by fluid seepage (e.g. Davie and Buffet, 2003; Hensen and Wallmann, 2005). At the absence of active upward advection, most of the dissolved Li is rapidly precipitated and the model curve traverses the domain of low-temperature diagenetic pore fluids (curve 1; Figure IV.6). Since much of the isotope fractionation in that scenario occurs in a narrow temperature range close to bottom water conditions, the resulting curve runs roughly parallel to the 5 °C-Rayleigh distillation line in Figure IV.3a. At a low advection rate of 0.003 cm a⁻¹, the effects of sediment burial, compaction and active fluid flow cancel out each other. A linear concentration-depth gradient (curve 2; Figure IV.7a) indicates that deep-sourced Li is transported upwards by molecular diffusion. Because of the slowness of this transport mechanism, however, intense precipitation of light Li prevents the deep-seated signal from reaching the sediment surface (Figure IV.6). The model curve corresponding to a moderate advection rate of 0.03 cm a⁻¹ traverses the lower half of the high-temperature diagenetic domain and follows the major trend of cold seep fluids (curve 3; Figure IV.6). The mixing zone between seawater and the original deep fluid is shifted into the uppermost 200 m of the modeled sediment column (Figure IV.7). This demonstrates that moderate pore water movement suffices to transmit a considerable portion of the deep-seated Li isotope signal into shallow sediments.

Increasing the advection rate by another order of magnitude results in Li concentrations and $\delta^7\text{Li}$ values equal to that of the original deep fluid in the entire sediment column (curve 4; Figure IV.6 and IV.7). This is in agreement with field observations at the eastern flank of the Juan de Fuca Ridge where hydrothermal basement fluids percolate through up to 900 m thick hemipelagic sediments. Because of low basement temperatures, the original Li concentration of fluids in that area is quite different from the one adopted in the present model.

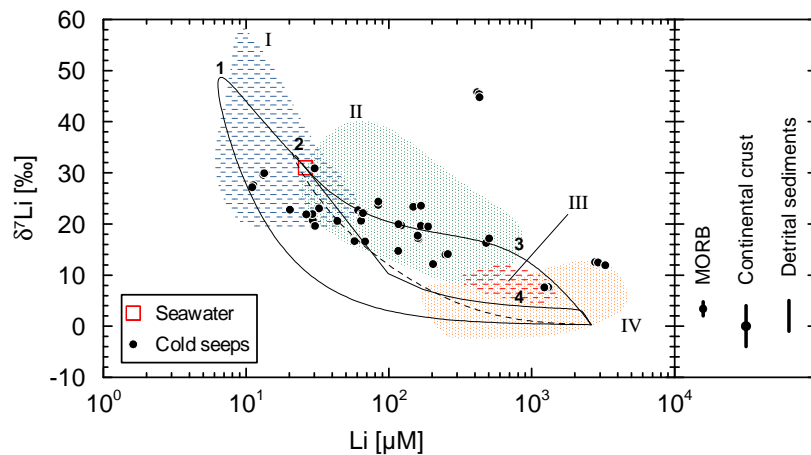


Figure IV.6. Plot of $\delta^7\text{Li}$ versus Li concentration showing results of the transport-reaction modeling. Note logarithmic scale of x-axis. The model simulates Li isotope fractionation during vertical transport of deep-seated pore fluids to the seafloor at different upward advection rates: 1: $v_{\text{TOP}} = 0.0 \text{ cm a}^{-1}$; 2: $v_{\text{TOP}} = 0.003 \text{ cm a}^{-1}$; 3: $v_{\text{TOP}} = 0.03 \text{ cm a}^{-1}$; 4: $v_{\text{TOP}} = 0.3 \text{ cm a}^{-1}$. Circles represent measured data of cold seep fluids. The colored domains depict the compositional ranges of reference fluid types: I = low-temperature diagenesis; II = high-temperature diagenesis; III = ridge-crest hydrothermal systems; IV = sediment-hosted hydrothermal systems.

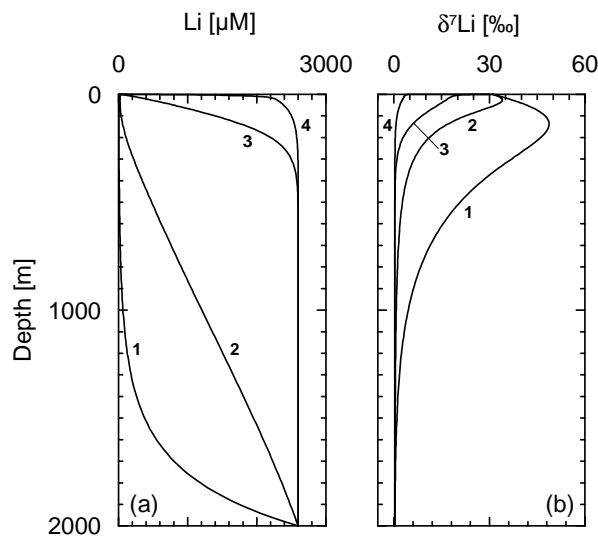


Figure IV.7. Pore water profiles of Li concentration (a) and $\delta^7\text{Li}$ (b) showing results of the transport-reaction modeling: 1: $v_{\text{TOP}} = 0.0 \text{ cm a}^{-1}$; 2: $v_{\text{TOP}} = 0.003 \text{ cm a}^{-1}$; 3: $v_{\text{TOP}} = 0.03 \text{ cm a}^{-1}$; 4: $v_{\text{TOP}} = 0.3 \text{ cm a}^{-1}$.

Nonetheless, Wheat and Mottl (2000) demonstrated, based on a comparative study of spring and pore fluids, that almost unaltered basement fluids may reach the top of the sediment column if fluid advection rates exceed a few mm a^{-1} . In an analogous manner, preservation of the deep-seated Li signal in fluids of Dvurechenskii MV may be explained with the high fluid advection rates prevailing at this site (Figure IV.2t and IV.3b; Aloisi et al., 2004). Higher temperatures at the model boundaries would further decrease Li precipitation during

upward transport and, thus, result in an even more pristine isotope signal at the sediment surface. The effect of high-temperatures (>300 °C) and advection rates on the $\delta^7\text{Li}$ of pore fluids is clearly demonstrated at Swallow Chimney, Okinawa Trough (Figure IV.3). At this site, rapid upward transport of fluids has pushed the mixing zone between seawater and hydrothermal pore fluids beyond the sediment/bottom water interface (Figure IV.2d) and the $\delta^7\text{Li}$ values are the lightest observed throughout this study.

IV.6. Summary and conclusions

In the present study, we evaluated the applicability of Li isotope systematics as a tracer for the origin and diagenetic evolution of pore fluids at cold seeps and similar submarine fluid escape structures. For that purpose, we established a general reference frame for Li isotope fractionation in marine systems. The major findings are summarized as follows:

- (1) Literature data for fluids from bare ridge crest and sediment-hosted hydrothermal systems as well as interstitial waters from normal ODP cores show a pronounced negative correlation between $\delta^7\text{Li}$ and Li concentration reflecting Li release from sediments or rocks and/or uptake of Li during clay mineral authigenesis.
- (2) Most cold seep fluids are in good agreement with this general trend and show higher Li concentrations and lower $\delta^7\text{Li}$ values than seawater. A common signal of clay mineral dehydration in most cold seep fluids indicates that diagenetic smectite/illite is the major sink for light pore water Li. Deviations from the general correlation trend are attributed to particularities in sediment composition and to transport-related fractionation mechanisms.
- (3) Pore fluids on passive margins receive high amounts of Li from intensely weathered, terrigenous and continental material. In contrast, on convergent margins and in other settings with strong volcanogenic input, Li concentrations in pore water are lower because of intense Li uptake during alteration of volcanic glass and other labile components. In addition, adsorption of Li by smectite at low temperature exerts an important control on pore water Li in volcanogenic settings. Separate investigation in shallow sediments revealed that this process is not accompanied by isotope fractionation.
- (4) The isotopic composition of two evolutionary distinct Mediterranean brines is in good agreement with the general correlation trend. It is inferred that saline pore fluids are

generally not affected by individual fractionation mechanisms related to evaporation or evaporite dissolution.

- (5) Application of a numerical transport-reaction model, simulating Li isotope fractionation during active upward transport of fluids, revealed that little upward advection suffices to transfer deep-seated diagenetic Li signals into shallow sediments. Once the advection rate exceeds a few mm a⁻¹ (assuming normal sedimentation rates) deep fluids that are almost unaltered by shallow fractionation processes may reach the upper end of the sediment column. The modeling results show that, if cautiously applied, Li isotope systematics of cold seep fluids may provide a valuable record of fluid/sediment or fluid/rock interaction that has been inherited several hundreds or thousands of meters below the seafloor.

Acknowledgements

We would like to acknowledge the support of officers and crews during seagoing expeditions with RVs *Aegeo*, *Marion Dufresne*, *Meteor*, *Pelagia*, *Poseidon* and *Sonne*. Furthermore, we are grateful to our colleagues A. Bleyer, B. Domeyer, A. Kolevica, C. Schulz and R. Surberg for assistance with analytical work at sea and in land-based laboratories. This is publication No. 185 of the Sonderforschungsbereich 574 “Volatiles and Fluids in Subduction Zones” at Kiel University. Financial support was obtained by RWE-Dea through R&D project West Nile Delta (WND) and by the Federal Ministry of Education and Research (BMBF) (Grant No. 03G0196B).

References

- Aloisi G., Drews M., Wallmann K. and Bohrmann G. (2004). Fluid expulsion from the Dvurechenskii mud volcano (Black Sea). Part I. Fluid sources and relevance to Li, B, Sr, I and dissolved inorganic nitrogen cycles. *Earth and Planetary Science Letters* **225**, 347-363.
- Berger G., Schott J. and Guy C. (1988). Behavior of Li, Rb and Cs during basalt glass and olivine dissolution and chlorite, smectite and zeolite precipitation from seawater: experimental investigations and modelization between 50° and 300 °C. *Chemical Geology* **71**, 297-312.
- Bernasconi S.M. (1999). Interstitial water chemistry in the Western Mediterranean: results from leg 161. *Proceedings of the Ocean Drilling Program Scientific Results* **161** (eds. Zahn R., Comas K.C. and Klaus A.), 423-432.
- Berner R.A. (1980). *Early diagenesis, a theoretical approach*. Princeton University Press, Princeton, NJ.

- Bohrmann G., Ivanov M., Foucher J.P., Spiess V., Bialas J., Greinert J., Weinrebe W., Abegg F., Aloisi G., Artemov Y., Blinova V., Drews M., Heidersdorf F., Krabbenhöft A., Klaucke I., Krastel S., Leder T., Polikarpov I., Saburova M., Schmale O., Seifert R., Volkonskaya A. and Zillmer M. (2003). Mud volcanoes and gas hydrates in the Black Sea: new data from Dvurechenskii and Odessa mud volcanoes. *Geo-Marine Letters* **23**, 239-249.
- Bottomley D.J., Katz A., Chan L.H., Starinsky A., Douglas M., Clark I.D. and Raven K.G. (1999). The origin and evolution of Canadian Shield brines: evaporation or freezing of seawater? New lithium isotope and geochemical evidence from the Slave craton. *Chemical Geology* **155**, 295-320.
- Boudreau B.P. (1996). The diffusive tortuosity of fine-grained unlithified sediments. *Geochimica et Cosmochimica Acta* **60**, 3139-3142.
- Boudreau B.P. (1997) *Diagenetic models and their implementation*. Springer-Verlag, Berlin.
- Castrec M., Dia A.N. and Boulègue J. (1996). Major- and trace-element and Sr isotope constraints on fluid circulation in the Barbados accretionary complex. Part II: circulation rates and fluxes. *Earth and Planetary Science Letters* **142**, 487-499.
- Camerlenghi A., Cita M.B., Hieke W. and Ricchiuto T. (1992). Geological evidence for mud diapirism on the Mediterranean Ridge accretionary complex. *Earth and Planetary Science Letters* **109**, 493-504.
- Chan L.H. and Kastner M. (2000). Lithium isotopic compositions of pore fluids and sediments in the Costa Rica subduction zone: implications for fluid processes and sediment contribution to the arc volcanoes. *Earth and Planetary Science Letters* **183**, 275-290.
- Chan L.H., Gieskes J.M., You C.F. and Edmond J.M. (1994). Lithium isotope geochemistry of sediments and hydrothermal fluids of the Guaymas Basin, Gulf of California. *Geochimica et Cosmochimica Acta* **58**, 4443-4454.
- Chan L.H., Edmond J.M. and Thompson G. (1993). A lithium isotope study of hot springs and metabasalts from mid-ocean ridge hydrothermal systems. *Journal of Geophysical Research* **98**, 9653-9659.
- Chan L.H., Starinsky A. and Katz A. (2002). The behavior of lithium and its isotopes in oilfield brines: evidence from the Heletz-Kokhav field, Israel. *Geochimica et Cosmochimica Acta* **66**, 615-623.
- Chan L.H., Leeman W.P. and Plank T. (2006). Lithium isotopic composition of marine sediments. *Geochemistry Geophysics Geosystems* **7**, Q06005, doi: 10.1029/2005GC001202.
- Dählmann A. and De Lange G.J. (2003). Fluid-sediment interactions at Eastern Mediterranean mud volcanoes: a stable isotope study from ODP Leg 160. *Earth and Planetary Science Letters* **212**, 377-391.
- Davie M.K. and Buffett B.A. (2003). Sources of methane gas hydrate: inferences from a comparison of observations and numerical models. *Earth and Planetary Science Letters* **206**, 51-56.
- Davis E.E., Fisher A.T., Firth J.V. and Shipboard Scientific Party (1997). 1. Introduction and summary: hydrothermal circulation in the oceanic crust and its consequences on the eastern flank of the Juan de Fuca Ridge. *Proceedings of the Ocean Drilling Program Initial Reports* **168** (eds. Davis E.E., Fisher A.T. and Firth J.V.), 7-21.
- De Lange G.J., Middelburg J.J., Van der Weijden C.H., Catalano G., Luther III G.W., Hydes D.J., Woititz J.R.W. and Klinkhammer G.P. (1990). Composition of anoxic hypersaline brines in the Tyro and Bannock Basins, eastern Mediterranean. *Marine Chemistry* **31**, 63-88.
- Fehn U., Snyder G.T. and Muramatsu Y. (2007). Iodine as a tracer of organic material: ¹²⁹I results from gas hydrate systems and fore arc fluids. *Journal of Geochemical Exploration* **95**, 66-80.
- Fisher A.T. (2004). Rates of flow and patterns of fluid circulation. In: *Hydrogeology of the Oceanic Lithosphere* (eds. Davis E.E. and Elderfield H.), 337-375. Cambridge University Press, Cambridge, NJ.
- Flesch G.D., Anderson A.R.Jr. and Svec H.J. (1973). A secondary isotopic standard for ⁶Li/⁷Li determinations. *International Journal of Mass Spectrometry and Ion Processes* **12**, 265-272.

- Fontes J.C. and Matray J.M. (1993). Geochemistry and origin of formation brines from the Paris Basin, France : 1. brines associated with Triassic salts. *Chemical Geology* **109**, 149-175.
- Foucault A. and Stanley D.J. (1989). Late Quaternary palaeoclimatic oscillations in East Africa recorded by heavy minerals in the Nile delta. *Nature* **339**, 44-46.
- Fouquet Y., Zierenberger R.A., Miller D.J. and Shipboard Scientific Party (1998). 1. Introduction: investigation of hydrothermal circulation and genesis of massive sulfide deposits at sediment-covered spreading centers at Middle Valley and Escabana Trough. *Proceedings of the Ocean Drilling Program Initial Reports* **169** (eds. Fouquet Y., Zierenberger R.A. and Miller D.J.), 7-15.
- Foustoukos D.I., James R.H., Berndt M.E. and Seyfried, J.W.E. (2004). Lithium isotopic systematics of hydrothermal vent fluids at the Main Endeavour Field, Northern Juan de Fuca Ridge. *Chemical Geology* **212**, 17-26.
- Gieskes J.M. and Mahn C. (2007). Halide systematics in interstitial waters of ocean drilling sediment cores. *Applied Geochemistry* **22**, 515-533.
- Glasby G.P. and Notsu K. (2003). Submarine hydrothermal mineralization in the Okinawa Trough, SW of Japan: an overview. *Ore Geology Reviews* **23**, 299-339.
- Grasshoff K., Erhardt M. and Kremling K. (2002). *Methods of seawater analysis*. Wiley-VCH, Weinheim.
- Haese R.R., Hensen C. and De Lange G.J. (2006). Pore water geochemistry of eastern Mediterranean mud volcanoes: implications for fluid transport and fluid origin. *Marine Geology* **22**, 191-208.
- Hensen C. and Wallmann K. (2005). Methane formation at Costa Rica continental margin - constraints for gas hydrate inventories and cross-décollement fluid flow. *Earth and Planetary Science Letters* **236**, 41-60.
- Hensen C., Wallmann K., Schmidt M., Ranero C.R. and Suess E. (2004). Fluid expulsion related to mud extrusion off Costa Rica - a window to the subducting slab. *Geology* **32**, 201-204.
- Hensen C., Nuzzo M., Hornibrook E., Pinheiro L.M., Bock B., Magalhães V.H. and Brückmann W. (2007). Sources of mud volcano fluids in the Gulf of Cadiz - indications for hydrothermal imprint. *Geochimica et Cosmochimica Acta* **71**, 1232-1248.
- Hyndman R.D. and Davis E.E. (1992). A mechanism for the formation of methane hydrate and seafloor bottom-simulating reflectors by vertical fluid expulsion. *Journal of Geophysical Research*. **97**, 7025-7041.
- Huh Y., Chan L.H., Zhang L. and Edmond J.M. (1998). Lithium and its isotopes in major world rivers: implications for weathering and the oceanic budget. *Geochimica et Cosmochimica Acta* **62**, 2039-2051.
- Ishikawa T. and Nakamura E. (1993). Boron isotope systematics of marine sediments. *Earth and Planetary Science Letters* **117**, 567-580.
- James R.H. and Palmer M.R. (2000). Marine geochemical cycles of the alkali elements and boron: the role of sediments. *Geochimica et Cosmochimica Acta* **64**, 3111-3122.
- James R.H., Rudnicki M.D. and Palmer M.R. (1999). The alkali element and boron geochemistry of the Escanaba Trough sediment-hosted hydrothermal system. *Earth and Planetary Science Letters* **171**, 157-169.
- James R.H., Allen D.E. and Seyfried W.E. (2003). An experimental study of alteration of oceanic crust and terrigenous sediments at moderate temperatures (51 to 350 °C): insights as to chemical processes in near-shore ridge-flank hydrothermal systems. *Geochimica et Cosmochimica Acta* **67**, 681-691.
- Jeffcoate A.B., Elliot T., Thomas A. and Bouman C. (2004). Precise, small sample size determinations of lithium isotopic compositions of geological reference material and modern seawater by ICP-MS. *Geostandards and Geoanalytical Research*. **28**, 161-172.
- Kastner M. and Rudnicki M.D. (2004). Ridge flank sediment-fluid interactions. In: *Hydrogeology of the oceanic lithosphere* (eds. Davis E.E. and Elderfield H.), 534-571. Cambridge University Press, Cambridge, NJ.

- Kastner M., Elderfield H. and Martin J.B. (1991). Fluids in convergent margins: what do we know about their composition, origin, role in diagenesis and importance for oceanic chemical fluxes. *Philosophical Transactions of the Royal Society of London: Physical Sciences and Engineering* **335**, 243-259.
- Kısakürek B., James R.H. and Harris N.B.W. (2005). Li and $\delta^7\text{Li}$ in Himalayan rivers: proxies for silicate weathering. *Earth and Planetary Science Letters* **237**, 387-401.
- Konno U., Tsunogai U., Nakagawa F., Nakaseama M., Ishibashi J.I., Nunoura T. and Nakamura K.I. (2006). Liquid CO_2 venting on the seafloor: Yonaguni Knoll IV hydrothermal system, Okinawa Trough. *Geophysical Research Letters* **33**, L16607, doi:10.1029/2006GL026115.
- Kopf A.J. (2002). Significance of mud volcanism. *Reviews on Geophysics* **40**, 1005, doi:10.1029/2000RG000093.
- Limonov A.F., VanWeering T.C.E., Kenyon N.H., Ivanov M.K. and Meisner L.B. (1997). Seabed morphology and gas venting in the Black Sea mud volcano area: observations with the MAK-1 deep-tow side scan sonar and bottom profiler. *Marine Geology* **137**, 121-136.
- Loncke L., Mascle J. and Fanil Scientific Parties (2004). Mud volcanoes, gas chimneys, pockmarks and mounds in the Nile deep-sea fan (Eastern Mediterranean): geophysical evidences. *Marine and Petroleum Geology* **21**, 669-689.
- Loncke L., Gaullier V., Mascle J., Vendeville B. and Camera L. (2006). The Nile deep-sea fan: an example of interacting sedimentation, salt tectonics, and inherited subsalt paleotopographic features. *Marine and Petroleum Geology* **23**, 297-315.
- Medialdea T., Somoza L., Pinheiro L. M., Fernández-Puga M.C., Vázquez J.T., León R., Ivanov M.K., Magalhaes V., Díaz-del-Río V. and Vegas, R. (2009). Tectonics and mud volcano development in the Gulf of Cádiz. *Marine Geology* **261**, 48-63.
- Millot R., Guerrot C. and Vigier N. (2004). Accurate and high-precision measurement of lithium in two reference materials by MC-ICP-MS. *Geostandards and Geoanalytical Research* **28**, 153-159.
- Moore J. C. and Vrolijk P. (1992). Fluids in accretionary prisms. *Reviews on Geophysics* **30**, 113-135.
- Müller D.W. and Mueller P.A. (1991). Origin and age of the Mediterranean Messinian evaporites: implications from Sr isotopes. *Earth and Planetary Science Letters* **107**, 1-12.
- Nikishin A.M., Korotaev M.V., Ershov A.V. and Brunet M.F. (2003). The Black Sea basin: tectonic history and Neogene-Quaternary rapid subsidence modelling. *Sedimentary Geology* **156**, 149-168.
- Pinheiro L.M., Ivanov M., Kenyon N., Maghalães V., Somoza L., Gardner J., Kopf A.J., Van Rensbergen P., Monteiro J.H. and the Euromargins Team (2005). Structural control of mud volcanism and hydrocarbon-rich fluid seepage in the Gulf of Cadiz: results from TTR-15 and previous cruises. *CIESM Workshop Monographs* **29**, 53-58.
- Pistiner J.S. and Henderson G.M. (2003). Lithium-isotope fractionation during continental weathering processes. *Earth and Planetary Science Letters* **214**, 327-339.
- Ranero C.R. and Von Huene R. (2000). Subduction erosion along the Middle America convergent margin. *Nature* **404**, 748-752.
- Reitz A., Haeckel M., Wallmann K., Hensen C. and Heeschen K. (2007). Origin of salt-enriched pore fluids in the northern Gulf of Mexico. *Earth and Planetary Science Letters* **259**, 266-282.
- Roberts H.H. and Carney R.S. (1997). Evidence of episodic fluid, gas, and sediment venting on the northern Gulf of Mexico continental slope. *Economic Geology and the Bulletin of the Society of Economic Geologists* **92**, 863-879.
- Robertson A.H.F. and Ocean Drilling Program Leg 160 Scientific Party (1996). Mud volcanism on the Mediterranean Ridge: initial results of Ocean Drilling Program Leg 160. *Geology* **24**, 239-242.

- Robertson A.H.F. and Kopf A.J. (1998). 50. Tectonic setting and processes of mud volcanism on the Mediterranean Ridge accretionary complex: evidence from leg 160. *Proceedings of the Ocean Drilling Program Scientific Results* **160** (eds. Robertson A.H.F., Emeis K.-C., Richter C. and Camerlenghi A.), 665-680.
- Ryan W.B.F., Venkatarathnam K. and Wezel F.C. (1973). 25.2. Mineralogical composition of the Nile Cone, Mediterranean Ridge, and Strabo Trench sandstones and clays. *Initial Reports of the Deep Sea Drilling Project* **13**, 731-745.
- Rudnick R.L., Tomascak P.B., Njo H.B. and Gardner L.R. (2004). Extreme lithium isotopic fractionation during continental weathering revealed in saprolites from South California. *Chemical Geology* **212**, 45-57.
- Scholz F., Hensen C., Reitz A., Romer R.L., Liebetrau V., Meixner A., Weise S.M. and Haeckel M. (2009). Isotopic evidence ($^{87}\text{Sr}/^{86}\text{Sr}$, $\delta^7\text{Li}$) for alteration of the oceanic crust at deep-rooted mud volcanoes in the Gulf of Cadiz, NE Atlantic Ocean. *Geochimica et Cosmochimica Acta* **73**, 5444-5459.
- Sonnenfeld P. (1984). *Brines and evaporites*. Academic Press, New York, NY.
- Środoń J. (1999). Nature of mixed-layer clays and mechanisms of their formation and alteration. *Annual Review on Earth and Planetary Sciences* **27**, 19-53.
- Stoffers P. and Müller G. (1978). 7. Mineralogy and lithofacies of Black Sea sediments Leg 42B Deep-sea Drilling Project. *Initial Reports of the Deep Sea Drilling Project* **42**, 373-411.
- Suess E., Torres M.E., Bohrmann G., Collier R.W., Greinert J., Linke P., Rehder G., Trehu A., Wallmann K., Winckler G. and Zuleger E. (1999). Gas hydrate destabilization: enhanced dewatering, benthic material turnover and large methane plumes at the Cascadia convergent margin. *Earth and Planetary Science Letters* **170**, 1-15.
- Teng F.Z., McDonough W.F., Rudnick R.L., Dalpe C., Tomascak P.B., Chappell B.W. and Gao S. (2004). Lithium isotopic composition and concentration of the upper continental crust. *Geochimica et Cosmochimica Acta* **68**, 4167-4178.
- Tomascak P.B. (2004). Developments in the understanding and application of lithium isotopes in the earth and planetary sciences. In: *Geochemistry of non-traditional stable isotopes. Reviews in Mineralogy and Geochemistry* **55** (eds. Johnson C.M., Beard C.L. and Albarède F.), 153-195. Mineralogical Society of America, Washington D.C.
- Tomascak P.B., Carlson R.W. and Shirley S.B. (1999). Accurate and precise determination of Li isotopic compositions by multi-collector sector ICP-MS. *Chemical Geology* **158**, 145-154.
- Tomascak P.B., Langmuir C.H., Le Roux P.J. and Shirley S.B. (2008). Lithium isotopes in global mid-ocean ridge basalts. *Geochimica et Cosmochimica Acta* **72**, 1626-1637.
- Vengosh A., De Lange G.J. and Starinsky A. (1998). Boron isotope and geochemical evidence for the origin of Urania and Bannock brines at the eastern Mediterranean: effect of water-rock interactions. *Geochimica et Cosmochimica Acta* **62**, 3221-3228.
- Venkatarathnam K. and Ryan W.B.F. (1971). Dispersal patterns of clay minerals in the sediments of the eastern Mediterranean Sea. *Marine Geology* **11**, 261-282.
- Vigier N., Decarreau A., Millot R., Carignan J., Petit S. and France-Lanord C. (2008). Quantifying Li isotope fractionation during smectite formation and implications for the Li cycle. *Geochimica et Cosmochimica Acta* **72**, 780-792.
- Wallmann K., Suess E., Westbrook G.H., Winckler G. and Cita M.B. (1997). Salty brines on the Mediterranean sea floor. *Nature* **387**, 31-32.
- Wallmann K., Drews M., Aloisi G. and Bohrmann G. (2006a). Methane discharge into the Black Sea and the global ocean via fluid flow through submarine mud volcanoes. *Earth and Planetary Science Letters* **248**, 545-560.

- Wallmann K., Aloisi G., Haeckel M., Obzhairov A., Pavlova G. and Tishchenko P. (2006b). Kinetics of organic matter degradation, microbial methane generation, and gas hydrate formation in anoxic marine sediments. *Geochimica et Cosmochimica Acta* **70**, 3905-3972.
- Wallmann K., Aloisi G., Haeckel M., Tishchenko P., Pavlova G., Greinert J., Kutterolf S. and Eisenhauer A. (2008). Silicate weathering in anoxic marine sediments. *Geochimica et Cosmochimica Acta* **72**, 2895-2918.
- Wedepohl K.H. (1978). *Handbook of geochemistry II*. Springer-Verlag, Berlin.
- Wheat C.G. and Mottl M.J. (2000). Composition of pore and spring waters from Baby Bare: global implications of geochemical fluxes from a ridge flank hydrothermal system. *Geochimica et Cosmochimica Acta* **64**, 629-642.
- Williams L.B. and Hervig R.L. (2005). Lithium and boron isotopes in illite-smectite: the importance of crystal size. *Geochimica et Cosmochimica Acta* **69**, 5705-5716.
- Wunder B., Meixner A., Romer R.L. and Heinrich W. (2006). Temperature-dependent isotopic fractionation of lithium between clinopyroxene and high-pressure hydrous fluids. *Contributions to Mineralogy and Petrology* **151**, 112-120.
- Wunder B., Meixner A., Romer R.L., Feenstra A., Schettler G. and Heinrich W. (2007). Lithium isotope fractionation between Li-bearing staurolite, Li-mica and aqueous fluids: an experimental study. *Chemical Geology* **238**, 277-290.
- You C.F., Chan L.H., Spivack A.J. and Gieskes J.M. (1995). Lithium, boron, and their isotopes in sediments and pore waters of Ocean Drilling Program Site 808, Nankai Trough: implications for fluid expulsion in accretionary prisms. *Geology* **23**, 37-40.
- You C.F., Castillo P.R., Gieskes J.M., Chan L.H. and Spivack A.J. (1996). Trace element behavior in hydrothermal experiments: implications for fluid processes at shallow depths in subduction zones. *Earth and Planetary Science Letters* **140**, 41-52.
- You C.F., Chan L.H., Gieskes J.M. and Klinkhammer G.P. (2003). Seawater intrusion through the oceanic crust and carbonate sediment in the Equatorial Pacific: lithium abundance and isotopic evidence. *Geophysical Research Letters* **30**, doi:10.1029/2003GL018412.
- Zhang L., Chan L.H. and Gieskes J.M. (1998). Lithium isotope geochemistry of pore waters from ocean drilling program Sites 918 and 919, Irminger Basin. *Geochimica et Cosmochimica Acta* **62**, 2437-2450.
- Zitter T.A.C., Huguenot C. and Woodside J.M. (2005). Geology of mud volcanoes in the eastern Mediterranean from combined sidescan sonar and submersible surveys. *Deep-sea Research. Part I* **52**, 457-475.

Synthesis

A two-tier approach was adopted in this thesis to investigate how geological factors, such as the tectonic setting or the composition and provenance of sediments, affect diagenetic signals in deep-seated pore fluids. Chapter II and III dealt with a geochemical transect across the Gulf of Cadiz continental margin. Deep-sourced seep fluids in this area reflect the seaward decreasing intensity of interactions with terrigenous sediments and the increasing influence of crustal fluids, originating in the oceanic basement, across the margin. In view of this well-defined transition, the Gulf of Cadiz turned out to be a prime locality to investigate regional differences in controls on fluid chemistry. A more global approach was chosen in Chapter IV, where new and literature data for seep and vent sites in different ocean basins and in a large variety of geological settings were compiled. Contrasting seep fluids with hydrothermal fluids and pore waters from ODP cores sharpened the understanding of how specific isotopic proxies respond to varying environmental conditions.

An important finding of this study is that many tracers for diagenetic or hydrothermal exchange processes behave markedly different in different geological settings. Especially the provenance of sediments, e.g. terrigenous on passive margins versus volcanogenic on convergent margins, exerts an important control on the presence and intensity of diagenetic processes in the subsurface. Such differences have to be considered and thoroughly cross-checked (e.g. using $^{87}\text{Sr}/^{86}\text{Sr}$ ratios) when defining global systematics for the geochemistry of seep fluids.

Particular emphasis was given to cosmogenic iodine isotopes and stable Li isotopes in this study. The Gulf of Cadiz is the first marine setting where $^{129}\text{I}/\text{I}$ ratios in pore water are found to be governed by in situ production of ^{129}I through spontaneous fission of ^{238}U rather than organic matter diagenesis. Seaward decreasing $^{129}\text{I}/\text{I}$ ratios along the continent-ocean transect revealed that the relative amount and thickness of terrigenous sediments is the major factor controlling ^{129}I accumulation in pore water. Comparison of the presented results with literature data for ODP cores and terrestrial groundwater aquifers provided fundamental insights into the behavior and cycling of ^{129}I in earth surface reservoirs.

A large set of Li isotope data was collected for seep fluids from different ocean basins and geological settings in order to better constrain the behavior of Li isotopes during diagenesis and fluid transport. A compilation of the new seep data and literature data for ODP cores and hydrothermal fluids was used to establish a general frame of reference for Li isotope exchange between fluids and minerals in marine systems. Transport-related isotope fraction trends were evaluated by the aid of a transport-reaction model. It could be demonstrated that little pore water movement suffices to convey much of the Li isotope signal generated at depth into shallow sediments.

Application and re-evaluation of up-to-date isotopic proxies revealed that deep-sourced fluid flow may occur in much more diverse manifestation than previously thought. Many cold seep fluids share geochemical characteristics with fluids from sediment-covered ridge crest and ridge flank hydrothermal systems. Pore fluids at the distal mud volcanoes in the Gulf of Cadiz carry a signature from interaction with the oceanic basement. This is a remarkable finding considering the 6 km thick sediment cover in this area. It represents new geochemical evidence for a hydrological connection between oceanic crust and the water column at this crustal age (>140 Ma; Müller et al., 2008) and distance from the spreading axis. Apparently, consecutive fluid flow through basement rocks and sediments is not restricted to near-shore ridge crests and flanks or convergent ocean margins. Further manifestations of such 'intermediate fluid pathways' (Scholz et al., 2009) are likely to become discovered when centering geophysical and geochemical research activities on sediment-covered seamounts and fracture zones in the deep-sea. Exploration of these largely disregarded structures is essential for a sound understanding of material exchange between the oceanic lithosphere and the ocean.

References

- Müller R.D., Sdrolias M., Gaina C. and Roest W.R. (2008). Age, spreading rates, and spreading asymmetry of the world's ocean crust. *Geochemistry Geophysics Geosystems* **9**, Q04006, doi:10.1029/2007GC001743.
- Scholz F., Hensen C., Reitz R., Romer R.L., Liebetrau V., Meixner A., Weise S.M. and Haeckel M. (2009). Isotopic evidence ($^{87}\text{Sr}/^{86}\text{Sr}$, $\delta^7\text{Li}$) for alteration of the oceanic crust at deep-rooted mud volcanoes in the Gulf of Cadiz, NE Atlantic Ocean. *Geochimica et Cosmochimica Acta* **73**, 5444-5459.

Appendix A. Supporting material to chapter IV

Appendix A. Compilation of literature data of Chapter IV. The classification in low-temperature diagenetic fluids (LTD) and high-temperature diagenetic fluids (HTD) has been done according to the original interpretation. Citations refer to the reference list of Chapter IV.

Location	Site	Depth [m]	Li [μM]	$\delta^7\text{Li}$ [‰]	Classification	Reference
<i>Hydrothermal systems, vent fluids</i>						
Juna de Fuca Ridge	Main Endeavour Field		521	7.9		(Foustoukos et al., 2004)
			497	7.2		
			399	7.9		
			346	8.9		
			410	7.6		
East Pacific Rise	21 °N		902	9.7		(Chan et al., 1993)
			887	9.3		
			1040	10.1		
			1340	6.6		
			979	8.7		
East Pacific Rise	11-13 °N		904	8.4		
			1420	6.9		
			617	11.0		
			904	8.2		
			477	10.8		
Mid Atlantic Ridge	23 °N		839	8.6		
			858	8.5		
<i>Sediment-hosted hydrothermal systems, vent fluids</i>						
Guaymas Basin			1070	5.0		(Chan et al., 1994)
			721	10.1		
			955	8.6		
			882	7.7		
			993	2.6		

continued on next page

Appendix A. Continued.

Location	Site	Depth [m]	Li [μM]	$\delta^7\text{Li}$ [‰]	Classification	Reference
Guaymas Basin			830	10.1		(Chan et al., 1994)
			853	10.3		
Escabana Trough			1280	8.0		
			1240	6.6		
Mariana Trough			832	8.5		
<i>Sediment-hosted hydrothermal systems, pore fluids</i>						
Escabana Trough	ODP Site 1038	76.3	1440	-0.6		(James et al., 1999)
		34.0	818	3.8		
		23.4	1640	5.8		
		39.0	2700	5.0		
		23.0	2180	3.3		
		37.5	3500	3.8		
		53.0	2520	7.3		
		24.5	24.0	22.8		
		34.3	1550	7.7		
		45.1	2330	2.4		
		77.0	1890	2.8		
		126.1	3190	2.7		
		12.3	29.0	27.5		
		50.3	403	15.0		
		77.4	716	8.0		
		152.0	3690	4.8		
		170.3	2790	9.6		
		180.0	2960	11.4		
		191.2	1800	6.4		
		287.6	674	7.9		

continued on next page

Appendix A. Continued.

Location	Site	Depth [m]	Li [μM]	$\delta^7\text{Li}$ [‰]	Classification	Reference
Escabana Trough	ODP Site 1038	368.9	569	6.5		(James et al., 1999)
		402.4	826	4.5		
<i>Sediment pore fluids</i>						
Nankai Trough	ODP Site 808	500	200	24.1	HTD	(You et al., 1995) ^a
		650	380	25.1	HTD	
		700	380	24.6	HTD	
		800	490	16.3	HTD	
		900	440	9.6	HTD	
		960	595	16.3	HTD	
		1000	620	17.8	HTD	
		1100	710	17.8	HTD	
		1190	750	15.2	HTD	
		0.0	27	34.0	LTD	
		80.0	19	38.0	LTD	
		100.0	18	40.0	LTD	
		130.0	15	40.0	LTD	
E Equatorial Pacific	ODP Site 844	220.0	13	49.0	LTD	(You et al., 2003) ^a
		230.0	10	48.0	LTD	
		260.0	10	48.0	LTD	
		290.0	14	39.0	LTD	
		0.0	28	31.0	LTD	
		5.0	25	31.0	LTD	
		50.0	22	38.5	LTD	
		110.0	16	42.0	LTD	
		140.0	10	45.0	LTD	
		190.0	10	56.0	LTD	

continued on next page

^a Approximate values drawn from published figures.

Appendix A. Continued.

Location	Site	Depth [m]	Li [μM]	$\delta^7\text{Li}$ [‰]	Classification	Reference		
E Equatorial Pacific	ODP Site 851	225.0	10	55.0	LTD	(You et al., 2003) ^a		
		250.0	10	54.0	LTD			
		300.0	18	34.0	LTD			
		320.0	28	20.0	LTD			
		7.8	15	37.6	LTD			
Irminger Basin	ODP Site 918	26.8	13	43.2	LTD	(Zhang et al., 1998)		
		55.3	15	43.2	LTD			
		139.0	13	40.3	LTD			
		168.0	18	36.7	LTD			
		206.0	20	38.3	LTD			
		232.0	23	32.5	LTD			
		276.0	27	29.6	LTD			
		322.0	29	36.9	LTD			
		515.0	57	39.2	HTD			
		575.0	59	35.8	HTD			
		632.0	94	31.6	HTD			
		660.0	116	32.2	HTD			
		728.0	126	28.3	HTD			
ODP Site 919	ODP Site 919	765.0	163	24.5	HTD			
		930.0	96	36.7	HTD			
		1157.0	91	24.7	HTD			
		6.0	19	40.7	LTD			
		11.0	18	43.2	LTD			
		30.0	17	42.9	LTD			
		50.5	16	43.7	LTD			
		60.0	16	37.4	LTD			
		continued on next page						

^a Approximate values drawn from published figures.

Appendix A. Continued.

Location	Site	Depth [m]	Li [μ M]	$\delta^7\text{Li}$ [‰]	Classification	Reference			
Irringer Basin	ODP Site 919	69.5	16	34.3	LTD	(Zhang et al., 1998)			
		79.0	16	34.1	LTD				
		88.5	15	33.0	LTD				
		94.5	15	37.8	LTD				
		105.0	15	31.4	LTD				
		133.0	16	33.9	LTD				
		Escabana Trough	ODP Site 1034	22.6	21		30.0	LTD	(James and Palmer, 2000)
				29.1	21		24.9	LTD	
				38.6	20		25.6	LTD	
				41.6	21		27.7	LTD	
67.9	16			26.1	LTD				
102.2	8.0			26.1	LTD				
108.1	8.5			24.2	LTD				
111.6	8.5			24.6	LTD				
3.0	15			42.6	LTD				
9.0	11			28.7	LTD				
ODP Site 1037	ODP Site 1037	19.1	11	25.7	LTD				
		30.1	10	25.7	LTD				
		39.6	10	25.2	LTD				
		68.1	9.0	27.2	LTD				
		77.6	10	26.9	LTD				
		125.0	10	22.1	LTD				
		163.1	13	22.1	LTD				
		196.7	18	19.7	LTD				
		225.5	37	20.3	HTD				
		292.6	97	19.6	HTD				

continued on next page

Appendix A. Continued.

Location	Site	Depth [m]	Li [μ M]	$\delta^7\text{Li}$ [‰]	Classification	Reference
Escabana Trough	ODP Site 1037	302.2	151	17.5	HTD	(James and Palmer, 2000)
		328.0	358	20.2	HTD	
		360.0	161	21.1	HTD	
		387.3	124	15.6	HTD	
		406.6	120	15.7	HTD	
		433.9	106	12.7	HTD	
		456.1	166	12.2	HTD	
		485.0	304	11.6	HTD	
		1.5	21	30.5	LTD	
		9.4	19	26.2	LTD	
Central American margin	ODP Site 1039	19.0	23	28.0	LTD	(Chan and Kastner, 2000)
		23.9	25	26.1	LTD	
		55.4	52	23.5	LTD	
		101.4	27	25.2	LTD	
		131.6	24	29.2	LTD	
		136.6	27	22.2	LTD	
		147.7	20	29.1	LTD	
		168.5	16	30.4	LTD	
		178.0	17	30.9	LTD	
		226.1	12	34.8	LTD	
		245.4	10	35.6	LTD	
		270.0	11	38.0	LTD	
		300.3	7.9	37.3	LTD	
		319.6	10	37.5	LTD	
		341.7	12	39.3	LTD	
		374.1	17	34.1	LTD	

continued on next page

Appendix A. Continued.

Location	Site	Depth [m]	Li [μ M]	$\delta^7\text{Li}$ [‰]	Classification	Reference
Central American margin	ODP Site 1039	365.3	10.7	38.9	LTD	(Chan and Kastner, 2000)
		393.2	14.8	35.8	LTD	
		417.0	17.7	33.7	LTD	
		421.7	15.8	35.2	LTD	
		12.9	27.0	30.2	LTD	
	ODP Site 1040	29.9	42.5	27.6	LTD	
		119.1	46.2	22.6	LTD	
		174.6	46.6	22.2	LTD	
		213.0	139	24.4	HTD	
		219.6	95.2	24.4	HTD	
ODP Site 1042	ODP Site 1042	306.4	96.2	30.8	HTD	
		316.0	81.4	28.4	HTD	
		335.3	134	25.4	HTD	
		357.6	261	23.6	HTD	
		367.1	33.2	26.2	HTD	
		401.1	28.0	25.4	HTD	
		461.7	26.8	25.9	HTD	
		519.6	13.6	36.1	LTD	
		564.7	11.4	35.6	LTD	
		620.0	8.90	34.9	LTD	
652.9	11.8	32.3	LTD			
333.0	68.5	27.0	LTD			

FLORIAN SCHOLZ

Diplom Geoökologe, Marine Geochemist

Address: Saarbrückenstraße 26
D-24114 Kiel

Phone: +49 (0)177 5671451

E-mail: fscholz@ifm-geomar.de

Date of birth: 05.02.1980

Place of birth: Karlsruhe, Germany

Nationality: German

Curriculum Vitae

Since 4/2007	Research associate at the Leibniz Institute of Marine Sciences at Kiel University, IFM-GEOMAR.
9/2004 – 6/2005	Studies of Marine Environmental Sciences at the University of Bordeaux 1, France.
10/2000 – 3/2007	Studies of Geoökologie at the University of Karlsruhe.
